Vascularization of Human Embryonic Stem Cell-derived Cardiac Tissues

Lara Filipa Ferreira Mil-Homens

Thesis to obtain the Master of Science Degree in

Biological Engineering

Supervisor(s): Dr. Marcelo Catarino Ribeiro

Prof. Tiago Paulo Gonçalves Fernandes

Examination Committee

Chairperson: Profª. Cláudia Alexandra Martins Lobato da Silva

Supervisor: Prof. Tiago Paulo Gonçalves Fernandes

Members of Committee: Profª. Maria Margarida Fonseca Rodrigues Diogo

October 2018

Acknowledgments

At first, I would like to express my sincere gratitude to Prof. Dr. Robert Passier for welcoming me in his team and to Dr. Marcelo Ribeiro for making everything that came afterwards achievable. Marcelo, even though a thank you will never be enough for all that you did for me, I will always be grateful for all the learning, guidance and support and foremost for your belief in myself even when I didn't.

To Aisen for all the insights given not only about work but also life outside it. To Andreia, AnneMarie, Dinis, José, Stefano and Thomas for never letting me feel that far from home. And to all the remaining members of the Applied Stem Cell Technologies group, without exceptions, for all the help provided along the way with any and everything.

Ao Prof. Tiago Fernandes por me ter estendido a mão nesta fase final.

Aos meus melhores amigos, Inês, Joana, Lili, Nídia, Rita, Patty e Bruno por caminharem comigo em todas as jornadas e me relembrarem diariamente que a distância é só um número.

Ao meu padrinho e "madrinha", Ernesto e Maria João, por todos os conselhos e energia positiva que me transmitem a cada passo da minha vida.

Aos meus tios "escolhidos", Paula e Carlos, e manas "escolhidas", Sofia e Mariana, por serem agora uma constante nos meus dias e que tanto têm contribuído para o meu crescimento.

Aos meus tios, Dalila e Ricardo, por sempre me mostrarem que empenho e resiliência se traduzem em prosperidade. Às minhas primas, Bruna, Lia e Inês, por nunca me deixarem esquecer o meu lado de criança pequena e feliz.

À Paulinha e Pipa por fazerem a diferença na minha vida e me mostrarem que família vai além do sangue e do tempo a que partilhamos memórias.

Aos meus avós, Alice e Feliz, Júlia e Ramiro, por me inspirarem a ser melhor a cada dia e me mostrarem que para todo o fim de túnel, há sempre uma luz.

A vocês, Mãe e Pai, um obrigada sem medida e jamais suficiente para agradecer não só todos os sucessos que me têm proporcionado como também todas as pedras que têm tirado do meu caminho. Hoje, esta vitória é tanto minha como vossa.

À melhor herança que os meus pais me deram, a minha irmã Rita, um obrigada por seres a minha fiel companheira e cúmplice para todos os momentos.

A ti, Carlos, não há língua ou palavras neste mundo que demonstrem o quão agradecida eu sou por te ter na minha vida. Obrigada por teres sido a minha calma quando eu não a soube ter ao longo deste processo. Obrigada por teres sempre segurado as pontas soltas quando a força me faltou. Obrigada por todo o amor desmedido. Obrigada, meu amor.

Vocês são tudo para mim. Esta tese é dedicada a vocês.

Abstract

Cardiovascular diseases can leave permanent lesions and cardiac repercussions, especially concerning extensive cardiomyocyte death and regression of coronary microvasculature, as a result of heart failure, myocardial infarction or ischemia/reperfusion episodes. In the past few decades, several approaches aiming to restore the native function in damaged hearts have been attempted, including through the application of tissue-engineered cardiac constructs that are intended to repopulate the injured cardiac muscle with a new group of contractile cells. However, the major limitation to these constructs has been their inadequate vascularization and reperfusion *in vitro* that highly limits their long-term efficacy and viability, particularly in thick complex tissue-constructs. Moreover, the paracrine cross-talk between endothelial cells and cardiomyocytes also plays a critical role in improving tissue functionality, which can further promote the tissue-engineered construct survival. Efforts employed in providing oxygen and nutrients to cells comprising bioengineered constructs have had variable rates of success, over the years. In the presented project, a fluidic device able to support the co-culture between cardiomyocytes, entrapped in a fibrin matrix, and endothelial cells, both derived from human sources, was successfully established. In the currently optimized fluidic device, it was possible to generate several human beating cardiac constructs with endothelial cells co-presented in their networks, establishing significant ground work for further formation of a vascular system throughout the entire construct. Such innovative approach could contribute largely to the emerging cardiovascular regenerative medicine field, as well to complement current research works regarding the study of key cellular interactions that intervene in tissue vascularization.

Key-words: Vascularization, Tissue Engineering, Cardiomyocytes, Endothelial Cells, Organ-on-a-Chip, Co-culture.

Resumo

Doenças cardiovasculares podem deixar lesões permanentes e repercussões cardíacas, especialmente envolvendo elevada morte de cardiomiócitos e regressão da microvasculatura coronária, como resultado de episódios de insuficiência cardíaca, enfarte do miocárdio ou isquemia/reperfusão. Nas últimas décadas, diversas abordagens que visam restaurar a função nativa em corações afetados têm sido testadas, inclusive através da aplicação de construções de tecidos cardíacos projetadas para repovoar o músculo cardíaco lesado com um novo grupo de células contraíveis. No entanto, o maior entrave a estas construções tem sido a sua vascularização e reperfusão inadequadas *in vitro*, que limitam altamente a sua eficácia e viabilidade a longo termo, particularmente em construções teciduais complexas e espessas. Além disso, comunicações parácrinas entre células endoteliais e cardiomiócitos também desempenham um papel crítico na fomentação da funcionalidade do tecido, o que pode mais tarde promover a sobrevivência da construção tecidual. Esforços empregues no fornecimento de oxigénio e nutrientes a células que compõem construções de bioengenharia têm tido taxas de sucesso variáveis ao longo dos anos. No projeto apresentado, um dispositivo fluídico capaz de suportar a co-cultura entre cardiomiócitos, aprisionados dentro de uma matriz de fibrina, e células endoteliais, ambos derivados de fontes humanas, foi estabelecido com sucesso. No dispositivo fluídico, atualmente otimizado, foi possível gerar várias construções cardíacas com batimento e com células endoteliais copresentes nas suas estruturas, estabelecendo um ponto de partida para a posterior formação de um sistema vascular ao longo de toda a construção. Esta abordagem inovadora pode contribuir largamente para o emergente campo de medicina regenerativa cardiovascular, bem como para complementar trabalhos de investigação correntes que envolvam o estudo de interações celulares chave intervenientes na vascularização de tecidos.

Palavras-chave: Vascularização, Engenharia de Tecidos, Cardiomiócitos, Células Endoteliais, *Organ-on-a-Chip*, Co-cultura.

List of Contents

List of Illustrations

List of Tables

List of Abbreviations

2D: Two-Dimensional

3D: Three-Dimensional

A: Cross-sectional Area

AA2P: L-Ascorbic Acid 2-phosphate Sesquimagnesium Salt Hydrate

ANG-1: Angiopoietin-1

AP: Action Potential

APC: Allophycocyanin

APTES: (3-aminopropyl)triethoxy Silane

ATP: Adenosine Triphosphate

bFGF: Basic Fibroblast Growth Factor

BM-EPC: Bone Marrow-derived Endothelial Progenitor Cell

BMP4: Bone Morphogenetic Protein 4

BPEL: Bovine Serum Albumin Polyvinylalchohol Essentials Lipids

BSA: Bovine Serum Albumin

CD: Cluster of Differentiation

CM: Cardiomyocyte

Cor VE: Coronary Vascular Endothelial Cell

CRISPR: Clustered Regularly Interspaced Short Palindromic

CVD: Cardiovascular Disease

DMEM: Dulbecco's Modified Eagle Medium

DPBS: Dulbecco's Phosphate-buffered Saline

EB: Embryoid Body

EC: Endothelial Cell

ECM: Extracellular Matrix

EDTA: Ethylenediaminetetraacetic Acid

EE: Endocardial Endothelial Cell

eGFP: Enhanced Green Fluorescent Protein

EHT: Engineered Heart Tissue

ET-1: Endothelin-1

FACS: Fluorescence-activated Cell Sorter

FGF: Fibroblast Growth Factor

Fp: Fibrinopeptide

GA: Glutaraldehyde

Gal: Galactose

GF: Growth Factor

Glc: Glucose

GTP: Guanosine-5'-triphosphate

h: Height

hESC: Human Embryonic Stem Cell

hESC-CM: Human Embryonic Stem Cell-derived Cardiomyocyte

hiPSC: Human Induced Pluripotent Stem Cell

hiPSC-EC: Human Induced Pluripotent Stem Cell-derived Endothelial Cell

hPSC: Human Pluripotent Stem Cell

HS: Horse Serum

HUVEC: Human Umbilical Vein Endothelial Cell

ICM: Inner Cell Mass

IGF: Insulin-like Growth Factor

IMDM: Iscove's Modified Dulbecco's Medium

iPSC: Induced Pluripotent Stem Cell

ITS-X: Insulin Transferrin Selenium Ethanolamine

Klf4: Kruppel-like Factor 4

$\boldsymbol{L}$**:** Lenght

LED: Light Emitting Diode

LowIns: Low Insulin

MEMS: Microelectromechanical System

MLC2v: Ventricular Myosin Light Chain 2v

MMP: Matrix Metalloproteinase

Myo Cap E: Myocardial Cardiac Endothelial Cell

$\boldsymbol{NaHCO_3}$**:** Sodium Hydrogen Carbonate

$\boldsymbol{NaOH}$**:** Sodium Hydroxide

NF1: Neurofibromatosis Type I

NO: Nitric Oxide

NOA81: Norland Optical Adhesive 81

Oct4: Octamer-binding Transcription Factor

OH: Hydroxyl Radical

$\boldsymbol{P}$: Wetted Perimeter

PDGF-B: Platelet-derived Growth Factor Subunit-B

PDMS: Polydimethylsiloxane

PECAM-1: Platelet Endothelial Cell Adhesion Molecule-1

PFHM-II: Protein Free Hybridoma Medium-II

PGS: Poly(glycerol sebacate)

PI: Phosphoinositide

PMMA: Poly(methyl methacrylate)

PVA: Poly(vinyl alcohol)

P/S: Penicilin-Streptomycin

$\boldsymbol{Q}$: Total Volumetric Flow Rate

$\boldsymbol{R}$: Radius

RAEC: Rat Aortic Endothelial Cells

$\boldsymbol{R_H}$: Hydraulic Resistance

$\boldsymbol{r_H}$**:** Hydraulic Radius

RyR2: Ryanodine Receptor 2

SOX2: Sex Determining Region Y-box 2

SA: Sinoatrial

SERCA: Sarco/endoplasmic Reticulum Ca^{2+}-ATPase

Si: Silicon

Si-OH: Silanol

SMC: Smooth Muscle Cell

SR: Sarcoplasmic Reticulum

TGF-β: Transforming Growth Factor-Beta

T-tubules: Transverse-tubules

T3: Triiodothyronine

UV: Ultraviolet

VE: Vascular Endothelial Cell

VEGF: Vascular Endothelial Growth Factor

$\boldsymbol{w}$: Width

αMTG: 1-Thioglycerol

$\Delta\boldsymbol{P}$: Pressure Drop

$\boldsymbol{\mu}$**:** Viscosity

I. Introduction

1. Cardiovascular Diseases

Cardiovascular diseases (CVD) include a range of conditions that affect the structures and/or function of the heart and blood vessels, and are among the leading causes of morbidity and mortality in the worldwide nations, representing 31% of all global deaths (17,7 million of people) in 2015, as reported by the World Health Organization [1]. Over 40% of these deaths, an estimated 7,4 million of people, were due to coronary heart diseases, being these the most common cause of death among cardiovascular diseases [1].

1.1. Myocardial Infarction: Clinical Implications and Therapies

Myocardial infarction is a serious result of coronary artery diseases and occurs when a coronary artery of the heart, responsible for the transportation of oxygenated blood to the right and left ventricles, gets a blockage leading to a prolongated hypoxic environment in several heart areas (Figure 1) [2]. If the depletion of oxygen is substantial, those areas will start presenting necrotic tissue and a massive inflammatory response is triggered by the organism [2]. Since adult cardiomyocytes are unable to regenerate, the inflammatory response of the body leads to the replacement of the infarcted tissue by dysfunctional fibrotic tissue produced by fibroblasts and myofibroblasts in the injured area [3]. The fibrotic tissue formed is permanent, incapable to contract and can lead to congestive heart failure as the heart is unable to meet the work load demand [2][3].

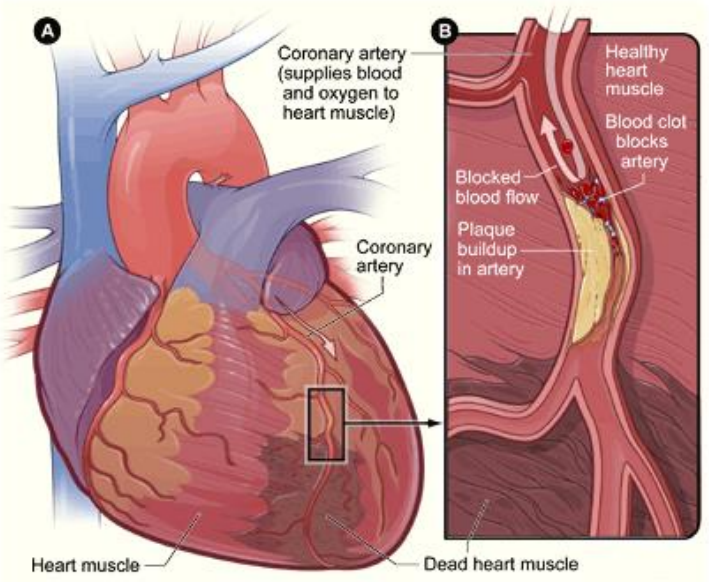

Figure 1: A) Overview of an infarcted myocardium as a result of a coronary artery disease. B) Cross-section of the coronary artery showing the plaque buildup and the blood clot blocking the blood flow to the progressive damaged area.

Although some pharmacological experiments have led to some improvements in patients with myocardial infarction, heart transplantation remains to be the gold-standard treatment. Due to the low availability of transplantable hearts and heart rejection scenarios, engineered cardiac constructs are one of the most promising alternatives to restore the native myocardial function [2].

1.2. Cardiovascular Pharmacology and Disease Models

Besides the development of engineered cardiac models for cardiac repair purposes, accurate prediction of proarrhythmic side effects of drugs in cardiovascular-related preclinical trials would also highly benefit from improved human heart models [4]. Additionally, most of these preclinical studies are currently performed using animal models which naturally exhibit substantial genomic and physiological differences relative to the human heart; hence, these fail to predict the toxicity of human cardiomyocytes and end up by leading to several patient deaths in advanced phases of the trials [4].

Therefore, the improvement of engineered cardiac models *in vitro*, that close mimic the complex structure of the human heart, should be an important motivation nowadays in order to develop reliable models for industrial and clinical applications, namely disease modeling, drug development and cardiac repair. These advances would contribute to move a step closer to a decrease in both mortality and morbidity rates associated with cardiovascular diseases, reducing one of the major loads to health care systems worldwide.

2. Cardiac Morphology and Physiology: Structure & Function

2.1. Cardiac Muscle: An Overview

The cardiac muscle or myocardium is composed by numerous cells that work together to pump blood from the heart throughout the body via a circulatory system.

The pumping mechanism is achieved through the process of contraction and relaxation of specific cardiac muscle cells (designated as cardiomyocytes) that make up the four contractile chambers (upper left and right atria and lower left and right ventricle) of the heart [5]. Besides being composed of strongly mechanically and electrically connected cardiomyocytes, the myocardium also contains cardiac fibroblasts, endothelial cells, vascular smooth muscle cells and macrophages [6].

2.1.1. Cardiac Electrophysiology

The activity of the human heart is characterized by auto rhythmicity which is the particular capacity to initiate an action potential (AP), rapid rise and subsequent fall in a cell membrane potential, followed by the spreading of that electrical impulse throughout the entire cardiac muscle, triggering continuous and synchronized contractions in the heart.

Usually, the action potential is generated in the sinoatrial (SA) node, located in the upper right atria, that comprises a specialized group of myocardial cells that exhibit automaticity, the unique ability of becoming spontaneously electrically active (depolarized), producing an electrical impulse (action potential) [7]. Therefore, these cells are the heart pacemaker, being for that reason designated as pacemaker cells, since they are responsible for the establishment of the normal sinus rhythm of the heart [7].

After the generation of the electrical impulse by the myocardial conducting cells, the impulse is spread to the adjacent myocardial cells (designated as cardiomyocytes) that have the ability to respond to the impulses by easily contracting, in a process known as excitation-contraction coupling process (Figure 2) [8].

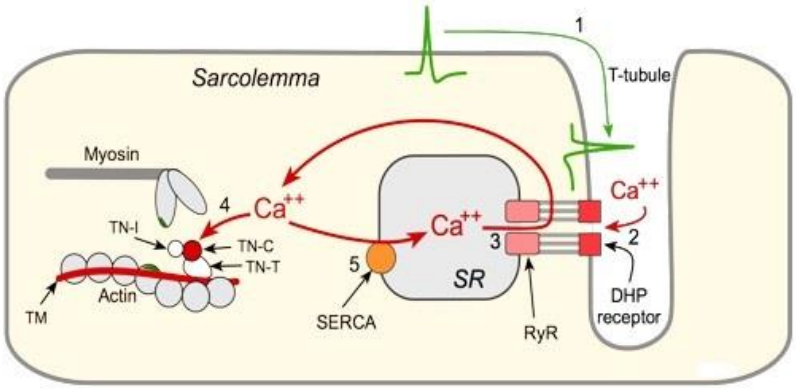

Figure 2: Schematic illustration of the excitation-contraction coupling process.
1) The action potential reaches the sarcolemma and travels along the transverse tubules (T-tubules), depolarizing the cardiomyocyte membrane; **2)** Voltage sensitive L-type calcium channels open allowing the entry of calcium into the cell; **3)** The influx of calcium triggers the release of calcium ions stored in the sarcoplasmic reticulum (SR); **4)** Calcium binds to a regulatory complex attached to the contractile filaments, inducing conformational changes that lead to the contraction of the actin and myosin; **5)** Calcium is newly sequestered into the SR, lowering the cytosolic calcium concentration and subsequently ending the signal, allowing the sarcomere to recover its initial length.

2.1.2. Cardiac Muscle Cells: Morphology

The size and morphology of the cardiomyocytes depend on their distribution in the adult heart. Specifically, ventricular cardiomyocytes are typically columnar shaped cells with 20 µm of diameter and 60 to 140 µm of length and atrial cardiomyocytes are usually ellipsoidal shaped with 5 µm of diameter and 10 to 20 µm of length [9].

The adult cardiomyocytes can be found aligned longitudinally in the heart and are composed of tubular myofibrils that comprise the myofilaments of the contractile proteins, including actinin and myosin [8]. These proteins are organized and aligned in repeated structures called sarcomeres that confer the striated appearance to the heart muscle and are responsible for the generation of the force of contraction [8]. The cardiomyocytes are connected by intercalated discs that facilitate the electrical conduction and muscle contraction by allowing the cardiomyocytes to work as a single functional syncytium [8]. These intercalated discs are mostly composed of gap junctions, that allow the spreading of the action potential between the cardiomyocytes, and desmosomes that hold together the cardiomyocytes upon the sliding of the cardiac myofibrils during the contraction process (Figures 3 and 4) [8].

Additionally, the cardiac muscle cells contain transverse-tubules (T-tubules), deep invaginations from the sarcolemma (cell membrane) that penetrate the cell, allowing the electrical impulses to reach the intracellular region (Figures 3 and 4) [8].

Apart from that, cardiac muscle cells also contain several mitochondrion to ensure the fulfillment of the high energy demands for the contractile process and are majorly single nucleated cells (Figures 3 and 4) [8].

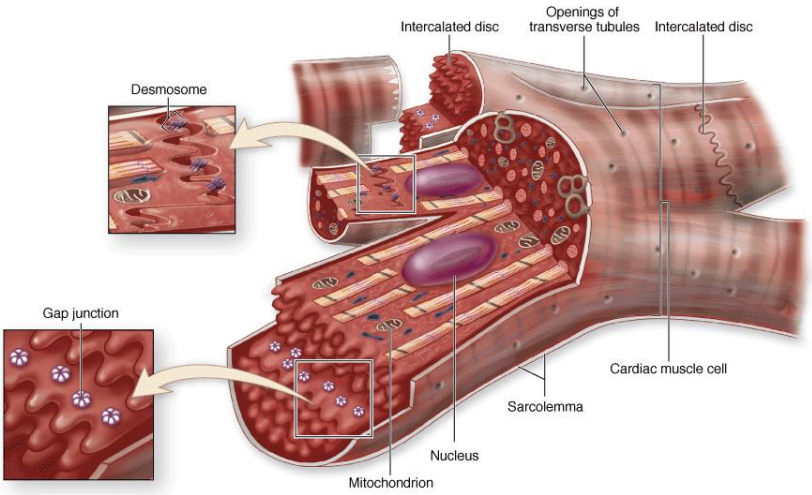

Figure 3: Schematic illustration of characteristic features of cardiac muscle cells.

Cardiomyocytes have a central nucleus and several mitochondrion to produce high amounts of adenosine triphosphate (ATP) to cover all the energetic demands. The cardiomyocytes are in close-contact with each other and are connected by intercalated discs, whose transverse regions are composed of desmosomes that hold the cells firmly together and longitudinal regions composed of gap junctions that allow the passage of the electrical signals from cell to cell as a single wave. The cell membrane of cardiac muscle cells is designated as sarcolemma and has invaginations that penetrate into the center of the cell, allowing the electrical signal to reach the intracellular region. Adapted from [10].

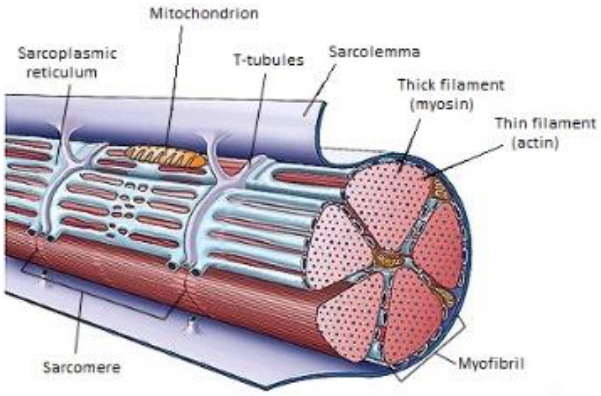

Figure 4: Schematic illustration of a cross-section of a cardiac muscle cell.

Cardiomyocytes are composed of myofibrils that consist in the contractile elements of the muscle. The myofibrils contain two different types of fibers: thin filaments made of actin and thick filaments made of myosin. These filaments are encircled by the sarcoplasmic reticulum and are arranged in compartments designated as sarcomeres.

3. Cardiac Muscle Cells: Models *In Vitro*

3.1. Human Pluripotent Stem Cells (hPSC)

In the last decade, several prominent advances have been accomplished, especially in the regenerative medicine field, with the development of human stem-cell derived three-dimensional engineered heart tissues [11]. Beyond that, these models also impact the drug modelling field due to their human origin that contribute to more predictive and relevant results compared to the ones obtained with existing animal-based models.

For that, many researchers have been using different types of proliferative cells that mostly comprise bone marrow cells, endogenous cardiac stem cells, embryonic stem cells and induced pluripotent stem cells [11]. Due to the low cardiac differentiation efficiency and low yield associated with the bone marrow and endogenous cardiac stem cells, their use has been limited, being often replaced by embryonic and

induced pluripotent stem cells that can effectively differentiate into cardiomyocyte (and non-cardiomyocyte) lineages [11].

Human embryonic and induced pluripotent stem cells are often grown on coated surfaces with vitronectin since this recombinant protein has been proved to maintain an undifferentiated state on multiple stem cell lines, by maintaining a compact cell morphology, expression of several stem cell markers, differentiation ability and others, even when cells are cultured for long-term periods [12].

3.1.1. Human Embryonic Stem Cells (hESCs)

Human embryonic stem cells (hESCs), derived from the pluripotent inner cell mass (ICM) of blastocyst-stage embryos (Figure 5), hold a great promise in the field of cell therapies due to their ability of unlimited self-renewal while maintaining an undifferentiated phenotype [13]. Therefore, hESCs can give rise to all somatic cell types present in the human organism by forming derivatives of all three germ layers: endoderm, mesoderm and ectoderm [13].

The ability to isolate and culture hESCs was reported for the first time in 1998 by Thomson et al. [14] and some of the first protein markers recognized as essential for the maintenance of their native pluripotency were the transcription factors OCT3/4, NANOG and sex determining region Y-box 2 (SOX2), reported by Nichols [15], Chambers [16] and Fong et al. [17], respectively.

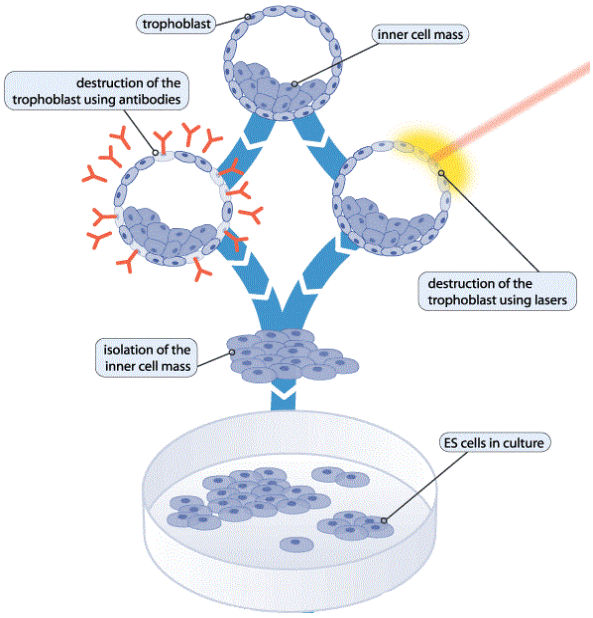

Figure 5: Schematic illustration of the embryonic-stem cell derivation process.
The blastocyst is composed of an outer cell layer (trophoblast) that envelops the inner cell mass, from where the stem cells can be obtained to be cultured after the destruction of the trophoblast layer.

Despite all the breakthrough created in the biomedicine field by the underlying potential of hESCs to specialize in all cell-types, several ethical issues regarding their embryo origin have been limiting their worldwide use [13].

3.1.2. Human Induced Pluripotent Stem Cells (hiPSCs)

Induced pluripotent stem cells (iPSCs) were first derived by the Shinya Yamanaka's group, in 2006, when they made the outstanding finding that the introduction of specific transcription factors, involved in the pluripotency of embryonic stem cells, in mature adult cells could induce them to an embryonic state [18]. Specifically, the Shinya Yamanaka's group showed that the introduction of four specific genes encoding transcription factors, namely the octamer-binding transcription factor 4 (Oct4), the SOX2, the Kruppel-like factor 4 (Klf4) and the c-Myc, all important to ESC function, in mouse adult cells induced them into pluripotent stem cells [18].

Based on this reprogramming approach, in 2007, the Yamanaka's [19] and Thomson's group [20], independently, reported the generation of human induced pluripotent stem cells (hiPSCs) from adult human skin fibroblasts. It was demonstrated that these reprogrammed cells display comparable morphology, surface antigens, gene expression, telomerase activity and properties of self-renewal and pluripotency with hESCs [19], being able to give rise to all the cell types present in the human body including the cardiac lineage.

The hiPSCs technology has an unequaled potential in the regenerative field since it bypass the need for embryo blastocysts and given that these cells can be directly derived from adult tissues, they allow the creation of patient-specific iPSCs (autologous cells). The patient-specific cells can then be used to screen effective disease-specific drugs *in vitro* or used to generate healthy tissue-engineered constructs passible to be transplanted into the patient body with minimal risk of immune rejection (Figure 6) [21].

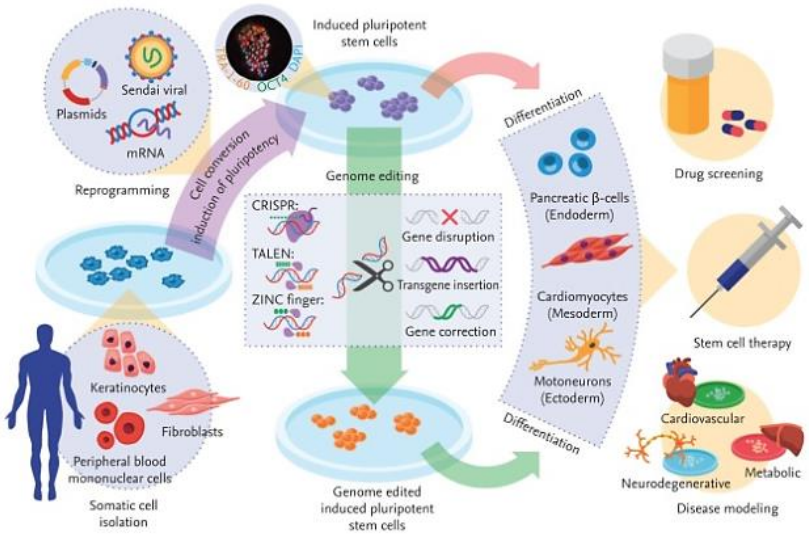

Figure 6: Schematic illustration of the generation of patient-specific induced pluripotent stem cells (iPSCs) and their possible clinical applications.
Somatic cells are firstly isolated from the patient and reprogrammed into iPSCs by transduction of 4 transcription factors: Oct4, SOX2, Klf4 and c-Myc. Genetic defects can be corrected by genome modifications through gene editing approaches. Afterwards, iPSCs can be differentiated into various cell-types and be used for drug screening, disease modelling and stem cell therapy purposes. Adapted from [21].

3.2. Differentiation of hPSC towards Cardiomyocytes

Human pluripotent stem cells can undergo differentiation *in vitro* in order to generate derivatives of all the three primary germ layers and, therefore, theoretically give rise to all the cell types present in the human body.

Significant progress has been made in developing efficient strategies for the production of functional cardiomyocytes from hPSC that mostly rely on the spontaneous differentiation by embryoid body (EB) formation, co-culture with endodermal cells or by directed differentiation using defined medium and inducers/growth factors (Figure 7) [22].

An embryoid body is a three-dimensional aggregate that contains tissues from all the three primary germ layers and is generated through the enzymatic dissociation of hPSCs colonies into small clumps (EBs)

[22][23]. Over time, some of the mesodermal layer derivatives will spontaneously differentiate into cardiomyocytes that start presenting beating activity after some days in culture. This approach was successfully reported in first place by Kehat et al. (2001) [23].

Another technique, firstly reported by Mummery et. al (2003), that can also be used to differentiate hPSCs into cardiomyocytes is the co-culture of these cells with the mouse visceral endoderm-like cell line END2 [24]. The drawback of this approach is the fact that the END2 cells are derived from mouse embryonal carcinoma, which implies that the hPSCs-derived cardiomyocytes will present xenogeneic components that therefore are genetically and immunologically incompatible with the human specie, limiting their use for clinical applications [22].

An alternative technique that can also be used to produced hPSCs-derived cardiomyocytes is the directed monolayer differentiation of hPSCs using specific growth factors and medium formulations [25]. Matrigel is a natural hydrogel, rich in extracellular matrix (ECM) proteins (e.g. laminin, collagen IV, proteoglycans, among others), that improves the attachment and differentiation of anchorage-dependent cells by better mimicking the *in vivo* ECM-environment [26], and it has been reported to promote cardiogenesis [25] with highly efficient cardiac differentiations associated to its use [27]. Laflamme et al. (2007) were the pioneers of this technique by using a combination of Activin and bone morphogenetic protein 4 (BMP4) in a serum free medium to generate cardiomyocytes from hPSCs [28].

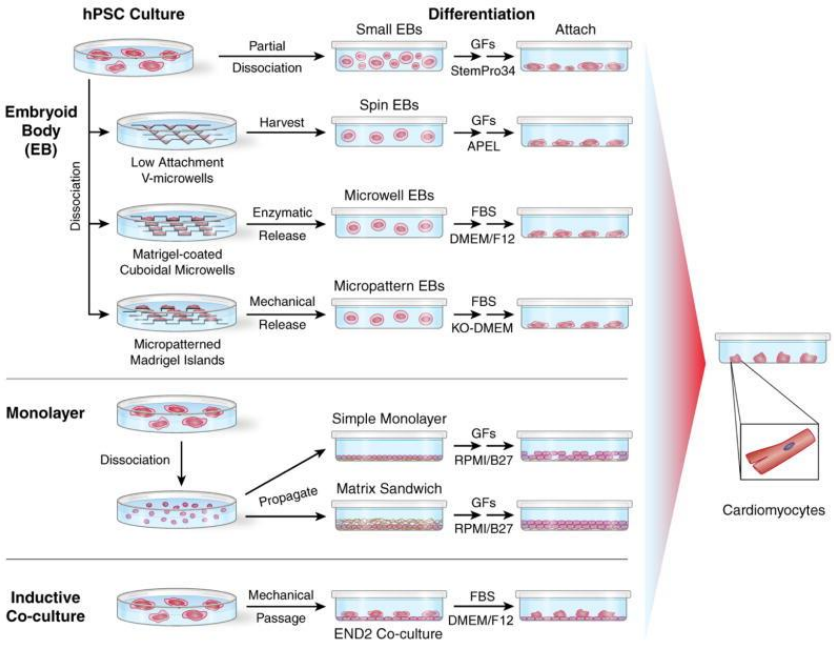

Figure 7: Overview of the three major approaches for differentiation of human pluripotent stem cells (hPSCs) into cardiomyocytes (CMs): embryoid-body (EB) formation, monolayer culture and inductive co-culture.
Embryoid-body formation consists in the enzymatic dissociation of hPSCs into 3D aggregates (EBs); a fraction of these EBs will exhibit spontaneously contracting regions containing CMs. Monolayer culture of hPSCs on Matrigel with defined media can also promote cardiogenesis. Stage-specific growth factors (GFs) are also applied for promoting an optimal cardiogenesis in these two approaches. Finally, co-culture of hPSCs with visceral endodermal-like END2 takes advantage of cell signaling from END2 cells to promote cardiogenesis. Adapted from [25].

3.3. Cardiac Maturation

3.3.1. Three-Dimensional Cardiac Microenvironments

The human heart is composed of contractile cardiac muscle cells and non-muscle cells types that are organized *in vivo* in a complex tridimensional structure. Nevertheless, hPSCs-derived cardiomyocytes are often grown on basic two-dimensional (2D) environments, usually flat petri dishes, that barely recapitulate the native cardiac environment. These 2D techniques were used for so long since they have been really well-established in the last decade, with several data available in the literature, the technology involved is not that expensive and usually cell observation and associated measurements are easily accessible.

Even though 2D culture systems had uncovered over the years many cellular mechanisms of the myocardial and vascular system, there are still a lot left to understand that is not reachable using these systems [29]. For instance, the interactions between myocytes and non-myocytes cell types present in the 3D cardiac environment (namely the electrical and paracrine crosstalk) is not assessible without resorting to a nature-3D mimicking environment [29]. Additionally to that, hPSC-derived cardiomyocytes obtained in 2D cultures greatly resemble immature cardiomyocytes exhibiting lower expression of specific cardiac genes, decreased force of contraction, morphological differences namely random sarcomere structures and distribution of nuclei, and electrophysiological differences affecting calcium handling and electric coupling when compared with adult mature cardiomyocytes [30][31]. The immaturity associated with the newly differentiated cardiomyocytes can negatively affect their functional properties as well their drug responses [31]. In order to address these limitations, more tissue-like 3D environments that can provide appropriate structural cues for cardiomyocytes *in vitro* maturation have been intensively explored in the last years [31].

3.3.2. Medium Formulations with Soluble Factors

Besides the use of 3D culture systems, the addition to the culture medium of certain soluble factors as the triiodothyronine (T3) hormone and the insulin-like growth factor 1 (IGF-1) can largely contribute to further the hPSC-committed cardiomyocytes *in vitro* maturation into adult mature-like cardiomyocytes by providing important biochemical cues to their adequate development.

T3 hormone has been shown to be involved in several physiological processes that directly affect the heart metabolism and rate [32]. More specifically, the T3 hormone is recognized by enhancing the expression of several cardiac genes, such as the sarco/endoplasmic reticulum Ca^{2+}-ATPase (SERCA), the ryanodine receptor 2 (RyR2), the NKX2.5 and the ventricular myosin light chain 2v (MLC2v), for instance, that play pivotal roles in hPSCs-derived cardiomyocytes function, positively contributing for the maturation of their calcium handling and electrophysiological properties [33]. In its turn, the IGF-1 is also known to enhance cardiomyocyte survival, growth, proliferation and metabolism *in vitro*, through the activation of specific signaling pathways, like the phosphoinositide 3-kinase/Akt (PI 3-kinase/Akt) pathway [34]. Even though, IGF-1 has been shown to inhibit cardiac differentiation from hPSCs [35], its

aforementioned positive role in hPSC-differentiated cardiomyocytes makes it a potential effector for promoting the maturation of these cells *in vitro*.

Along with that, the addition of galactose to the culture medium greatly contributes to improve the metabolic maturity of the cultivated cardiomyocytes, by improving their oxidative capacity [36]. The transition for a non-glucose enriched medium forces the cardiomyocytes to rely on the oxidative phosphorylation pathway instead on the glycolytic one, since the latter does not produce enough ATP capable of covering all the cell energetic demands using galactose as substrate [37]. Cardiomyocytes maturation *in vivo* is associated with the transition of an embryonic-like glycolytic metabolism to an adult-like oxidative metabolism; hence, adapting cardiomyocytes to galactose as energy source also contributes for moving a step further in promoting their maturation *in vitro* [36]. However, glucose should not be dismissed from the culture medium, after the adaption of the cardiomyocytes to the galactose source, since cardiomyocytes also depend *in vivo* on the glycolytic pathway to produce part of the needed ATP [36]. Besides that, when cardiomyocytes are lately involved in 3D-tissue structures, the access to energy sources is hampered. Thus, the adaptation of cardiomyocytes to the use of more than one energy source will always be beneficial and helpful especially in this type of culturing conditions.

3.3.3. Other Strategies

Other strategies that can be pursuit *in vitro* for promoting cardiomyocytes maturation can include other types of biophysical cues, as mechanical and electrical stimulation, substrate stiffness and topography, or biochemical cues, as substrate chemistry, co-culture systems, long-term cultures or by genetic manipulation of the cells (Figure 8) [30].

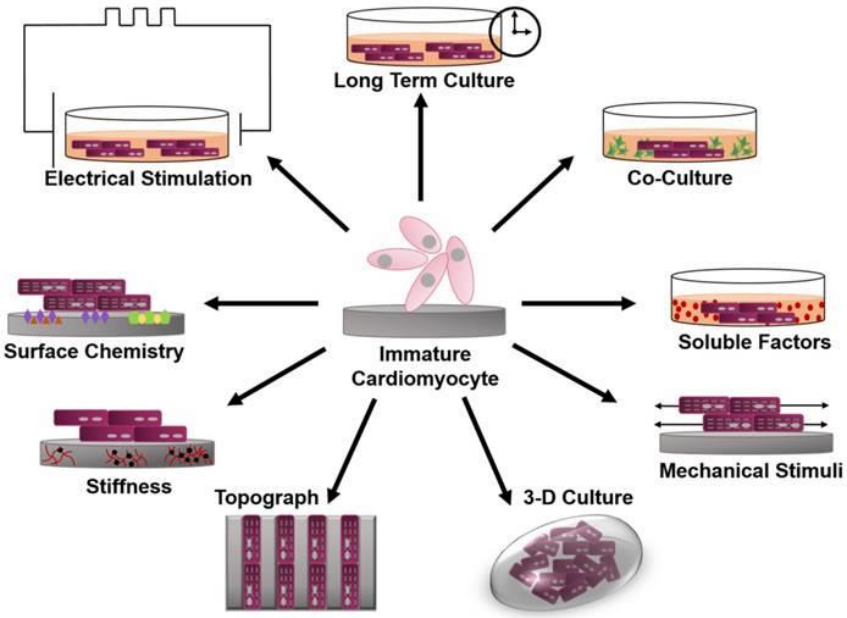

Figure 8: Schematic illustration of engineered microenvironments that can be employed to promote the *in vitro* maturation of human pluripotent stem cell-derived cardiomyocytes by mimicking the natural physiological conditions of cardiomyocytes during their development.
Adapted from [30].

4. Three-Dimensional (3D) Cardiac Tissue Engineering Models

4.1. Methods for Engineering Heart Tissues

There are several approaches that can be pursued in order to generate 3D cardiac tissues *in vitro*, being the most common to take advantage of the endogenous ability of cardiomyocytes to naturally assemble and form organized 3D functional networks, together with engineering techniques to form those constructs with the desired size, geometry and orientation [38].

Considering this approach, there are several strategies that are commonly followed, including: hydrogel encapsulation, prefabricated matrices or scaffolds, recellularization of decellularized heart tissues and cell sheet technology [6][38]. Most of these approaches still rely on the supplementation with horse serum (HS) since the withdrawal of this component from the culture medium leads to a rapid decline in the contractile activity of the cardiomyocytes that culminates in the complete absence of a beating activity over time for still unknown reasons; in fact, several successfully reported engineered heart tissues (EHTs) are dependent on the continuous presence of horse serum at 10% (v/v), like fully investigated by Eschenhagen et al. (2002) [39].

4.1.1. Hydrogel Encapsulation Methods

Hydrogel encapsulation methods are probably the most used technology to generate heart muscles *in vitro* due to its simplicity, straightforward measurements of force and other relevant parameters of heart muscle function, miniaturization and automatization [38], structural similarities to the extracellular matrix (ECM) and intrinsic ability to support cell adhesion and growth [40].

This technology requires 4 main factors that can be listed as: cardiac cells (or cardiomyocytes), solutions of gelling natural products or hydrogels (e.g. collagen I, fibrin, among others), casting molds and a mechanic or anchoring support for the cells [6][38].

Shortly, the liquid hydrogel entraps the cells during the gelation time in the 3D shape provided by the casting mold, promoting an *in vivo*-like environment in which the cells can interact between themselves in an organ-like architecture; while the supportive or anchoring points allow the growing tissue to fix to the casting mold and to develop mechanical tension between the anchoring points [6][38]. The anchoring points expose the cells to a continuous mechanical strain, which consists in one of the main advantages of this approach since it allows the cardiomyocytes to align parallel to the force lines, resembling their alignment in the myocardium, and largely contributing to their development and maturation [6][38].

<u>Types of Hydrogels</u>

Natural and synthetic hydrogels are both suitable for tissue engineering purposes due to their soft and viscoelastic properties that closely mimic the native cardiac tissue [41]. Nevertheless, natural hydrogels are biodegradable, non-cytotoxic as some synthetic polymers and are naturally compatible with cell adhesion [41].

Collagen I is one of the most used natural hydrogels since it is a major component of the extracellular matrix (ECM) of the myocardium, being a natural and biodegradable polymer, that presents negligible antigenic and inflammatory responses. Taking this into account, well-defined protocols considering diverse approaches with different types of casting molds have been established using this component. However, collagen I presents some remarkable drawbacks namely high stiffness, extensive handling that can lead to experimental variations, procedures difficult to miniaturize and gelation times considerably long, incurring into the possibility of having cells flushed away in this period [42].

On the other hand, fibrin is also a biodegradable and natural gel that has an inherent production in the human plasma blood from which can be purified, allowing its autologous use, eliminating potential immunologic responses [43]. Besides its autologous source, fibrin can easily be synthesized *in vitro* by the thrombin-catalyzed conversion of fibrinogen into fibrin [43].

In fact, after mixing the fibrinogen with the protease thrombin, the release of the fibrinopeptides A (FpA) and B (FpB) from the fibrinogen is promoted [44]. Thereby, occurs the sequential exposure and activation of 2 polymerization sites that readily interact with other monomers permanently present in the fibrinogen molecule [44]. As a result of these interactions, the monomers are able to self-assemble into fibers that ultimately form the fibrin-hydrogel mesh (Figure 9) [44].

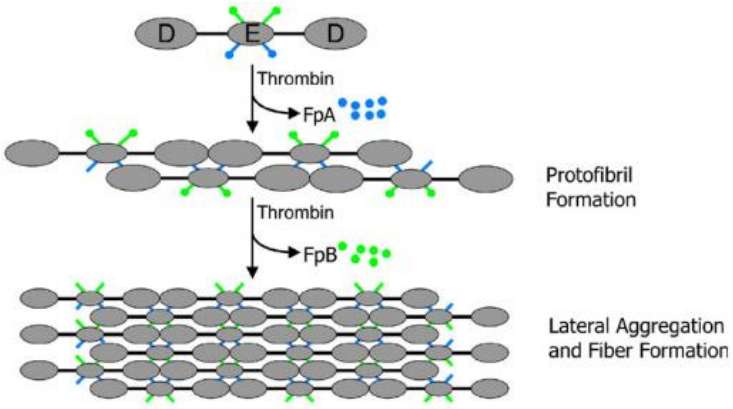

Figure 9: Schematic representation of the fibrin gel formation. The thrombin promotes the successive release of the fibrinopeptides A (FpA) and B (FpB) from the central E nodule of the fibrinogen. The fibrinopeptides release allows the interaction and aggregation of the fibrinogen chains, leading to the formation of the first protofibrils that readily form the fibrin fibers through lateral aggregations between the protofibrils. Adapted from [45].

The exchange of collagen I for fibrin(ogen) has been extensively investigated in the last few years since it presents a faster gelation time contributing to a more homogenous cellular distribution [43], versatile mechanical properties namely its nonlinear elasticity, that is expressed in a higher elastic modulus when exposed to shear stress, and finally, its softness that contributes to cardiomyocytes with higher motility [6][42].

Types of Casting Molds

Besides conferring the 3D shape to the developing tissue, the casting molds are also responsible for the establishment of its size. There are a lot of conformations that can be used as casting molds, all dependent and defined based on the final application envisioned for the cardiac tissue in development (Figure 10).

For example, Eschenhagen et al. (1997) reported the generation of plane collagen-based engineered heart tissues (EHTs) using Velcro-covered rods as casting molds [46], being one of the first hydrogel-

based techniques reported in the literature [38]; whereas Zimmermann et al. (2002) reported the creation of ring-shaped collagen-based EHTs [47]. Regarding fibrin-based engineered heart tissues, one of the first innovative approaches using this hydrogel was reported by Hansen et al. (2010) that described the generation of mini-EHTs on polydimethylsiloxane (PDMS) flexible racks [42]. All these different geometries were idealized in order to be biologically relevant for the authors purposes, as well the choices of the hydrogel used.

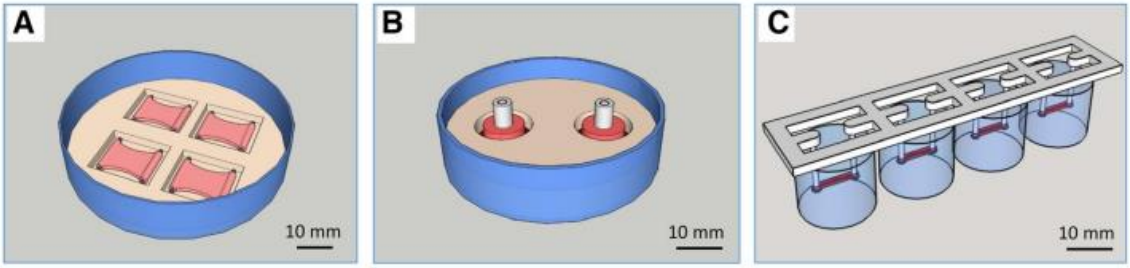

Figure 10: Schematic illustration of some strategies, with illustrated casting molds, used to generate cardiac tissues based on hydrogel encapsulation methods.
A) Plane collagen-based engineered heart tissues (EHTs) on Velcro-covered rods; **B)** Ring collagen-based EHTs; **C)** Fibrin-based mini-EHTs on (polydimethylsiloxane) PDMS racks. Adapted from [6].

Expected Development of Hydrogel-based Engineered Heart Tissues

Directly after casting the cardiac tissues, it is expected to observe single and round-shaped cells (resulting from the dissociation step) englobed in a uniform and amorphous (without a defined spatial organization) cell suspension contained in the hydrogel. Human adult-like cardiomyocytes exhibit a structural rigid architecture, whereby after their dissociation, they remain rod-shaped; while immature hESC-derived cardiomyocytes remain round-shaped after their dissociation, resembling fetal-like cardiomyocytes [48].

Natural occurring hydrogels provide biochemical cues to the entrapped cells, stimulating their spreading on their surface that, in its turn, enables the progressive establishment of novel intercellular connections; hence, within days the cells start recovering their beating activity as single cell clusters [38]. Along with that, the increased compression of the gel, due to the increase presence of novel contractions areas, contributes for reducing the water content of the hydrogel, contributing to its shrinkage several times in size and consequently, also stimulating the cell remodeling [38].

Parallel to that, the progressive degradation of the hydrogel by the plasmin and other components present for example in serum [42], and by the increased production of ECM proteins as matrix metalloproteinases (MMPs) by the cardiomyocytes [49], also contributes to reduce the tissue size and consequently to increase the proximity between cells, allowing the establishment of cell-cell interactions that start to be translated in a coherent and synchronous beating tissue with time. Thus, the degradation and remodeling of the hydrogel is marked by a combination of all the aforementioned biological events.

Clearly, the timeframe that defines each developing stage of an EHT is highly dependent on a set of variables, namely: the type of mechanical load exerted into the construct, the cell concentration applied in the reconstitution mixture, the addition of agents that control the rate of degradation of the hydrogel

in vitro (e.g. aprotinin is a commonly used antifibrinolytic agent that slows down the *in vitro* rate of degradation of the fibrin (fibrinolysis) by inhibiting active fibrinolytic components present in the serum, for instance [43]), the age and state of maturation of the cardiomyocytes, among others.

4.1.2. Prefabricated Matrices Methods

Prefabricated matrices or scaffold-based approaches rely on seeding cardiomyocytes onto porous solid scaffolds, usually constructed from biodegradable polymers [38]. Evident advantages of this type of techniques are related to the feasibility of engineering any designed form and to the easiness of manipulating and handling the constructs in culture [38]. This approach was pioneered a long time ago, with publications resorting the 1990s and the early 2000s, that describe the use of polymers like gelatin, polyglycolic acid, alginate and collagen, respectively, reported by Li et al. (1999) [50], Carrier et al. (1999) [51], Leor et al. (2000) [52] and Radisic et al. (2004) [53] to grow cardiac tissues. Clearly, the properties of the material that composes the scaffold construct influences the cell function, migration, force of contraction, calcium transients, state of differentiation, among others; whereby its choice should be adapted to the biological circumstance in study [54].

4.1.3. Recellularization of Decellularized Heart Tissues

Some successful attempts have been made in the last years, regarding the generation of artificial hearts directly by decellularizing whole hearts and repopulating the remaining ECM with cardiac cells (Figure 11) [6]. Protocols using detergents for decellularization are well advanced, allowing the eradication of all possible immunogenic cellular components from the tissue without disturbing the architecture of blood vessels. This approach was pioneered in 1999 by the company CryoLife (Kennesaw, GA, USA) that decellularized a porcine heart valve that received the approval for commercialization in 2001 [55]. Since then, different types of animal hearts and tissue products have been decellularized, including human hearts. For instance, in a recent study (2016) reported by Guyette et al., hiPSC-derived cardiomyocytes were injected in the free left ventricular wall of a decellularized human heart; the cardiomyocytes were able to survive in the matrix and formed an immature beating cardiac tissue [56].

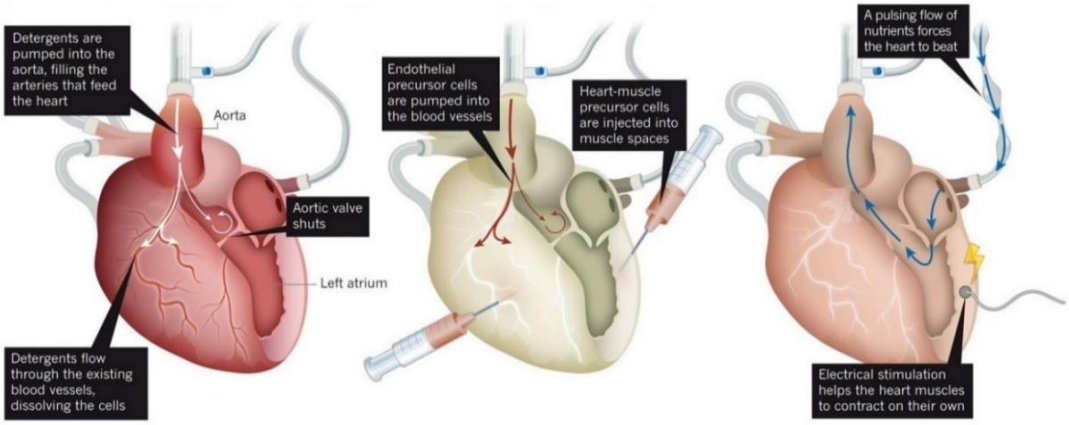

Figure 11: Schematic illustration of a recellularization process of a decellularized heart.
Left picture: The cells are removed from the organ by application of suitable detergents, leaving a protein scaffold. **Center picture:** The protein scaffold is seeded with new cardiac cells: endothelial precursor cells and heart-muscle precursor cells. **Right picture:** The heart can be matured under the influence of growth factors and mechanical stimulation.

4.1.4. Cell Sheet Technology

Monolayers of cardiomyocytes cultured on standard plastic petri dishes tend to spontaneously detach from their surface overtime [38]. In 2002, Shimizu et al. made use of this principle by exploiting thermosensitive surface materials that lose their adhesive properties at room temperature, enabling in this condition the easy detachment of intact monolayers contrary to the results obtained using conventional enzymatic methods (Figure 12) [57]. After having the cell monolayers or sheets properly detached and isolated, 3D cardiac tissues can be simply generated by stacking the sheets on top of each other [57].

Since this is a scaffold-free technology, putting aside biological questions like biocompatibility of materials and other concerns, it is a technique that is well-suited and promising for cardiac repair applications [38]. On the other side, it is not suitable for drug screening or disease modelling applications due to the fact that monolayers would need to be attached to enable the connection of force transducers needed for functional testing and analysis, for instance [6].

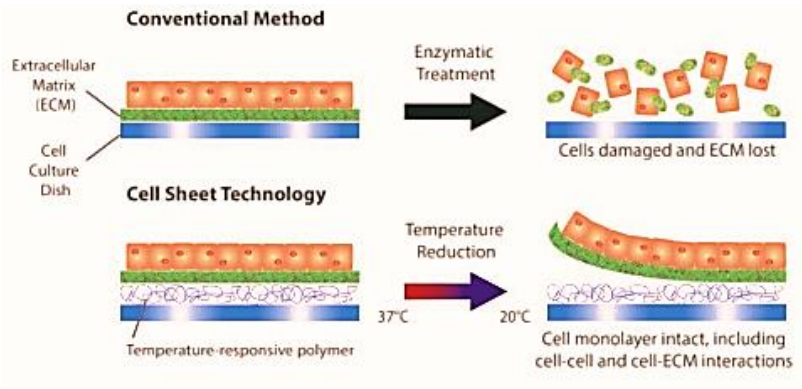

Figure 12: Schematic illustration of a conventional enzymatic method and a cell sheet method to harvest cardiomyocytes in culture.
Conventional method: The cells are harvested by resorting to enzymatic treatments that result in the disruption of membrane proteins and the extracellular matrix (ECM). **Cell sheet technology:** Contiguous monolayers of cardiomyocytes can be harvested from temperature-responsive culture surface with intact cell-cell connections and deposited ECM.

4.2. Scaling-up Cardiac Tissues *In Vitro*: The Need for Vascularization

Most of the aforementioned approaches to generate cardiac tissues *in vitro*, except the ones concerning recellularization of decellularized heart tissues that already include a native vascular system, are limited to a certain thickness due to the lack of efficient vascularization strategies. The lack of a functional vascular system that can assure constant flows of oxygen and nutrients to the tissue, as well as escape routes to eliminate the carbon dioxide and other cellular wastes that are generated inside it (Figure 13), in order to maintain its long-term viability and functionality is currently one of the major limitations in every 3D-engineered tissue field [58], but especially for the cardiac system.

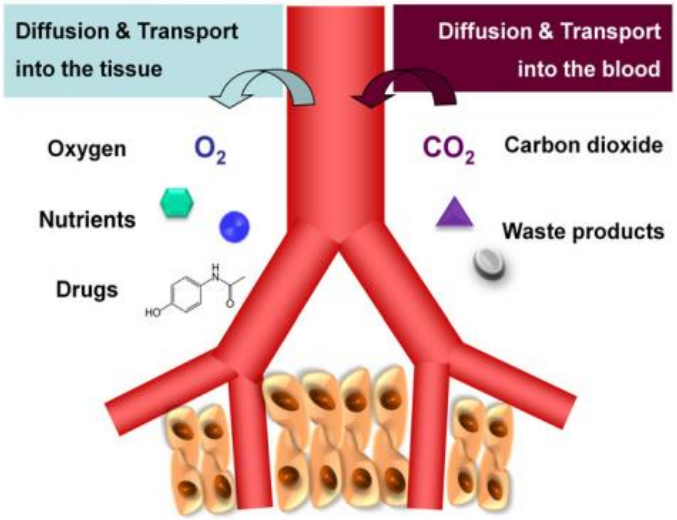

Figure 13: Schematic exemplification of diffusion and transport processes that occur between tissues and the vascular system.

The vascular system provides oxygen, nutrients and drugs to the surrounding tissue and carries waste products and carbon dioxide away from it, ensuring its long-term functionality. Adapted from [58].

The demanding metabolic requirements of the cells can be attested *in vivo* by the high capillary density observed in the mammalian myocardium, actually almost every cardiomyocyte has a neighbor capillary in order to facilitate an efficient mass transfer, since the diffusion of a given factor is inversely proportional to the square of distance the factor has to travel [59]. In fact, the intercapillary distance observed in the mammalian myocardium is as tiny as 15-50 µm [59]. So, in theory, any 3D-cardiac tissue construct that exceeds these dimensions in any aspect should be vascularized to ensure its long term-survival and efficient physiological activity, being this the current limitation for scaling-up tissues *in vitro*.

5. The Vascular System

5.1. Endothelial Organization in the Heart

Endothelial cells are present in the three layers of the human heart wall (endocardium, myocardium and epicardium), specifically, they arise from two different classes: cardiac endothelial cells that form the myocardial capillaries (Myo Cap E) and the endocardium (EE) and vascular endothelial cells (VE) that contribute to the coronary vasculature (arteries and veins) at the epicardium and to smaller intramyocardial coronary vasculature, as well (Figure 14) [11][60].

In a general morphological description, endothelial cells are usually flat cells with a central nucleus and present about 1 to 2 µm of thickness and 10 to 20 µm of diameter [61].

The vascular endothelial cells are not in direct contact with cardiomyocytes, only indirectly contributing to the cardiac function by controlling the coronary blood supply to the myocardium mainly through changes in the coronary vasomotricity [60].

On the other hand, the cardiac endothelial cells are in direct contact with the adjacent cardiomyocytes and influence several cardiac parameters such as hypertrophy, contractility, metabolic activity and rhythmicity through several paracrine signaling mechanisms [11][60].

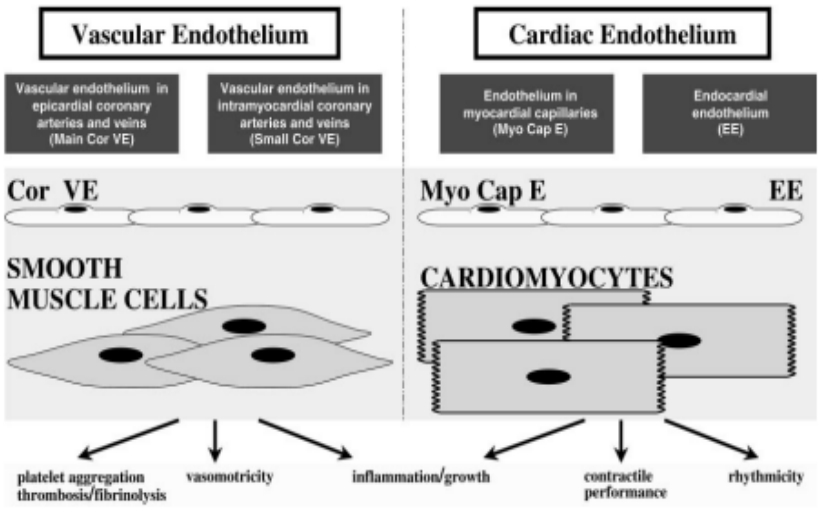

Figure 14: Schematic representation of the organization of endothelial cells in the human heart.
Left picture: The epicardial and intramyocardial coronary vascular endothelial cells (Cor VE) only influence the myocardium indirectly by controlling the myocardial blood supply. **Right picture:** Contrary to the Cor VE, the myocardial cardiac endothelial cells (Myo Cap E) and the endocardial endothelial cells (EE) directly influence the myocardium activity by signaling mechanisms trade with the adjacent cardiomyocytes that affect the cardiac growth and hypertrophy, contractile function and rhythmicity. Adapted from [60].

5.1.1. Endothelial-Cardiomyocyte Interaction

Like previously mentioned, cardiac endothelial cells are in close contact with cardiomyocytes (intercapillary distance in human myocardium around 15-50 µm), not only just to ensure an efficient physiological transport of nutrients and oxygen as well the essential removal of cellular waste, but also to allow a local communication between the cardiomyocytes and the endothelial cells through several paracrine signaling [59].

Although further studies should be performed in order to fully understand the cross-talk mechanisms between cardiomyocytes and cardiac endothelial cells, it is already known that endothelial cells secrete several mediators that influence the cardiomyocyte development (e.g. neuregulin growth factor, platelet-derived growth factor subunit B (PDGF-B) and neurofibromatosis type I (NF1)), survival (e.g. neuregulin and PDGF-B) and contraction (e.g. nitric oxide (NO) and endothelin 1 (ET-1)). Likewise, cardiomyocytes also promote the endothelial cell survival and assembly through the release of other mediators mainly angiogenic factors, like the vascular endothelial growth factor A (VEGF-A) and angiopoietin-1 (ANG-1) (Figure 15).

Beyond these paracrine signaling, autocrine signaling between cardiomyocyte-cardiomyocyte and endothelial cell-endothelial cell is also involved in the development of a normal cardiac function through complex mechanisms, some of them not completely understood (Figure 15) [11][59].

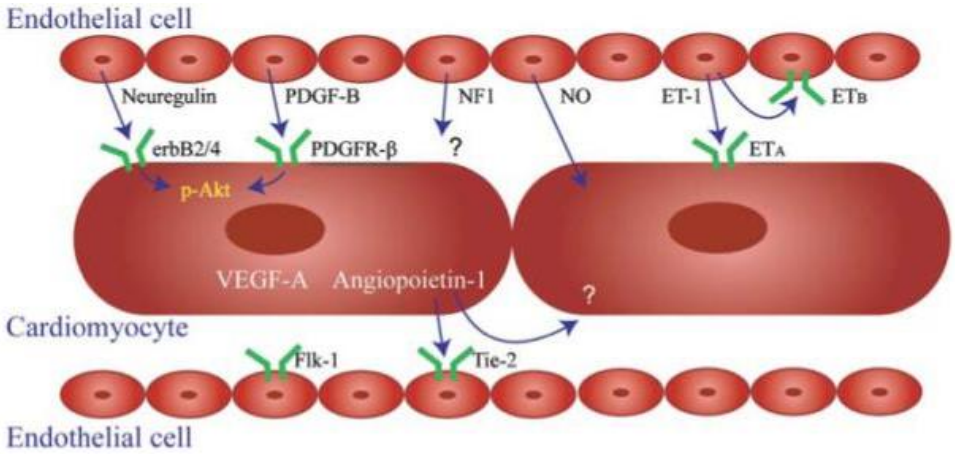

Figure 15: Schematic illustration of the endothelial-cardiomyocyte cross-talk through several paracrine and autocrine signaling mechanisms.
Endothelial cells secrete signaling mediators that control cardiomyocyte development (e.g. neuregulin, PDGF-B and NF1), survival (e.g. neuregulin and PDGF-B) and contraction (e.g. NO and ET-1); whereas cardiomyocytes secrete angiogenic mediators (e.g. VEGF-A and angiopoietin-1) that influence the ECs survival and assembly. Autocrine signaling involved between cardiomyocytes (possibly through the angiopoietin-1 mediator) and endothelial cells (e.g. through the mediator ET-1) also influences the development of a normal cardiac function. Adapted from [59].

5.2. Blood vessels: Formation and Assembly

All blood vessels, including arteries, veins and capillaries, are composed of three sub-layers: an innermost layer that is lined by endothelial cells, a middle layer composed of a large population of well-organized smooth muscle cells (SMCs) and an outermost layer mainly composed of extracellular matrix and fibroblasts [62].

In early embryogenesis, vascular progenitor cells from the mesoderm layer (angioblasts) coalescence with each other forming small cell clusters (called blood islands) [63]. In these islands, the peripheral cells differentiate into endothelial cells and the core cells differentiate into blood cells, in a process designated by vasculogenesis [64]. After the formation of a primary network, that happens due to the rearrangement of the cells, they start producing matrix-degrading proteases that degrade their surrounding extracellular matrix, allowing them to escape from the network walls and proliferate into the surrounding matrix to form new vessels [62][63]. Endothelial cells also secrete factors (like the transforming growth factor beta 1 (TGF-β1)) that recruit mural cells (pericytes in case of smaller vessels and smooth muscle cells in case of larger vessels) that start producing extracellular matrix to stabilize the network [63]. After the angiogenic process (angiogenesis), pro-angiogenic factors (e.g. acidic fibroblast growth factor (FGF) and VEGF) are released from fibroblasts in order to direct the migration and sprouting of the endothelial cells (Figure 16) [63]. After the growth and proliferation of the newly formed vessels, they link to existing neighboring vessels through a process called anastomosis [63].

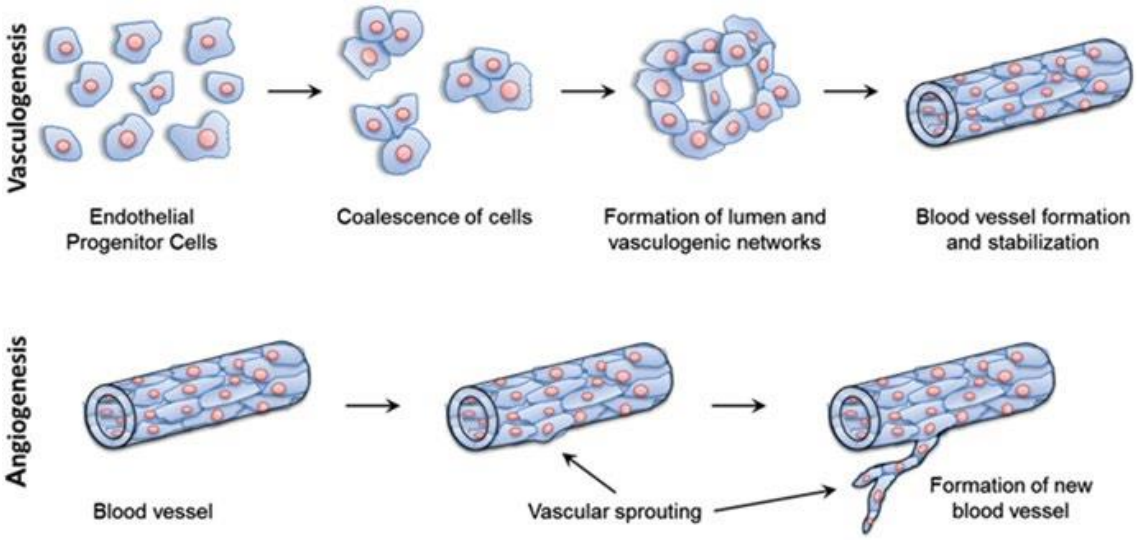

Figure 16: Schematic illustration of the blood vessel formation via vasculogenisis and angiogenesis. The vasculogenisis corresponds to the spontaneous process in which endothelial progenitor cells proliferate and form lumen structures that lately will develop in blood vessels. After the formation of a primary network, new blood vessels are formed from these pre-existing ones through a vascular sprouting phenomena, designated as angiogenesis. Adapted from [62].

6. Human Endothelial Models

6.1. Sources of Human Endothelial Cells

The layer of endothelial cells that lines the interior surface of blood vessels (endothelium) is highly influenced by the extracellular microenvironment of its native organ [65]. Due to this influence, endothelial cells located in different tissues display different phenotypes, giving rise to a structural and functional heterogeneity between different types of endothelial cells [65].

Human umbilical vein endothelial cells (HUVECs), cells derived from the endothelium of veins from the umbilical cord, are among one of the most popular models for vasculature studies *in vitro*, since they are easy to obtain and handle and display a high proliferative rate in culture [65][66]. However, the use of HUVECs as a universal endothelial model should be taken carefully, since, like aforementioned, the expression profile and functional responses from HUVECs varies from other endothelial cells types with different vascular origins [65].

On other hand, bone marrow-derived endothelial progenitor cells differentiated towards endothelial cells and human induced pluripotent stem cell-derived endothelial cells (hiPSC-ECs) present several endothelial surface markers, as well physiological functions of native ECs, being suitable to be used as better *in vitro* models [65]. These stem cell sources can provide specific ECs phenotypes and valuable information regarding the key intervenient mechanisms and molecules involved in each specific endothelial cell type.

6.2. Differentiation of Stem Cells towards Endothelial Cells

Bone marrow-derived circulating endothelial progenitor cells (BM-EPCs), display similar properties to embryonic angioblasts, including the potential to differentiate into mature endothelial cells and further involvence in the postnatal neovascularization process [67]. BM-EPCs can be isolated for selection for either the CD34 or CD133 markers [65] and can be induced to differentiate towards endothelial cells by stimulation with VEGF through still unclear mechanisms, like reported, for instance, by Li et al. (2017) [68].

Human induced pluripotent stem cells (hiPSC) can also be differentiated into endothelial cells when cultured either in a growth factor cocktail (with VEGF and FGF) or on a feeder layer of mouse fibroblasts followed by the purification of the obtained cells by flow cytometry, like reported, for instance, by Lin et al. (2012) [69] and Taura et al. (2009) [70], respectively. Afterwards, endothelial cells are often maintained in surfaces coated with fibronectin, since this protein promotes the endothelial adhesion, growth and spreading *in vitro* [71], and using culture mediums containing VEGF and SB, since SB is a synthetic molecule that blocks the transforming growth factor-beta (TGF-β) and the activin activity, known endothelial inhibitors *in vitro*, facilitating the proliferation and sheet formation of the hPSC-derived endothelial cells [72]; and the VEGF is the most important regulator of blood vessel formation *in vivo*, being an essential factor for promoting vasculogenesis and angiogenesis *in vitro*, as well [73].

7. Cardiac Tissue Vascularization

To accomplish the goal of cardiac vascularization in 3D engineered tissue constructs, several solutions have been raised in the last few years. Some approaches are more biological-based, relying on the induction and guidance of the endogenous ability of assembly of blood vessels; while other approaches are more engineered-based including the direct generation of microvasculature through a conjugation of microfluidic techniques and tissue engineering approaches, mainly [74][75].

The more biological-based strategies can be cataloged in two major types: co-culture systems with growth factors induction and bioactive scaffolds [74]; whereby the more engineered-based techniques, also designated as microelectromechanical systems (MEMS)-related approaches, can be divided into three major categories: microfluidics systems using synthetic polymers, biodegradable microfluidics and modular tissue assembly [74]. In particular, cardiac cell sheets systems are in the edge between the biological-based and engineered-based techniques.

7.1. Co-culture Systems with Growth Factors Induction

Strategies involving standard co-culture systems of cardiomyocytes and endothelial cells highly rely on the intrinsic communication pathways that are established between these two types of cells, specifically through cell-cell interactions and diffusion of signaling molecules (growth factor delivery), to promote the growth of microvasculature [75][76]. For instance, cardiomyocytes secrete the vascular endothelial

growth factor (VEGF) which is one of the driving pro-angiogenic factors involved *in vivo* in the formation of vessels.

The endothelial cells can be simply mixed with cardiomyocytes in culture or can be introduced via 3D cellular spheroids [74]. These endothelial cell spheroids are able to produce spontaneously capillary-like sprouts, particularly in the presence of angiogenic factors externally supplemented to the culture or in co-culture with fibroblasts, mimicking adequately the *in vivo* angiogenesis process [74]. Beyond these spheroid cultures, standard co-cultures of endothelial cells are also efficient in promoting spontaneous formation of tubular structures in the presence of the required growth factors [74]. These communication pathways are also highly beneficial for the cardiomyocytes, since these co-culture systems also contribute in large scale to the enhancement of cardiomyocytes survival and spatial organization, and consequently maturation *in vitro* (Figure 17), like reported by Narmoneva et al. (2004), for instance [77]. The major drawback of these systems is related to their lack of mechanical support and guidance that culminates in a random vascular network without any specific special organization [74].

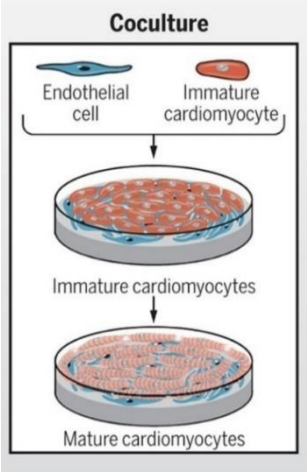

Figure 17: Schematic illustration of a method to generate mature hPSC-derived cardiomyocytes (CMs).
Morphological and physiological characteristics of hPSC-derived CMs greatly resemble those of fetal CMs, instead of those of adult CMs. Coculture with non-myocyte cells, especially endothelial cells, can drive hPSC-derived CMs towards a more mature adult phenotype, through several signaling mechanisms. Adapted from [78].

7.2. Cardiac Cell Sheet Systems

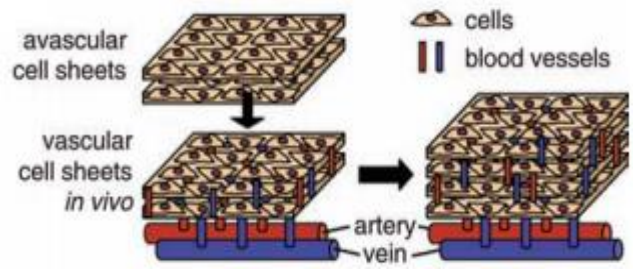

Figure 18: Schematic illustration of a cardiac cell sheet system.
Contiguous cell sheets, composed of cardiomyocytes and endothelial cells, are stacked together and vascularized upon direct and adjacent implantation into host arteries and veins. Endothelial cells from the stack are able to connect to the host vascular bed through points of anastomosis and form lumen structures that can be perfused. Thicker tissues can be built up afterwards through the overlay of more avascular cardiac sheets for vascularization. Adapted from [74].

Cell sheet systems or *in vivo* systems consist in confluent cardiac cell sheets, co-cultured with endothelial cells, that are grown and then stacked together to form thicker tissues; the stack is then vascularized *in vivo* through its adjacent transplantation to host arteries and veins (Figure 18) [74]. By this direct transplantation over the host arteries and veins, points of anastomosis are incorporated into the cardiac stack that enable its connection to the host blood vessels [74]. As soon as this connection occurs, vascular blood flow from the host

body immediately supplies the cardiac stack with the needed oxygen and nutrients, as well as waste removal, ensuring its prolonged functionality and survival [74]. Thicker tissues can be then assembled by the overlap of new cardiac sheets, that are then vascularized through the same process but this time by establishing points of anastomosis with the initial vascularized stack [74].

For instance, Sekine et al. (2013) overlaid triple-layer neonatal rat cardiac sheets, produced from co-culture with endothelial cells, on top of a resected rat femoral tissue with a perfusable artery and vein (vascular bed) [79]. The authors were able to observe the connection of the endothelial cells, present in the cardiac sheets, to the capillaries, present in the host vascular bed, and the formation of tubular structures that could be perfused afterwards; thus creating perfusable blood vessels [79]. The cardiac cell sheets were able to survive through the media supplied through the new vessels formed *in vitro* [79].

7.3. Bioactive scaffolds

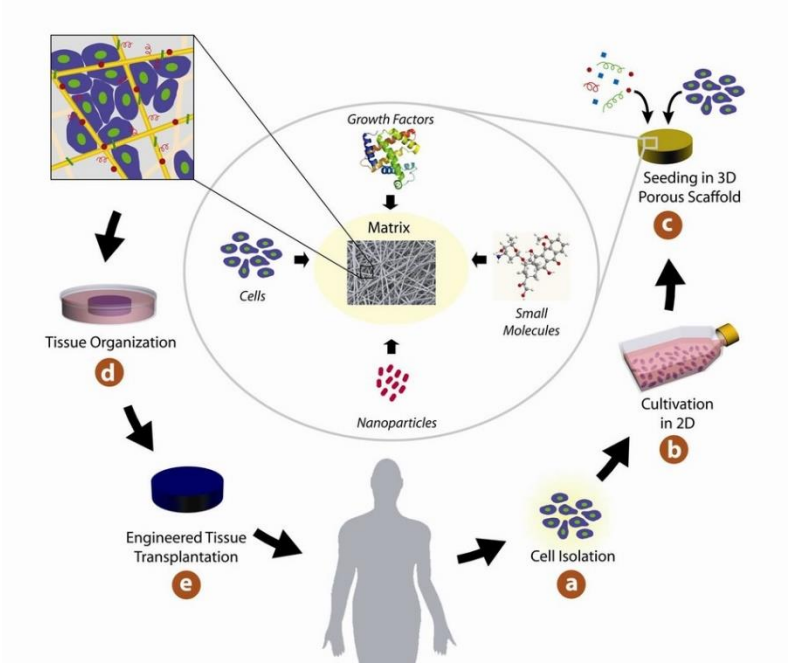

Figure 19: Schematic illustration of a bioactive scaffold approach. **a)** Cells are isolated from the patient; **b)** The cells are cultured *in vitro* using two-dimensional standard surfaces to enable an efficient cell expansion; **c)** The cells are then seeded in three-dimensional porous scaffolds that can be loaded or coupled with growth factors, small molecules and micro and/or nanoparticles to promote cell proliferation and differentiation. **d)** The cellular scaffolds are ultimately cultivated in bioreactors to provide optimal conditions for cell organization into a functional tissue; **e)** After the production of a functional tissue, the construct can be transplanted into the patient to restore the defective function. Adapted from [80].

Scaffold functionalization or bioactive scaffolds consist in scaffolds, natural or synthetic, that are loaded or chemically coupled with pro-angiogenic factors, usually with VEGF and the basic fibroblast growth factor (bFGF) [74]. This approach aims to mimic the *in vivo* situation, since after the growth factors being secreted, they associate with the extracellular matrix in order to stabilize their conformation as well to protect themselves from proteolytic digestions [74]. Basically, in this approach vascularized cardiac tissues are generated by seeding cardiomyocytes, endothelial cells (and fibroblasts) onto these scaffolds, preferentially composed of natural ECM proteins (Figure 19). The timing and the ability to direct the progressive release of these growth factors (e.g. using drug-load microspheres) controls the degree of neovascularization within the cardiac tissue [74].

These techniques may also be applied to hydrogels, like for instance, Hao et al. (2007) reported the use of alginate hydrogels to differentially release VEGF and other angiogenic factors that efficiently promoted the growth of mature vessels and enhanced cardiac function in rat infarcted hearts [81].

Due to the high dependence on endogenous mechanisms regarding cell response (e.g. endothelial cell migration, proliferation, formation of capillary-like structures) to vascularize the tissue, these techniques are not well controllable, similar to what happens with the standard co-culture systems [74]. Nevertheless, cues can be applied to the scaffold design like porous microgrooves that contribute to the vascular cell alignment instead of the production of random organizations as in the standard co-culture systems [74].

7.4. Modular Tissue Assembly

Another emerging technique is the modular tissue assembly approach that consists in microtissues (cells-embedded in a hydrogel), coated with endothelial cells (ECs), that are packed in a mold or tube to form a large macrotissue, with an endothelialized interstitial space for media perfusion (Figure 20) [75]. This approach has some advantages regarding other biological-based methods, namely the quickness of assembly the vascular network into the tissue and the feasibility of scaling-up the technique [75]. However, this technique faces a major challenge concerning cardiovascular tissues due to the fact that the module arrangement in microtissues, physiologically isolated from each other by the endothelial cell coating, can be problematic to allow the formation of a synchronous beating macroscopic tissue [75]. Functional contractile cardiac tissues rely on tiny intercellular junctions between cardiomyocytes, to ensure the electrical signal propagation through the entire tissue, that are considerably separated in this approach specifically between microtissues [75].

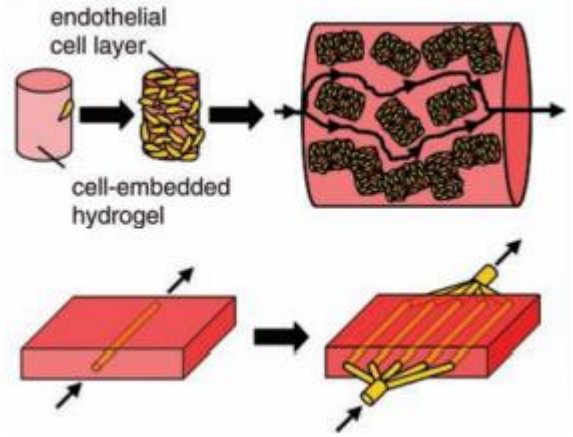

Figure 20: Schematic illustration of a modular tissue assembly approach.
Microtissues, composed of cardiac cell-embedded hydrogels, are covered with an endothelial cell layer. Several covered microtissues are then assembled together in a mold to form a vascularized macrotissue under perfusion. Adapted from [74].

Nevertheless, for instance, Leung et al. (2010) reported the use of a successful modular tissue engineering approach to create functional cardiac tissue [82]. The authors seeded rat aortic endothelial cells (RAEC) onto micromodules, made of collagen supplemented with Matrigel, with embedded cardiomyocyte-enriched neonatal rat heart cells [82]. The micromodules were then assembled into a contractile sheet-like construct that was excitable when exposed to external field stimulation, representing the viability of producing functional cardiac tissues with this type of approach [82].

7.5. Microfluidic Systems

Microfluidic techniques enable the formation of vascular tree-like organizations in synthetic (e.g. poly(dimethylsiloxane) (PDMS)) or biodegradable polymers (e.g. poly(glycerol sebacate) (PGS)) that can be seeded with endothelial cells in order to allow the *in situ* formation of primary vasculatures [74].

7.5.1. Synthetic Polymers

Considering the synthetic polymers, the most used approach consists in the generation of negative molds of the desired vascular pattern that will lately be used as molding templates for the chosen synthetic polymer (usually, PDMS), in a process called replica molding (Figure 21) [74]. The intended features in the negative mold can be engraved with a micron-scale precision through plasma etching or lithographic techniques [74], micromilling and microprinting techniques, among others. After the production of the positive molding template, it can finally be perfused and endotheliazed to give rise to the formation of a microvasculature in a controlled microenvironment [74].

The vascular pattern is designed to mimic the native *in vivo* environment by using relevant conformational and geometrical aspects to the tissue in question, in order to give rise to more biological significant results, since cultivated cells in the absence of their native environment, tend to lose their specific tissue physiology [83]. For this ability, this kind of technologies can also be referred as "organ-on-chip platforms". For example, Borenstein et al. (2002) reported the fabrication of vascular network templates (negative mold) by silicon etching that were then molded in PDMS, to form the vascular network, in which were seeded endothelial cells [84]; this approach was one of the first to be reported regarding the use of synthetic polymers.

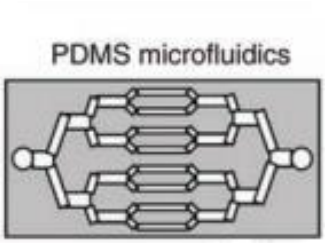

Figure 21: Example of a microelectromechanical-system (MEMS) related approach. PDMS microfluidics allows the creation of vascular tree-like organization within this polymer. Endothelial cells can be then seeded in these features, guiding the vasculogenesis and angiogenesis process. Adapted from [74].

<u>Comparison Between Synthetic Polymers</u>

The replica molding process is not suitable for glass surfaces due to their rigid properties, whereby the fabrication of glass-based microfluidic devices has to be made out of fused silica, turning the process expensive and highly complex in terms of hardware use.

However, despite fabricating PDMS microfluidics devices being a relatively simple and inexpensive process, there are several drawbacks linked to this polymer. Regardless of PDMS being an optically clear polymer, it can easily include air bubbles during its fabrication that may scatter the light [85], that along with its soft composition, that leads to elastic deformations when studying flow and pressure rates [86] and propensity to swell, when its brought in contact with commonly use chemicals [85], have been limiting its intended use in several microfluidic applications. Along with that, for cell culturing purposes, its poor cell adhesion due to its high surface hydrophobicity [87], and its adsorption of small compounds as drugs that impact the drug bioavailability on its surface, limits its broad use for drug testing purposes

[88]. In order to overcome all these limitations, the use of glass for fabricating microfluidic devices has been gaining attention due to its optimal optical characteristics, namely its high transparency that allows high-resolution imaging, its resistance to several solvents allowing its easy cleaning and consequently reuse, dimensional stability and low auto-fluorescence. Additionally, glass presents a well-understood surface chemistry [89], which is a relevant knowledge when performing drug testing assays, as well as a good cell adhesion [90], representing a gold standard for several applications.

7.5.2. Biodegradable Microfluidics

The demand for biodegradable microfluidics arises from the discovery of biocompatibility problems associated with synthetic and non-biodegradable materials, such as the PDMS and silicone polymers [74]. In order to try to overcome these problems, elastomers such as the poly(glycerol sebacate) (PGS), which are biocompatible and biodegradable, started being explored to be used in the vascular tissue engineering field [74].

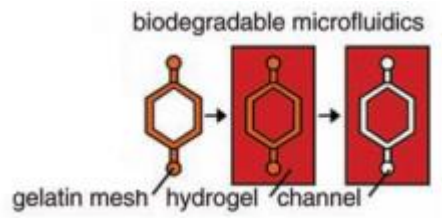

Figure 22: Example of another microelectromechanical-system (MEMS) related approach.
Biodegradable microfluidics allows the creation of vascular tree-like organization within biodegradable polymers. For instance, sacrificial materials (e.g. gelatin meshes) are used to leave interconnected free grooves in cellularized hydrogels. These grooves or channels are then used to seed the endothelial cells. Adapted from [74].

In this type of approach, the microfluidic devices are produced using similar techniques as the ones employed in the synthetic polymers, with the molding templates being produced from negative molds [74]. For obtaining the molding template, the negative mold is coated with a surface coating material followed by the deposition of the biodegradable polymer. Afterwards, the coating material is sacrificially removed to enable the intact release of the molded polymer layer (Figure 22) [74]. Several molded polymer layers can be bonded together by physical interactions and curing steps under vacuum, in order to enable the formation of complex vascular templates [74].

For instance, Golden et al. (2007) reported the use of a biodegradable microfluidic approach that relies in having a cellularized hydrogel that is molded from a vascular network of micropatterned meshes of gelatin (negative mold) [91]. The gelatin is then melted (sacrificial material) in order to leave behind interconnected channels in the hydrogel that can be used to seed the endothelial cells [91]. This approach can easily be applied to the cardiac field by embedding cardiomyocytes in the hydrogel.

II. Project Motivations

Cardiovascular diseases, besides representing one of the major economic burden on health care systems, are among the leading causes of death and disability worldwide. Given the magnitude of the problem, the number of transplantable hearts or efficient pumping assisting devices is not sufficient to cover all the heart disease population; and the drugs developed so far are meant to alleviate the events after heart failure instead of to restore the native function of the myocardium, acting as a palliative treatment. Taken into account the continuing occurrence of cardiovascular diseases and the emergent demand for new cell-based therapies, to repair, improve or replace the defective heart, and for new cardiac tissue-analogous models to enable the development of novel drugs to be used as palliative and expectantly as curative therapies for heart failure events, in the last few decades, the scientific community has been striving for discovering new tissue engineering methods that can give answer to the reported needs. However, the preparation of engineered 3D cardiac tissues, that closely resemble the native environment of the human heart, is hampered by the lack of an intrinsic vascular system able to nourish such engineered constructs. In fact, most of the engineered cardiac tissues either are established with dimensions that go beyond the practical perfusion limits, which compromises their long-term survival and functionality, or are established *in vivo* using a host vasculature to induce the formation of natural vascular-like networks into the construct, which limits their envisioned regenerative applications. Along with that, since most of these tissue-like systems created *in vitro* are not set for enabling the inclusion of a vascular network as previously reported, they are not able to support the scaling up of the developing engineered construct to physiological increasingly relevant sizes. And, ultimately, efficient differentiation and culturing protocols towards the obtention of mature adult-like cardiomyocytes and endothelial cells descendant from human cell lines are still lacking, since a considerable amount of the current established cardiac tissue engineering approaches have only been reported using animal models, that as expectable, comprise several genomic and physiological differences that can contribute for a failing prediction of human responses and outcomes.

As an attempt to provide answer to these limitations, this project was envisioned to focus in the development of a novel fluidic device able to support the co-culture between fibrin-based cardiac tissues and endothelial cells, both derived from human sources, aiming to further promote the formation *in vitro* of a primary vascular network throughout the cardiac tissue, enabling its prolonged maintenance, without depending on body-in approaches. Optimization regarding device fabrication and culturing conditions were also implemented during this project. The fluidic system was also projected to be compatible with the most common microscopy imaging techniques and to easily allow the scaling up of the bioengineered construct when intended. The outlined objective regarding the establishment of an efficient fluidic device for co-culturing cardiomyocytes and endothelial cells was successfully accomplished, even enabling the migration of the endothelial cells into the tissues, highlighting the important ground work provided by this project regarding the pursuit of innovative vascularization strategies *in vitro*.

III. Materials and Methods

1. Cell Culture

In all of the following procedures, the cells were kept in culture in tissue culture incubators (Sanyo) with humidified atmospheres and 5% CO_2 at 37°C.

1.1. Maintenance of Human Embryonic Stem Cells (hESCs)

The human embryonic stem cell line HES3-NKX2-5-eGFP, formerly described by Elliot et al. (2011) [92], in which a sequence encoding an enhanced green fluorescent protein (eGFP) was introduced into the locus of the cardiac transcription factor NKX2-5 to enable the identification and selection of hESC-derived cardiomyocytes (hESC-CMs), was used to generate cardiomyocytes *in vitro*. A fusion protein (α-actinin-mRuby), consisting of the sarcomeric α-actinin and a red fluorescent protein (mRuby), was also overexpressed in this stem cell line, through Clustered Regularly Interspaced Short Palindromic Repeats (CRISPR) mediated gene editing, to enable the observation and analysis of the sarcomere movement during the cardiomyocyte's contractile activity.

The HES3-NKX2-5-eGFP line was cultured and maintained in Essential 8™ medium (E8 medium, Life Technologies) on 6-well plates (Greiner) coated with vitronectin (Life Technologies). The protocol for coating 6-well plates with vitronectin is fully described in Appendix "Coating with Vitronectin".

The hESCs were passaged using ethylenediaminetetraacetic acid (EDTA, Life Technologies) and seeded at $1{,}7 \times 10^5$ cells/well on Mondays and at 1×10^5 cells/well on Thursdays. The medium was then refreshed on Mondays, Tuesdays, Thursdays and Fridays.

1.2. Monolayer Differentiation of hESCs towards Cardiomyocytes

One day before starting the differentiation protocol, between $2{,}2 \times 10^5$ to $2{,}5 \times 10^5$ cells/well were seeded in E8 medium and left incubating overnight.

The monolayer differentiation protocol was performed on a 6-well format coated with Matrigel (Corning), whose coating was performed as elucidated in Appendix "Coating with Matrigel".

In day 0 of differentiation, the hESCs were plated in Bovine Serum Albumin (BSA) Polyvinylalchohol Essentials Lipids (BPEL) medium [93] (Appendix "Preparation of the BPEL Medium") supplemented with 20 ng/mL of bone morphogenetic protein 4 (BMP4) (R&D Systems), 20 ng/mL of Activin A (Miltenyi) and 1,5 µM of CHIR99021 (Axon Medchem). On day 3, the medium was refreshed with BPEL medium together with 5 µM of XAV-939 (R&D Systems) and 50 µg/mL of Matrigel. At day 6 and 9 of differentiation, the medium was refreshed with fresh BPEL without any supplementation. After day 13 of differentiation, the cardiomyocytes could be dissociated and seeded for subsequent experiments.

1.3. Maintenance of hESC-derived Cardiomyocytes

On day 13 of differentiation, the medium was refreshed with a non-enriched glucose, cardiomyocyte (CM) medium supplemented with galactose (Gal) (Sigma-Aldrich®) and low insulin (LowIns), henceforth addressed as CM+Gal+LowIns (see Appendix "Preparation of the CM+Gal+LowIns Medium"). Long R3 insulin like-growth factor-1 (IGF-1) (Sigma-Aldrich®) and triiodothyronine hormone (T3 hormone) (Sigma-Aldrich®) were also added to this medium at a concentration of 100 ng/mL and 10 nM, respectively. Hereafter, the final formulated medium will be referred as CM+Gal+LowIns+IGF+T3 or equivalent.

The switch to this medium is driven by the fact that the T3 hormone, IGF and galactose are known positive effectors in promoting the *in vitro* maturation of cardiomyocytes into more adult-like cardiomyocytes, as already brought to analysis in the introductory remarks (see Section "Medium Formulations with Soluble Factors").

1.4. Dissociation of hESC-derived Cardiomyocytes

On day 16 of differentiation, the dissociation of the monolayer-derived cardiomyocytes was performed using a 1xTrypLE-Select (Gibco™, Life Technologies) solution for 10 minutes at 37°C. The dissociated cardiomyocytes were then suspended in CM+Gal+LowIns medium supplemented with 100 ng/mL of Long R3 IGF-1 (Sigma-Aldrich®), 100 nM of T3 hormone (Sigma-Aldrich®), 4,5 mM of glucose (Glc) (Sigma-Aldrich®) and 10% (v/v) of horse serum (HS) (Gibco™, Life Technologies). The aforementioned medium will be addressed as CM+Gal+LowIns+IGF+T3+Glc+HS or equivalent from this point forward.

The cardiomyocytes were placed in this medium since they will be use thereupon to generate the fibrin-based cardiac tissues and the supplementation with horse serum is crucial for their maintenance, as already stated in the introduction chapter (see Section "Methods for Engineering Heart Tissues"). The glucose concentration was set to 4,5 mM in order to recapitulate the physiological levels (around 5 mM) [94].

1.5. Generation of Fibrin-based Cardiac Tissues

To generate the fibrin-based cardiac tissues, firstly, the cell suspension in CM+Gal+LowIns+IGF+T3+Glc+HS medium, obtained from the dissociation step, was concentrated into the desired density to be used for the cardiac tissue (after optimization, 4×10^7 cells/mL).

After that, a reconstitution mixture was prepared on ice containing the following components: fibrinogen (1:10 dilution (v/v)) (Sigma-Aldrich®) (Appendix "Preparation of the Fibrinogen Stock"); Matrigel (1:10 dilution (v/v)); two times concentrated CM+Gal+LowIns medium (1:10 dilution (v/v)), named as 2xCM medium; aprotinin (1:100 dilution (v/v)) (Sigma-Aldrich®) (Appendix "Preparation of the Aprotinin Stock"); cell suspension (remaining volume to address the final volume of cardiac tissue in preparation) and thrombin (after optimization, a ratio of 1 µL of thrombin/150mL of final volume was used; this component

should be the last to be added since after its addition the polymerization reaction is immediately initiated) (Sigma-Aldrich®) (Appendix “Preparation of the Thrombin Stock”).

The 2xCM medium was used to restore the isotonic conditions of the medium, since the fibrinogen is dissolved in a saline solution (see Appendix “Preparation of the Fibrinogen Stock”).

1.6. Maintenance of hiPSC-derived Cardiac Endothelial Cells

HiPSC-derived cardiac endothelial cells, generated in house by a group’s collaborator, were cultured and maintained in BPEL medium supplemented with 50 ng/mL of VEGF (Miltenyi) and 5 µM of SB431542 (Tocris Bioscience), henceforth addressed as BPEL+VEGF+SB medium, in 6-well plates previously coated with fibronectin (Sigma-Aldrich®) (see Appendix “Coating with Fibronectin”).

The hiPSC-derived cardiac endothelial cells were passaged before reaching a high confluency level (approximately of 70%-80%) for 6-well plates previously coated with fibronectin using a seeding density of $1{,}5 \times 10^5$ cells/mL. The passage was performed using a 1xTrypLE-Select solution for 3 minutes at 37°C and the endothelial cells were only used from passage 1 to 3.

Depending on the culturing purpose, after each passage, the cells were left in BPEL+VEGF+SB medium (control) or in a combination of a BPEL and CM-derived medium named as BPEL+CM+VEGF+SB+IGF+HS (see Appendix “Preparation of the BPEL+CM+VEGF+SB+IGF+HS Medium”).

2. Fluidic Device

A novel fluidic device aiming to support the vascularization of hESC-derived fibrin-based cardiac tissues was projected and optimized along this project. Shortly, the designed fluidic device is comprised by three modules: an upper PDMS reservoir in where the endothelial cells can be plated, a middle triple-layered stack with several holes drilled along it where the fibrin-based cardiac tissues will be seeded; and a layer of PDMS with engraved channels that in a general way has the same purpose as the reservoir layer.

2.1. The Design

The envisioned fluidic device, aiming to combine the technology of multilayered systems with microfluidic techniques, is, to our best knowledge, completely brand-new and novel, hence its design and final dimensions were progressively adapted and optimized along the project according to the obtained results (see Chapter “Results and Discussion”).

2.2. The Fabrication

2.2.1. Triple-layered Stack Fabrication

For economical and practical motivations, commercial 76 x 26 x 1 (mm) microscope glass slides (Thermo Scientific Menzel™) were used to produce the first (top) layer of the triple-layered glass stacks, while 24 x 50 x 0,15 (mm) microscope glass coverslips (Thermo Scientific Menzel™) were used to produce the second (middle) and third (bottom) layer of the designed glass stack. The dimensions of the glass slides were adapted to the dimensions of the glass coverslips in parallel with the drilling process.

In its turn, plastic (vinyl) coverslips (Fisherbrand™) presenting 22 x 22 x 0,2 (mm) as external dimensions were chosen as raw materials for the second and third layers of the plastic stack; while casted poly(methyl methacrylate) (PMMA) slides presenting 2 mm of thickness were chosen to be used as the first layer of the plastic stack and cut, using a laser-cutting machine (Speedy 400™, Trotec), to the external dimensions of the plastic coverslips (22 x 22 (mm)).

Drawings from SolidWorks2017®, with the design and correspondent measurements of the three layers that compose the triple-layered glass stack, were delivered to a collaborator at the Techno Center for Education and Research (TCO), University of Twente (The Netherlands), that kindly provided the working glass layers. The layers that compose the triple-layered plastic stack were handled and drilled by the author using regular drillers with appropriate steel bits according to the drawings projected for these stacks.

2.2.2. Channel Layer Fabrication

The negative mold of the channels was engraved in a PMMA material (8 mm thick) using micromilling technology. Micromilling is a subtractive method in which small pieces of the initial block of material are progressively removed using a rotating mill that moves up, down and sideways in the material according to the file given as input to the machine with the drill bit path code. The machining of all the negative channels features was accomplished in a CNC-milling machine (Model 5410, Sherline Products Inc., Vista, CA) using micro tungsten carbide end mill drill bits with a diameter of 2 mm. A CAM plug-in available to the SolidWorks® (Autodesk HSMXpress) was used to translate the SolidWorks drawings into machine code (G-code).

The original model of the channels was afterwards produced in an injection molding system, in which the negative mold of the channels was hold together against another PMMA block with the same external dimensions, using a metal clamp as holding system. This auxiliary PMMA block has a 4 mm diameter hole that allows the injection of PDMS into the system through a syringe (BD plastipak). The PDMS was obtained by mixing the pre-polymer (PDMS base) and the curing agent (Sylgard 184 Silicone Elastomer Kit, Dow Corning®, Midland, MI, USA) in a 10:1 (w/w) ratio. The mixture was then degassed, previous to its injection in the molding system, in order to remove all the air bubbles. The system was then cured in an oven (Quincy Lab Inc., Model 10) at 67°C for at least 2 hours. After the curing step, the injection

molding system was opened and the PDMS channels were peeled off, covered with tape (Scotch®) to preserve the PDMS surface clean and cut into the desired dimensions.

2.2.3. Reservoir Fabrication

The reservoir layer was obtained by pouring PDMS to a petri dish (Greiner) up to a final height of approximately 0,2 mm of PDMS. Afterwards, the PDMS was cured in the oven at 67°C for at least 2 hours. After the curing step, the PDMS layer was peeled off the petri dish, covered with tape and cut to the desired dimensions followed by its punching with an adequate puncher (Robbins Instruments) in the intended positions.

2.3. The Assembly

In each set of experiments, the three layers that compose the triple-layered stack were always assembled first. Only afterwards, the PDMS surfaces (either the channels or the reservoir, depending on the purpose) were assembled to the triple-layered glass stack.

2.3.1. Triple-layered Stack Assembly

The assembly of both triple-layered stacks, either produced from glass or plastic, was accomplished using two different assembling agents depending on the stage of the project.

Using a 10% Gelatin Solution

The assembly of the triple-layered stack was initially performed using an autoclaved 10% (w/v) gelatin solution in Dulbecco's phosphate-buffered saline (1xDPBS) (Gibco™, Life Technologies) from porcine skin powder (Sigma Aldrich®). The choice of gelatin was motivated by its biocompatibility and easy-handling that simplified the assembly process to pipetting around 150 µL of gelatin solution on one layer followed by the aligned overlap of the second layer under a sterile microscope (Leica). The two layers were then gently pushed against each other, followed by the aspiration of the gelatin from the holes using a suitable vacuum cleaner (Cardinal Health) in order to keep them open. Afterwards, the ongoing assembly was placed in the fridge (Haier) at 4°C for at least 15 minutes, so that the gelatin could solidify to allow the overlap of the third layer without affecting the alignment of the layers already laid.

Using the Norland Optical Adhesive 81 (NOA81)

Afterwards, the assembly of the triple-layered stack was carried out using NOA81 (Norland Products Inc.), which is a promising ultraviolet (UV)-curable and low-cost optical adhesive that has been used on several microfluidic applications [95]. NOA81 is sensitive to wavelengths between 320 to 380 nm with a peak sensitivity around 365 nm and can be cured using a powerful UV curing system with a full power of 2,5 W/cm^2 for 5 to 10 seconds at 365 nm or equivalent [96]. Remarkably, after being properly cured, NOA81 is no longer toxic for cells, affording the possibility of being used for cell culturing purposes [95].

To perform the assembly of the triple-layered stack using the NOA81, around 100 µL of this optical adhesive were spread on top of the intended layer using an oral swab to allow the production of a really thin and uniform top layer of NOA81. Afterwards, the second layer was aligned and overlapped over the first and the NOA81 trapped inside the holes was aspirated using the vacuum cleaner. To cure the NOA81, an UV-gun with a full power of $400\ mW/cm^2$ was used 7 times in the maximum intensity for at least 10 seconds in each side of the ongoing assembly in order to meet the curing requirements. After that, the third layer was overlaid using the same approach. Finally, after optimization and to ensure an aggressive curing step, the assembly was left overnight inside a beaker (VWR) full of deionized water (Milli-Q®, Merck Millipore), agitated by a magnetic stirrer bar, in order to ensure that any remaining of liquid NOA81, and therefore non-cured, could be released from the assembly before its use for cell culture.

2.3.2. Channel Assembly to Triple-layered Glass Stacks

To assemble the channel layer to the bottom of the triple-layered glass stack, a plasma treatment process was used to covalently bond the glass to the PDMS surface. The plasma treatment process can be used not only to bond the two modules, but also to sterilize and surface functionalize the PDMS channels and the triple-layered glass stack, by turning their interior walls temporarily hydrophilic through the insertion of polar groups on both surfaces [97]. For that, the PDMS channels were place inside of a plasma cleaner (PDC-002-HP, Harrick Plasma), faced up, along with the triple-layered glass stack that was also placed with the intended surface faced up. This configuration exposes both modules to the reactive species of the air plasma, created by a radio frequency generator, at a pressure of 500 mTorr and for about 45 seconds. The plasma treatment introduces polar silanol groups (Si-OH) in the PDMS surface and OH groups in the glass surface, allowing the irreversible bonding of the surfaces by Si-O-Si bonds, formed when the surfaces are brought together (Figure 23) [97]. Therefore, after the plasma treatment, the channels and the glass stack were bonded together by placing the channels facing the exposed glass layer and exerting a subtle pressure to enable their connection.

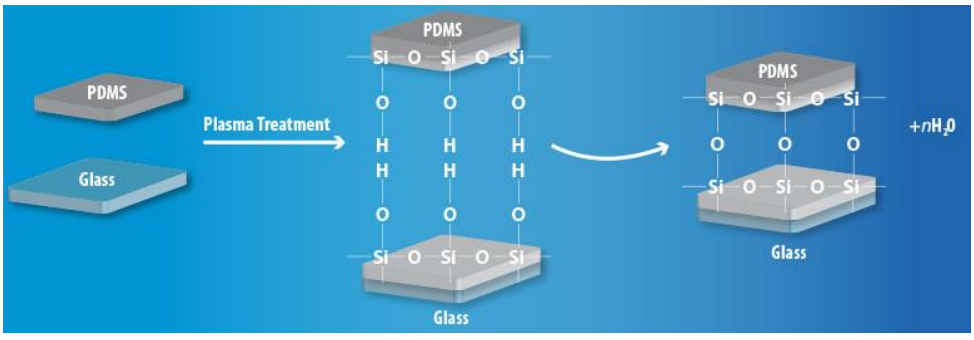

Figure 23: Schematic illustration of the plasma treatment process.
By exposing the glass and the PDMS surface to a reactive air plasma, polar groups are introduced in both surfaces (Si-OH groups in case of the PDMS and OH groups in case of the glass) at the expense of methyl groups (CxHy). When both surfaces are brought together, strong Si-O-Si covalent bonds are established between the two layers, enabling the irreversible bonding of these layers. Adapted from [97].

2.3.3. Reservoir Assembly to Triple-layered Glass Stacks

The reservoir was only assembled in the chip device when the purpose of the ongoing experiment was to seed hiPSC-derived cardiac endothelial cells on top of the fibrin-based cardiac tissues, otherwise the chip was used without containing the reservoir layer. The reservoir layer was bonded to the top of the triple-layered glass stack following the same approach described for bonding the channel layer to the glass stack (see Section “Channel Assembly to Triple-layered Glass Stacks”); since this module is also made of PDMS and is intended to be bonded to a glass surface, the plasma treatment principle can also be applied to this case.

2.4. Optimizing Conditions for Cell Culturing

2.4.1. Silane and Glutaraldehyde Functionalization

Apart from allowing the direct and irreversible bonding between glass and PDMS surfaces, the plasma treatment also contributes for reducing the hydrophobicity of these surfaces through the introduction of polar groups as already explained above (see Section “Channel Assembly to Triple-layered Glass Stacks”). Cell adhesion is highly favored by surface wettability, but the hydrophilicity conferred by the plasma treatment is only temporary since overtime partial or full hydrophobicity recovery is observed, which eventually can lead to the removal of cells from the PDMS surface [87][98].

To address this issue, a surface functionalization process using (3-aminopropyl)triethoxy silane (APTES) (Sigma-Aldrich®) and glutaraldehyde (GA) (Merck Millipore) was performed in the channels and reservoir to immobilize fibronectin on their walls (Figure 24); since fibronectin highly favors the adhesion of hiPSC-derived cardiac endothelial cells contributing for their survival and proliferation (see Introduction Section “Differentiation of Stem Cells towards Endothelial Cells”).

For that, right after the plasma treatment, and consequently after the bonding of the PDMS surfaces to the respective glass surfaces, the PDMS channels and reservoir were infused with a 3% (v/v) APTES solution in deionized water (Milli-Q®, Merck Millipore) and incubated for 5 minutes at room temperature (approximately, at 24°C). The APTES solution should be opened and closed under nitrogen flow, since APTES is very reactive with water; if it is open to air, it will react with water and it will be damaged quickly. After the incubation period, the PDMS surfaces were abundantly washed with ethanol 70% (v/v) (Azlon) and dried with an air gun. Then, the surfaces were filled with a 10% (v/v) GA solution in DPBS and incubated at room temperature for another 5 minutes, followed by the abundant rinsing with distilled water and drying with the air gun. Afterwards, the surfaces were coated with a fibronectin solution to promote the seeding of the endothelial cells and their adhesion on the protein layer through the inherent biocompatibility with ECM proteins and molecular recognition properties [87].

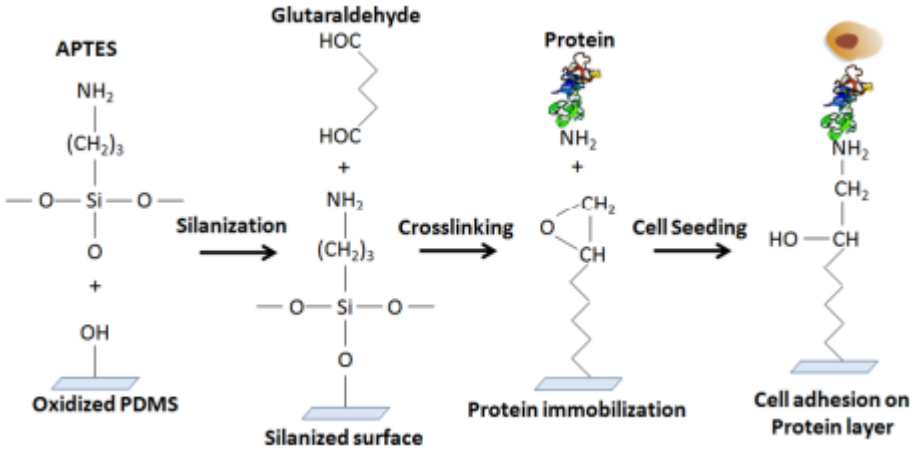

Figure 24: Schematic illustration of a surface chemical modification process of poly(dimethylsiloxane) for an enhanced cell adhesion on these surfaces.
Hydroxyl (OH) groups created in the plasma-activated PDMS surface are used to chemically react with the (3-aminopropyl)triethoxy silane (APTES), allowing its bonding to the oxidized PDMS surface. The free reactive amine group (NH2) present in the APTES molecule is used to react with the glutaraldehyde (GA) that in its turn, interacts and covalent binds to the fibronectin protein through its functional group CHO. The modified surface is highly efficient to promote the adhesion of cells like hiPSC-derived cardiac endothelial cells due to the fibronectin coating. Adapted from [87].

2.4.2. Practical Considerations

The resulting fluidic device was placed inside an open section (free of PDMS) of 60 mm x 34 mm created in a 90 mm standard petri dish filled with cured PDMS. This working concept, addressed from this point forward as shortened-volume petri dish, was adopted to minimize the amount of medium needed to cover all the chip in the end. The petri dish was previously sterilized using the aforementioned plasma treatment technology (see Section “Channel Assembly to Triple-layered Glass Stacks”) in the day before to its utilization. After the plasma treatment, the chip was placed inside the petri dish and, leaving the lid open, sterilized under the UV light of the laminar flow hood (Telstar) for at least 30 minutes. The chip was used for cell seeding purposes no longer than 1 hour after this procedure.

3. Cell Seeding in the Fluidic Device

3.1. Seeding the Fibrin-based Cardiac Tissues in Triple-layered Stacks

After a soft resuspension of the reconstitution mixture obtained in Section “Generation of Fibrin-based Cardiac Tissues”, 2 µL for glass stacks and 4 µL for plastic stacks of the prepared mixture were added to each intended space of the stack in a timeframe of 1 minute, corresponding to the period in which the newly formed fibrin is still accessible. The cellular tissue should be pipetted using a micropipette with a tip that allows its respective threading into each working space, therefore a P20 micropipette (Greiner Bio-One™) was used for the purpose. The plunger of the micropipette should only be pressed until the first downward position and only be released with the pipette already out of the working space to avoid the formation of air bubbles in the seeding tissue. Thereafter, the chip was allowed to rest for 10 minutes to allow the complete polymerization of the fibrin-based cardiac tissue without any disturbance.

Aftterwards, around 150 µL of CM+Gal+LowIns+T3+IGF+Glu+HS or BPEL+CM+VEGF+SB+IGF+HS medium, depending on the purpose of the ongoing experiment, and previously left overnight in the incubator to release all possible air bubbles, was slowly infused in each channel. The medium was carefully added to each channel in order to ensure that the liquid level in the inlets and outlets was never higher than the seeded tissues; otherwise the liquid would tend to flow in the direction of the configuration with lower height, ending up by disrupting the tissues. Afterwards, around 8 mL of the same medium infused in the channel was added to the shortened-volume petri dish in order to completely immerse the chip.

3.2. Seeding the hiPSC-derived Cardiac Endothelial Cells in the Channels

The endothelial cells were dissociated using the same dissociation protocol described in Section "Maintenance of hiPSC-derived Cardiac Endothelial Cells" for cell passaging. The dissociated endothelial cells were seeded at 5×10^5 cells/mL in the channels (value previously optimized) in BPEL+VEGF+SB or BPEL+CM+VEGF+SB+IGF+HS medium, depending on the state of progress of the project at the moment. Each channel was filled with approximately 150 µL of cell suspension, having in mind that before the seeding, the channels were coated with a fibronectin solution, for the stated reasons in Section "Silane and Glutaraldehyde Functionalization", that was aspirated immediately before seeding. The fluidic device was then incubated up-side down for around 2 hours to enable the seeding of the endothelial cells on top of the tissues, instead on the bottom of the channels, and then placed in its original position after the incubation period mentioned.

3.3. Seeding the hiPSC-derived Cardiac Endothelial Cells in the Reservoir

The hiPSC-derived cardiac endothelial cells were only seeded in the reservoir, that in its turn was only assembled in the fluidic device, when the purpose was to perform experiments regarding promoting vascularization in the fibrin-based cardiac tissues using top-bottom approaches and/or to allow the imaging of the fluidic device from a top perspective using the confocal microscope, due to the low thickness of the reservoir.

The dissociated endothelial cells were seeded at 5×10^5 cells/mL in the reservoir in BPEL+VEGF+SB or BPEL+CM+VEGF+SB+IGF+HS medium, according to the stage of the work. Each cavity of the reservoir was filled with 20 µL of the aforementioned cell suspension, while the remaining volume of the petri dish was also full either with BPEL+VEGF+SB or BPEL+CM+VEGF+SB+IGF+HS medium, in agreement with the medium present in the reservoir itself.

4. Medium Change during Operation of the Fluidic Device

The medium was partially changed every 7 days after the fibrin-based cardiac tissues were seeded in the fluidic device. To accomplish this, the petri dish medium (and reservoir medium, in case of its presence) was aspirated until just a thin layer of medium was on top of the seeded tissues, to prevent them from drying. Right after, the medium was changed from the channels by pipetting out the spent medium and infusing 150 µL of new medium. The refreshment of the fluidic device was only effected

partially, because the tissues were too small to justify a full change since they would never consume all the nutrients available in the medium as well filling it up with cellular waste; whereby a partial change would still ensure a viable cell growth and productivity.

5. Re-utilization of the Fluidic Device

Since the fabrication of the triple-layered glass stack is economically expensive and the chip assembly is also time-consuming, when needed, the fluidic devices were cleaned, functionalized and sterilized again to allow their re-utilization.

The cleaning step was initiated by the aspiration of all the medium present in the fluidic device, as well as the aspiration of the remaining cardiac tissues. After that, a 1% (w/v) Terg-A-Zyme® (Alconox, Inc.) solution was prepared in distilled water (Gibco™, Life Technologies) and used to dive the chip that was then left overnight in the solution. The Terg-A-Zyme® is an anionic detergent with a proteolytic enzyme suitable for the removal of tissues from glassware without leaving any interfering residues. In the next day, the chips were diped in a petri dish full of distilled water that was placed in a rotating platform (IKA) for at least 10 minutes. This process was repeated three times to ensure the complete removal of the Terg-A-Zyme® solution from all the surface of the material. Right before the utilization of the chip, the channels and reservoir (when being used) were once again functionalized (see Section “Silane and Glutaraldehyde Functionalization”); followed by the sterilization of the petri dish together with the fluidic device (already functionalized) as described in Section “Practical Considerations”.

The re-utilization of the chip was only possible when the fluidic device was assembled using the optical adhesive glue NOA81, since the Terg-A-Zyme® solution contains proteolytic enzymes that would degrade the gelatin content when using the gelatin solution for assembling the triple-layered stacks.

6. Microscopy

All the micrographs referring to bottom views, later shown in the Chapter “Results and Discussion”, were taken using an inverted microscope (Nikon Eclipse Ts2) connected to a computer (Dell) with the Nikon’s NiS Elements Software installed; whereas the micrographs concerning top views, also later shown in the Chapter “Results and Discussion”, were taken using a sterile upright microscope (Leica) and a microscope smartphone camera adaptor (Carson). Fluorescence micrographs were also taken using the inverted microscope or the confocal microscope (Nikon Confocal A1).

6.1. Cell Staining

Since the hiPSC-derived cardiac endothelial cells are not genetically fluorescently labeled, a cell tracking staining, Vybrant DiD® cell-labelling solution (Molecular Probes™), was added to the cell suspension before its seeding in the fluidic device according to the manufacturer’s protocol, to enable the analysis of both co-cultured cells. For that, the hiPSC-derived cardiac endothelial cells were dissociated and suspended at a density of 1×10^6 cells/mL in serum-free culture medium, specifically, in BPEL medium. Afterwards, 5 µL of the cell-labelling solution/mL of cell suspension were gently added. The cell

suspension was incubated for 20 minutes at 37°C followed by its centrifugation at 1500 rpm for 5 minutes, removal of the supernatant and resuspension of the cells in 1 mL of warm BPEL+CM+VEGF+SB+IGF+HS medium (at 37°C). The latter steps of washing were repeated two more times.

6.1.1. Cell Staining Probes

The fluorescent dye used for staining the endothelial cells was chosen so its emission spectrum could overlap minimally, or ideally not at all, the emission spectra of the two fluorescent reporter genes that are present in the cardiomyocytes cell line (eGFP and mRuby), in order to enable the easy distinction of their fluorescence signals. Since the eGFP has a maximum emission at 510 nm and the mRuby has a maximum emission at 605 nm, the best option would be a fluorescent dye with a maximum emission wavelength in the far-red spectrum region as the DiD® -labelling solution that has a maximum emission at 670 nm, as illustrated in Figure 25 [99][100]. In Figure 25, the mRuby is represented by the mCherry fluorescent protein, since the database of the SpectraViewer® does not include yet the mRuby protein; nevertheless both of these proteins have excitation and emission spectrums highly comparable, for instance, the maximum excitation for mCherry is at 587 nm and for mRuby is at 558 nm, and the maximum excitation is at 610 nm for mCherry and at 605 nm for mRuby [99][100].

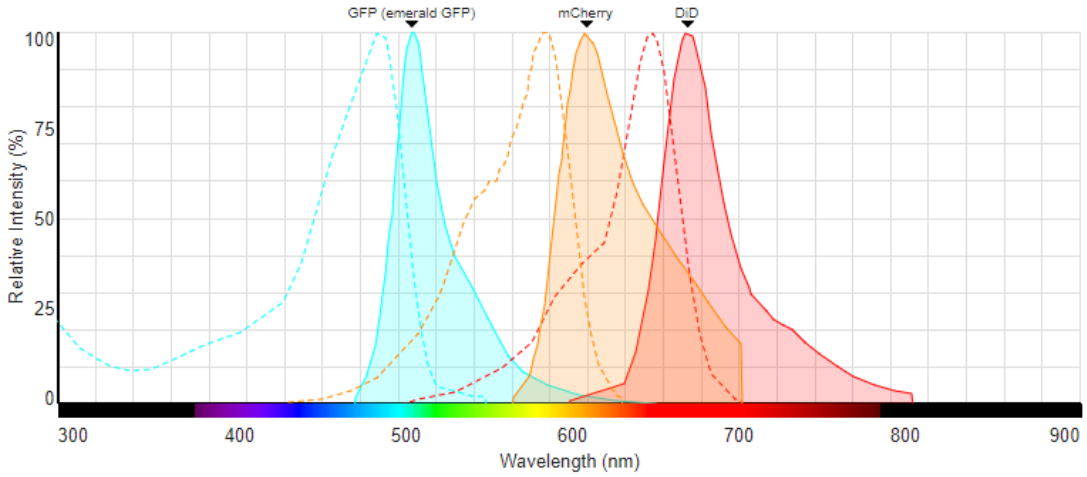

Figure 25: Fluorescent SpectraViewer® tool from ThermoFisher displaying the excitation and emission spectrums of the GFP, mCherry protein and DiD fluorescent dye.
The mCherry protein is representing the mRuby protein, since the mRuby protein cannot be found in the Fluorescent SpectraViewer® yet, and their excitation and emission spectrums are sufficiently similar to enable the comparison. Adapted from [99].

7. Flow Cytometry

A flow cytometer (MACSQuant VYB, Miltenyi Biotech) was used to quantify the population of endothelial cells in the control medium (BPEL+VEGF+SB) and in the new formulated medium to co-culture both endothelial cells and cardiomyocytes (BPEL+CM+VEGF+SB+IGF+HS), in order to firstly assess the viability of using this latter medium for culturing endothelial cells. Later on, the viability of the new

formulated medium was also tested in a culture of cardiomyocytes to further validate its use as culture medium for the co-culture system.

Endothelial cells were dissociated from wells in BPEL+VEGF+SB medium and in BPEL+CM+VEGF+SB+IGF+HS medium, centrifuged at 1100 rpm for 3 minutes and resuspended in FACS buffer (250 µL/well) composed of 0,5% BSA (w/v) (Sigma-Aldrich®) and 2 mM of EDTA, after the removal of the supernatant from each cell suspension. The cell suspensions were then placed in FACS tubes after passing through the strainer. The filters were washed with another 250 µL of FACS buffer to wash leftovers of single cells through the strainer. Before adding the antibody, 200 µL of each cell suspension were isolated in order to be used as negative control for each medium, centrifuged (1100 rpm at 3 minutes) and resuspended in 50 µL of FACS buffer. The remaining cell suspensions were stained with the Monoclonal Anti-Human-CD31-APC Antibody (eBioscience™) (3 µL/sample) and incubated for 30 minutes at 4°C. Next, 1 mL of FACS buffer was added to each tube to wash them followed by their centrifugation at 240 g for 5 minutes, removal of the supernatant and resuspension in 100 µL of FACS buffer. Afterwards, all the contents of the FACS tubes, including the negative controls, were transferred to a 96-well plate (Greiner) to be run and analyzed on the flow cytometer.

IV. Results and Discussion

1. Fluidic Device Concept

A novel fluidic device was created in house to support the culture of multiple fibrin-based cardiac tissues and their further co-culture with endothelial cells to promote the vascularization of the tissues *in vitro*. This fluidic device was envisioned to be composed by three sections, namely an upper PDMS reservoir, a middle triple-layered stack with several holes drilled along it and a bottom PDMS layer with engraved channels.

1.1. Triple-layered Stack

The hESC-derived cardiomyocytes, and also the fibrin-based cardiac tissues, are anchorage dependent relying on the adherence to supportive structures to ensure their normal development and survival. Having that in mind, a triple-layered stack with holes with different diameters drilled along its layers, henceforth addressed as working setups, was thought out in order to promote the establishment of several anchoring points to where the cardiomyocytes could attach (Figure 26). Additional to that, these anchoring structures will allow the spanning of the tissue between the interior walls of the holes imposing a static mechanical tension to the developing tissue [101]. This mechanical load creates multiple force lines that contribute for the cell alignment along these axes [102], promoting their maturation *in vitro* without initially depending on external stimuli, conferring a design advantage over other constructs such as, for instance, the ones that completely rely on electrical stimulation to stimulate cardiomyocyte alignment in scaffold structures [53].

Apart from the variable diameter of the holes, the top layer that composes the triple-layered stack was also designed to be thicker than the middle and bottom layer to ensure a substantial thickness capable to withhold the seeded tissue but not too high to compromise and hind the survival of the tissue before vascularization is possible.

Figure 26: Cross view of a triple-layered stack, highlighting their anchoring points.
The green and pink layers (top and bottom sheets) that compose the triple-layered stack present holes with a higher diameter than the blue layer (middle layer) allowing the formation of anchoring structures. These structures can then be found in the regions of the stack in which the layer is switched, and consequently the diameter is altered, and are identified with a black contour in this illustration. The cross view was obtained using the SolidWorks® 2017 Software.

Additionally, the conformation of the triple-layered stack allows the developing tissues to grow in a scaffold-free environment, maintaining intact their matrix contrary to scaffold-based approaches whose stiffness and composition critically influences the ECM synthesis by cardiomyocytes [103].

The device was also envisioned to easily allow the scaling-up of the bioengineered cardiac constructs by the direct overlap of new layers or by increasing their thickness; or even by increasing the diameter of the holes that compose the stack with low practical adjustments to be performed, conferring another distinct advantage over other available devices that are dependent on the progressive overlap of 2D temperature-responsive culture surfaces to form an increasingly thicker 3D structure, as the one reported by Shimizu et al. (2002) [57].

Finally, the triple-layered stack was also envisioned to be composed by multiple working setups, enabling the creation of several bioengineered cardiac constructs at once, reducing volume amounts needed and cost per sample, contrary to other devices that only allow the fabrication of a single EHT at a time, as an example the one reported by Zhao et al. (2005) [104].

1.2. Channel Layer

The channel layer was projected to support the culture of the hiPSC-derived endothelial cells and simultaneously, since the channels are intended to be bonded underneath the triple-layered stack, the co-culture of these cells with the cardiomyocytes trapped in the fibrin-based cardiac tissues. In this way, the top of the cardiac tissues could stay free and accessible for further experiments regarding scaling-up, for instance. The channels are also intended to support the sprouting and formation of tubular like-structures by the endothelial cells through local gradients with pro-angiogenic factors [105], for instance, in order to further promote the infiltration of these blood-vessels like-structures in the avascular regions of the tissues, without depending on animal host vasculatures to promote these events like other approaches do, such as the one reported, for example, by Sekine et al. (2013) [79].

1.3. Reservoir Layer

The reservoir layer was developed to help the seeding of the endothelial cells on top of the fibrin-based cardiac tissues, instead of the bottom, presenting in part the same function as the channel layer. Since the central goal of this project was focused in the vascularization of the fibrin-based cardiac tissues, and not in their immediate scaling-up, it was not a problem to have the top layer of the triple-layered stack bonded to other layers.

2. Culturing Fibrin-based Cardiac Tissues in the Fluidic Device

In the first set of experiments, the goal was to assess the viability of using triple-layered stacks to culture fibrin-based cardiac tissues, in order to validate the underlying proof of concept. For that, the generation of fibrin-based cardiac tissues, and their corresponding behavior after seeding inside the working setups of the triple-layered stacks, was dully evaluated and further optimized in this Section.

2.1. General Considerations of the Fabrication of Triple-layered Stacks

Initially, the triple-layered stacks were envisioned to be made from glass, due to the optimal cell adhesion and optical properties of this material (see Section “Comparison Between Synthetic Polymers”).

However, the drilling in glass surfaces needs to be provided by a specialized glass technician due to the fragility and difficulty of handling this material; and even if that was not the case, the need for diamond coated drill bits, to drill in glass, which are expensive to acquire, would turn the fabrication of the triple-layered glass stack in a time and cost-limiting step.

Considering the undesired dependency on third party, the replacement of the glass material by plastic was assessed. Plastic materials are theoretically easier to handle, cheaper than glass and can be drilled using regular drillers with conventional steel bits, eliminating all the aforementioned limiting steps associated with glass.

2.2. Initial Design of the Triple-layered Plastic Stack

The initial design defined for the triple-layered plastic stacks, including the initial diameters of the holes composing the working setups and other relevant dimensions for its construction, are depicted in Figure 27.

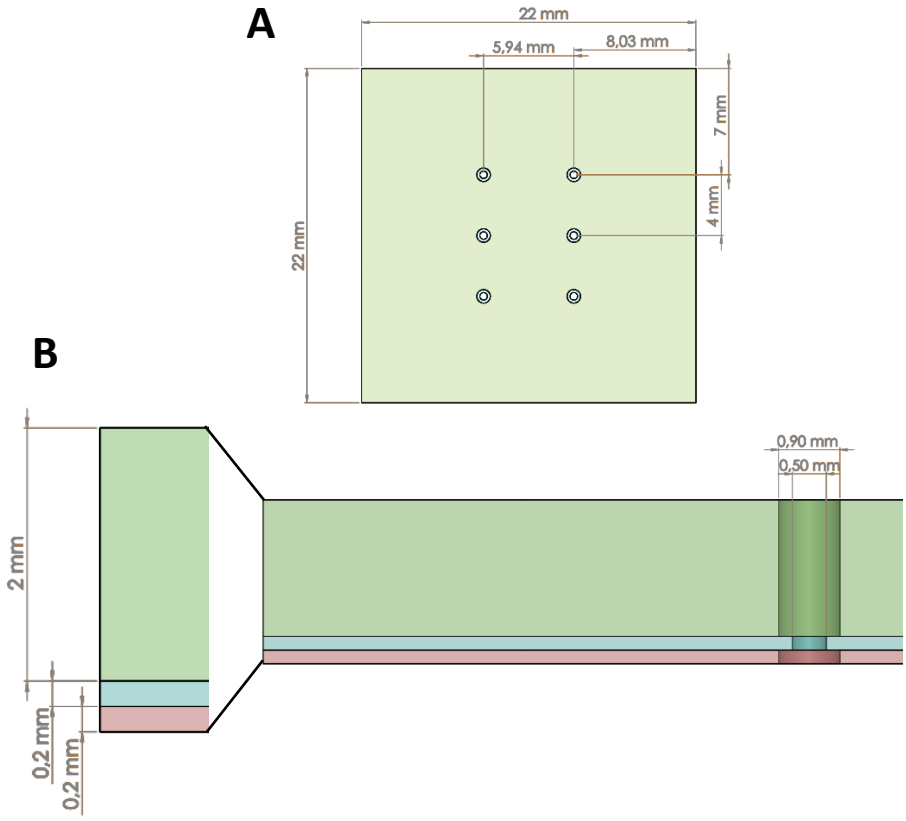

Figure 27: A) Top view of the triple-layered plastic stack and some of its corresponding dimensions. B) Cross view of the triple-layered plastic stack and associated thicknesses and diameter of holes.
The green, blue and pink layers illustrate the first (PMMA slide), second (vinyl coverslip) and third (vinyl coverslip) layers of the triple-layered plastic stack, respectively, from a top to bottom perspective, whose relevant dimensions for its construction are properly discriminated in this Figure. All the views were obtained using SolidWorks® 2017 Software.

2.3. Triple-layered Plastic Stacks Assembled with a 10% Gelatin Solution

2.3.1. General Considerations

Concerns were raised regarding not only the feasibility of assembling the PMMA and vinyl materials in the desired stack but also concerning the viability of further seeding the fibrin-based cardiac tissues in them; therefore, the first experiments performed with these materials intended to give answer to these open questions. Thus, the first experiments were performed using these materials, that were firstly assembled using a 10% gelatin solution, according to the specified in Section “Using a 10% Gelatin Solution”.

Gelatin has been described as an attractive polymer for tissue engineering approaches due to its biological origin, extraordinary biodegradability, cost-efficiency, non-antigenicity and easy handling [106]. Hence, the selection of the gelatin, to perform the bonding of the stack layers, was exactly driven by these factors, especially by its assumed biocompatibility with the seeded tissues, wide availability and low costs-associated. Nevertheless, gelatin usage also has some major drawbacks, being one of the most characteristic, its solubility at temperatures of 37°C or above, dissolving as a colloidal sol [106]. Hereupon, to further prevent the leakage of gelatin from the sides of the stack after its placement inside the incubator (set at 37°C), the four sides of the stack were isolated with PDMS afterwards cured in the oven. The final results of the assembled-plastic stack before and after its isolation with PDMS are shown in Figure 28.

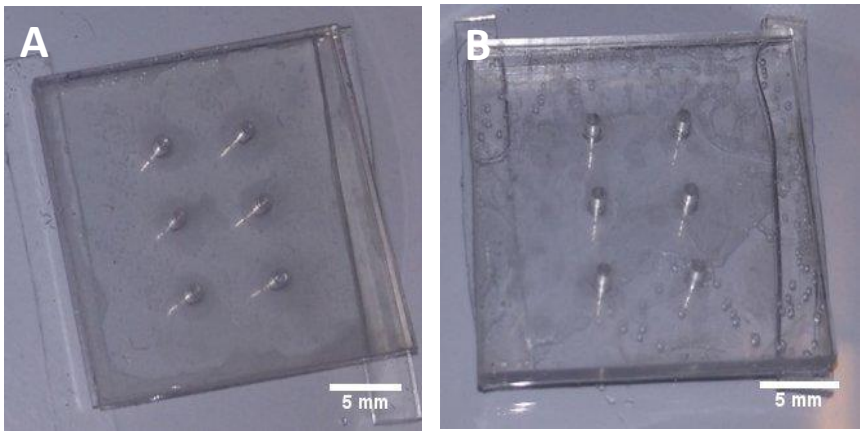

Figure 28: A) Photograph taken to the triple-layered plastic stack right after its assembly using a 10% gelatin solution. B) Photograph taken to the triple-layered plastic stack after being assembled and isolated on the sides with PDMS that was cured in an oven.
All the scale-bars were added resorting to Fiji Software.

2.3.2. Culturing Conditions Before Optimization

Given the nature and objectives of the first set of experiments, neither the channel or the reservoir layer were bonded, hence the device layout was resumed to the assembled triple-layered plastic stack. After

the apparent successful assembly of the triple-layered plastic stack using a gelatin solution, the compatibility of the device to culture fibrin-based cardiac tissues was assessed.

For that, a fibrin-based cardiac tissue was generated, using initially a cell concentration of 2×10^7 cells/mL, value previously optimized in previous work; and seeded in the respective working setups of the triple-layered plastic stack. Given the selected seeding density used, the ratio of thrombin to final volume was set at 0,5 µL of thrombin/150 mL, given its proportionality to the amount of cells intended to be entrapped within the fibrin network.

Some of the micrographs taken to a working setup, kept in culture for 10 days, comprising all the testing culturing conditions aforementioned are presented in Figure 29.

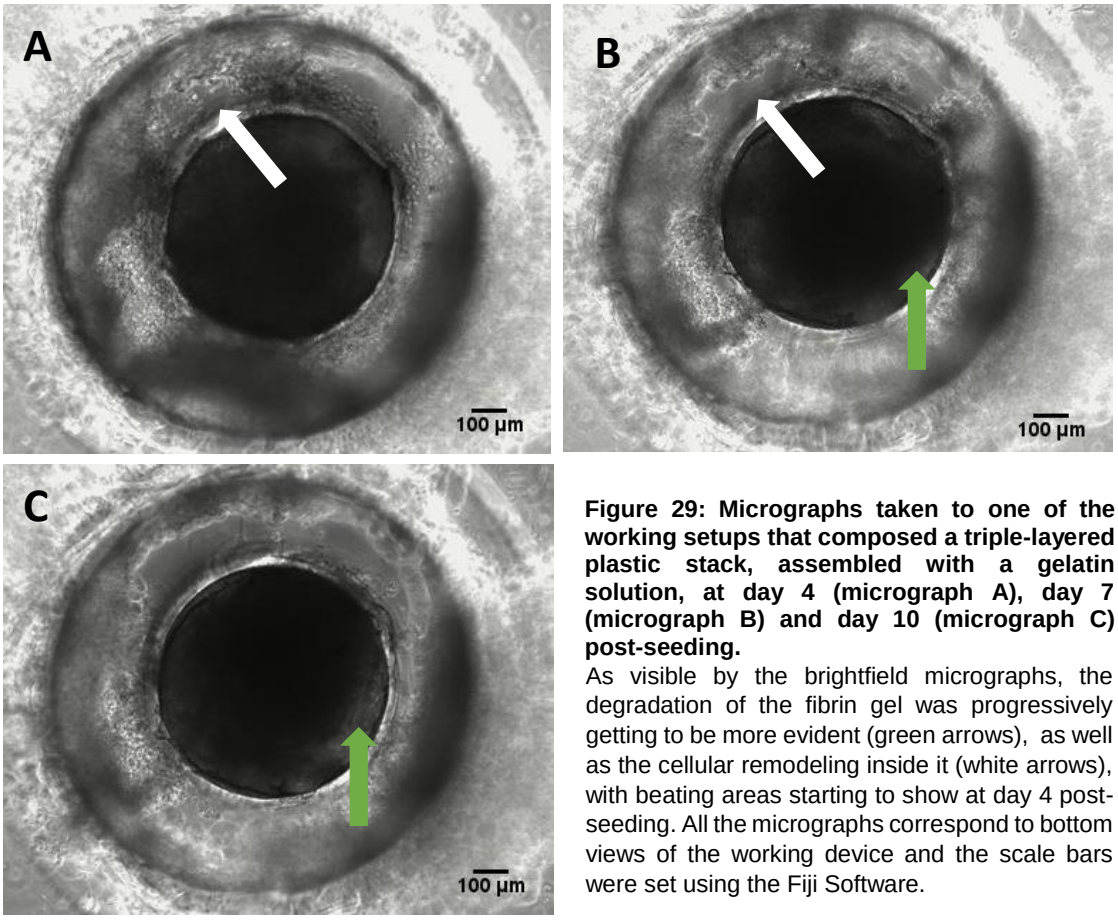

Figure 29: Micrographs taken to one of the working setups that composed a triple-layered plastic stack, assembled with a gelatin solution, at day 4 (micrograph A), day 7 (micrograph B) and day 10 (micrograph C) post-seeding.
As visible by the brightfield micrographs, the degradation of the fibrin gel was progressively getting to be more evident (green arrows), as well as the cellular remodeling inside it (white arrows), with beating areas starting to show at day 4 post-seeding. All the micrographs correspond to bottom views of the working device and the scale bars were set using the Fiji Software.

2.3.3. Analysis of the Experimental Data Before Optimization

By analyzing Figure 29, it is visible that over time of cultivation, some of the cardiomyocytes were indeed able to spread out inside the fibrin matrix (white arrows) and form new cell-cell interactions, that led to spontaneous contracting areas that started at day 4 and extended until day 10 post-seeding. From day 4 to day 10, it was noticeable not only the remodeling of the hydrogel, but also its progressive degradation (green arrows) probably by the plasminogen in the culture medium and by the increased cellular production of ECM proteins [107], that greatly contributed to a decrease of the size of the fibrin-based cardiac tissue. The degradation of the hydrogel was already to be expected since even though

its degradation rate is remarkably slowed, and consequently controlled, by the use of the antifibrinolytic agent aprotinin, it is never stopped even when using aprotinin concentrations way higher than the ones used in this project [42]. Nevertheless, the remodeling of the hydrogel was never complete, since it was never noticeable a synchronously contracting tissue englobing all cells; in fact, it is easily seen in Figure 29 a significant amount of cells that never remodeled and maintained their original positions in the working space. A possible reason for the incomplete cell remodeling could be the cell density used not being adequate, meaning that, there might not be enough cells sufficiently close to each other to initiate novel intercellular connections; hence, the cell density should be increased, in order to rise the amount of contacting cells.

2.3.4. Analysis of the Limitations of Gelatin as Assembling Agent

Nevertheless, the results presented above were not always reproducible in all of the working setups, in fact, the patterning efficiency was around 20%, meaning that only 20% of the working setups were filled with a promising fibrin-based cardiac tissue in each set of experiments. The remaining 80% greatly resemble the examples depicted in Figure 30.

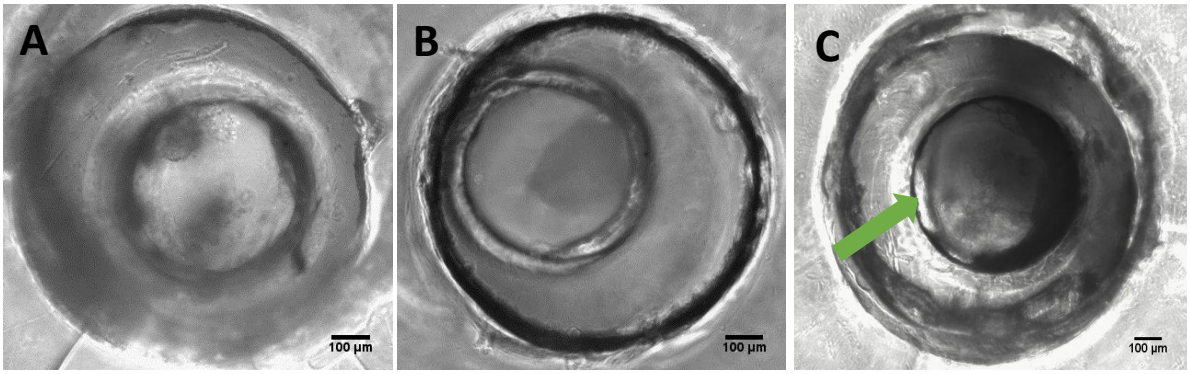

Figure 30: Micrographs taken, at different days post-seeding, to multiple working setups that composed different triple-layered plastic stacks, all assembled with a gelatin solution, showing some of the limitations faced with this culturing system.

A) Micrograph taken 4 days-post seeding. The fibrin-based cardiac tissue was almost completely ruptured, no longer being possible to observe a tissue covering all the area of the working setup. **B)** Micrograph taken 4 days-post seeding. Similar situation as reported in micrograph A; only a partial remain of the original tissue survived anchored to the working space. **C)** Micrograph taken 8 days-post seeding. Even though, in this case, the tissue was not disrupted, the cell concentration is really low, despite the use of the same cell density as the optimistic results reported in Figure 29. The green arrow points to the fact that the formed tissue was getting smaller than the middle hole. All the micrographs correspond to bottom views of the working device and the scale bars were set using the Fiji Software.

In micrographs 30A and 30B, it is visible that the forming tissues were considerably damaged following their casting, only persisting small remaining of the original casted tissues, that remarkably exhibited smooth beating areas at day 4 post-seeding. This large number of ruptures could be explained by the release of air bubbles, trapped inside the layers of the triple-layered stacks, that had origin in the partial boiling of the gelatin when the working device was placed inside the oven at 67°C to cure the PDMS from its sides. In fact, in picture 28B, after the isolation of the sides of the triple-layered stack, a considerable amount of cloistered bubbles is visible between the layers.

Furthermore, in micrograph 30C, it is visible a uniform and coherent beating tissue but with a really low cell concentration, almost depleted of cells, although the seeding density was the same used in other experiments (2×10^7 cells/mL). This can be explained by the low sealant properties offered by the gelatin that is liquid at room temperature; hence, following aspiration of the excess liquid gelatin, some open areas are left in these regions, as partially noticeable in picture 28A. After the seeding of the cardiac tissues, some cells were able to infiltrate and disperse through these free-gelatin spaces, turning the remaining tissue more thinned.

2.3.5. Optimizing the Assembling Agent

Considering all these hardly predictable and controllable events, and in order to try to obtain reproducibility and repeatability in the further trials, a new alternative to the gelatin was brought to analysis, specifically the use of the optical adhesive glue NOA81.

Like already described in Section “Using the Norland Optical Adhesive 81 (NOA81)”, NOA81 is a UV-curable liquid photopolymer that presents several characteristics really valued for microfluidic operation, namely, its entire transparency and non-scattering in the visible spectrum, enabling the use of brightfield microscopy for imaging purposes; its low auto-fluorescence that negligible would influence fluorescence imaging techniques; its good chemical resistance to organic solvents, allowing the cleaning and successive re-utilization of chips assembled with it; its impermeability to oxygen and water vapor, so even if any air bubble gets trapped on its surface during the assembly process, it would never be released from there, since neither the NOA81 or the plastic/glass materials are permeable to air; its stability during surface treatments (e.g. plasma treatment using an oxygen plasma); its biocompatibility after being cured and finally its good adhesion to glass and plastic materials without showing any leakage for up to months [108]. All the aforementioned characteristics of the NOA81 would be highly beneficial for the ongoing project for all the stated reasons, and expectantly would end by solving the faced challenges, motivating in this way the choice of this polymer for the next set of experiments.

2.3.6. Optimizing Design Features

Apart from that, it is also visible in micrograph 30C (see green arrow), that overtime, the degradation of the tissue was so prominent that, in some cases, its size was getting smaller than the middle hole, causing a lack of physical support that lately, was translated in the progressive detachment and consequent loss of the tissue. Therefore, it was clearly that the ratio between the diameter of the middle and the upper and bottom holes needed to increase, to ensure that regardless of how much the tissue was compacting overtime, it would never be sufficient to cause displacement from the middle hole. For practical limitations, namely lack of availability of drill bits with a diameter smaller than 0,5 mm, it was chosen to increase the diameter of the bottom and upper holes from 0,9 mm to 1,2 mm.

2.4. Triple-layered Stacks Assembled with NOA81

2.4.1. Optimizing the Curing Step

Representative results obtained for the first set of experiments using a plastic triple-layered stack assembled with NOA81, and whose top and bottom layers were drilled with a 1,2 mm drill bit, are depicted in Figure 31.

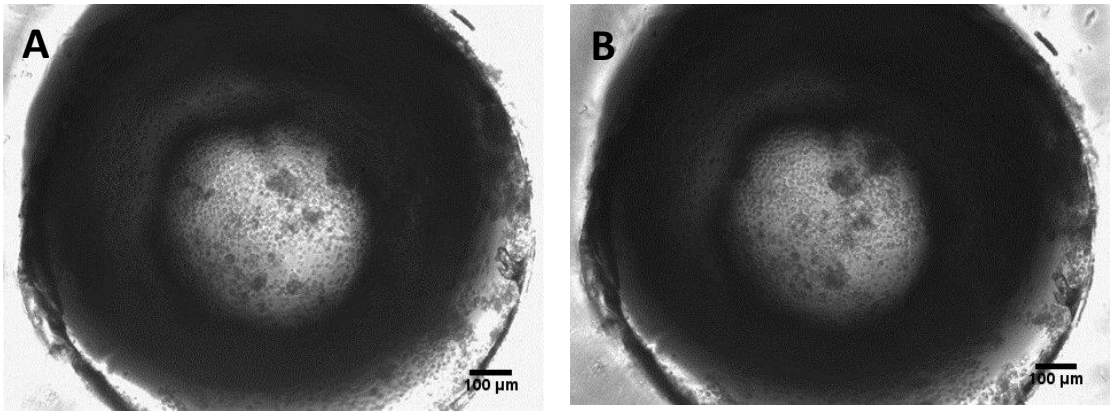

Figure 31: Micrographs taken to one of the working setups that composed a triple-layered plastic stack, assembled with NOA81, at day 8 (micrograph A) and day 11 (micrograph B) post-seeding.
As visible by the micrographs, the remodeling of the tissues never occurred, at least the majority of it, associated to an assumable cell death caused by the toxicity of the NOA81; only some small clusters survived and started presenting contractions at day 8 post-seeding, much later than in the gelatin experiments. All the micrographs correspond to bottom views of the working device and the scale bars were set using the Fiji Software.

Unfortunately, these results were not as promising as expected, since the cells were never able to remodel into a synchronously beating tissue, as visible by Figure 31. As a matter of fact, even synchronous contractions of small cell clusters only started after 8 days of culture, long after of what was observed with the previous experiments with gelatin, remaining as distinctive beating clusters until the end of the experiment (on day 15 of culture). The remaining cells never recovered their contractile activity, even as single cells, being assumingly dead. Based on these observations, and after some of the encouraging results obtained with the gelatin assembled stacks, it was presumable a problem related to the biocompatibility of the NOA81. In fact, the first developed experiments performed with NOA81 started with a curing step slightly different of the enunciated in Section “Using the Norland Optical Adhesive 81 (NOA81)”, since despite the curing step having been performed with the same UV-LED system, the exposure time was only of 10 seconds, considering that this was already a process previously optimized by colleagues at the University of Twente, The Netherlands. In fact, after 10 seconds of exposure to the UV-light system, the NOA81 had become rigid turning into a hard polymer that clearly sealed every space between each assembled layer.

However, after consultation of the NOA81 datasheet, it was clear that the NOA81 should be exposed to an UV power of $2{,}5\ mW/cm^2$ for 5 to 10 seconds, or equivalent, in order to be properly cured. Taken into account that the working UV-light has a full power around 7 times lower than the recommended, it

was established that from this point forward, every area of the stack would be exposed at least 7 times in a row for 10 seconds to the available UV system, to allow an effective curing step. After that, the samples were left overnight inside an agitated beaker with distilled water to ensure that any uncured residue, which would still be liquid, would be release from the sample surface, corresponding to the procedure described in Section "Using the Norland Optical Adhesive 81 (NOA81)".

2.4.2. Analysis of the Experimental Data after Optimization of the Curing Step

By implementing the previous alterations to the NOA81 curing method, it was possible to obtain results analogous to the ones presented in Figure 32.

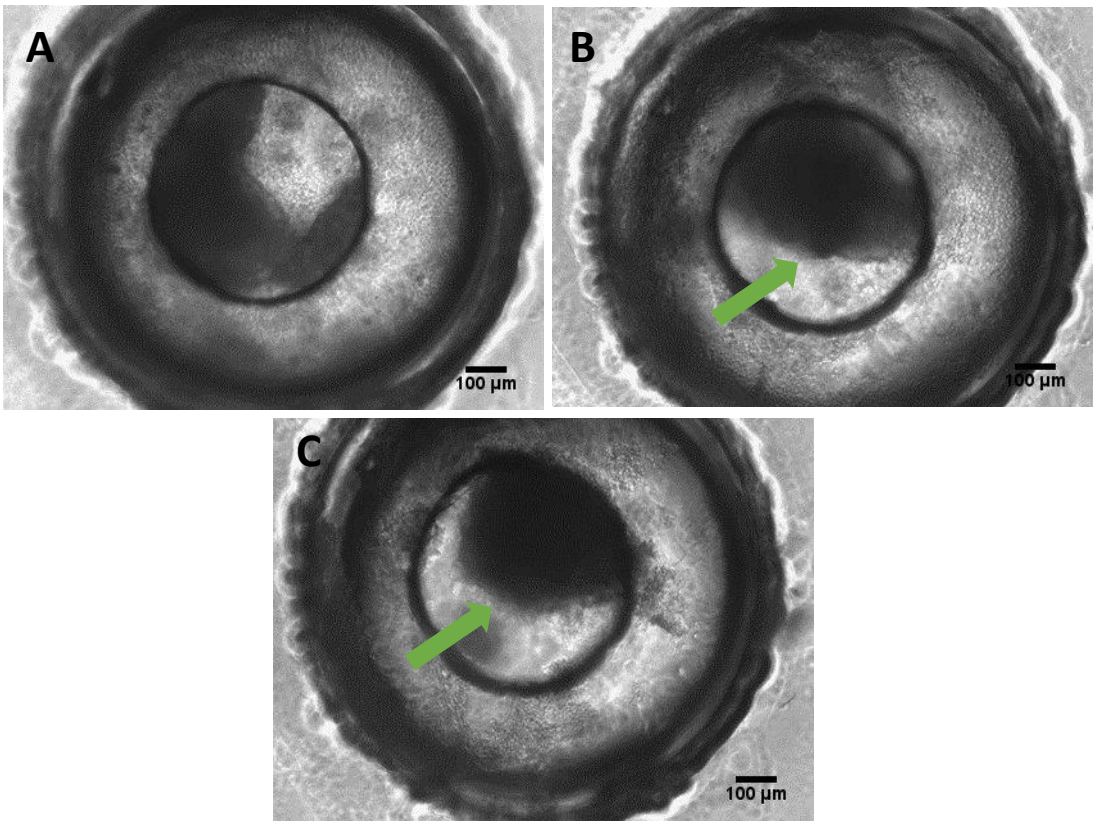

Figure 32: Micrographs taken to different working setups that composed a triple-layered plastic stack, assembled with NOA81, at day 4 (micrograph A), day 6 (micrograph B) and day 11 (micrograph C) of culture after optimizing the curing step.

Micrographs B and C concern the same working setup at different days of culture, in order to enable the evaluation of the development of the casted tissue. As visible by the micrographs, it is clear that, after using a more aggressive curing step, the majority of the cells were able to remodel into a synchronous beating tissue that started contracting at day 4 post-seeding, in all cases. The extensive compaction (green arrows) of the tissue was also visible from day 6 to day 11 as noticeable by looking at micrographs B and C. All the micrographs correspond to bottom views of the working device and the scale bars were set using the Fiji Software.

Overtime, it was possible to observe a higher number of cells, compared to the previous set of experiments (Figure 31), concentrated around the middle hole, remodeling in a consistent tissue. Along with that, during the culture time, it was also visible the progressive degradation and sequential compaction of the tissue (green arrows), in which the cardiomyocytes occupy the space of the degraded

fibrin, by looking, for instance, to the evolution of the same tissue from day 6 (micrograph 32B) to day 11 post-seeding (micrograph 32C). The first contractions of these developing tissues started at day 4 post-seeding, resembling the previous results obtained using gelatin as assembling agent. The contractions were kept regular and vigorous until the end of the experiment (at day 15 after seeding), revealing some promising results regarding the use of NOA81 as assembling agent.

2.4.3. Optimizing the Cell Density

However, a significant amount of cells was not able to remodel into the tissue; showing that either there was still toxic residues of uncured NOA81 inside the working setups, or the cell density applied was not high enough to allow the complete remodeling, as already assumed in the gelatin experiments. In order to evaluate the second hypothesis, it was decided to increase the working cell concentration to the double (4×10^7 million cells/mL), to analyze if a higher cell density, translated into a closer proximity of the cells with their neighbors, could facilitate and promote the remodeling process. Even if the problem was centralized in possible uncured residues of NOA81, a higher cell density should also work to minimize this issue, by compensating the number of viable cells over the dead ones. Besides that, it was also chosen to increase the working concentration of thrombin to the double (1 µL of thrombin/ 150 µL of final volume) since this increase would accelerate the gelation time of the hydrogel resulting in a more densely cross-linked mesh with thinner fibers, allowing the generation of a hydrogel with lower porosity [109] and subsequent with a higher trapping efficiency. Besides these motivations, and given that the cell density was increased to the double, the thrombin concentration should really be increased at least twice to answer to the current higher cell trapping requirement.

2.4.4. Analysis of the Experimental Data after Optimization of the Cell Density

In Figure 33 some representative results obtained for a triple-layered plastic stack are illustrated, taken into consideration the aforementioned modifications to the working cell density and concentration of thrombin.

After these adjustments, it was possible to obtain a spontaneously and synchronously contracting tissue, formed not only in the majority of the working setup, but also in a large extension of the outer space of the bottom layer (Figure 33). The casting of the tissue was always a delicate step highly dependent on the time available to do it (around 1 minute) that sometimes compromised the positioning of the micropipette, ending up by positioning it deeper in the working setup resulting in the escape of the extra tissue through the bottom layer. The cardiomyocytes started beating spontaneously and at the same pace as part of a synchronous tissue, englobing all the cells and not only enclosing some major cell clusters as in previous experiments, at day 4 after the casting and continued for several days until the end of the experiment (at day 15 of culture).

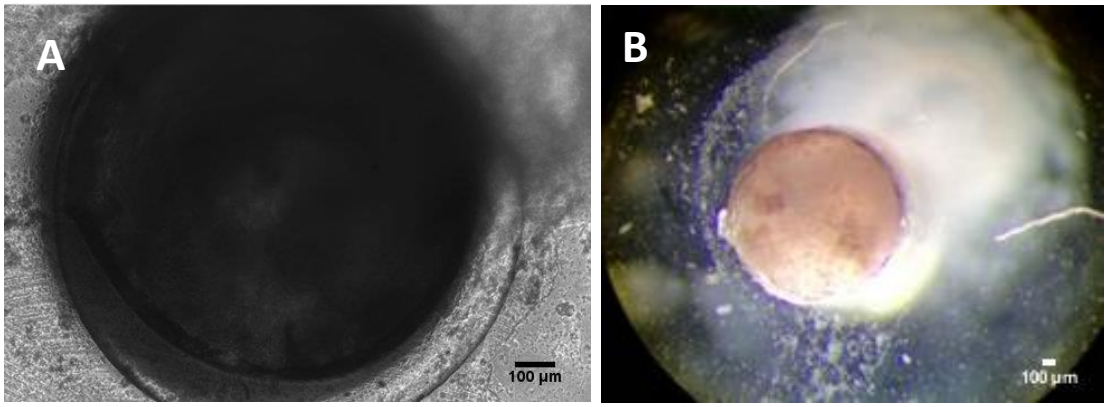

Figure 33: Micrographs taken to different perspectives of the same working setup that composed a triple-layered plastic stack, assembled with NOA81, at day 4 of culture (both micrographs A and B) after optimizing the cell density.

A) Bottom perspective of the working setup where is visible that the cardiomyocytes were able not only to attach to the anchoring points of the working setup but also to the bottom layer of the device, forming there a synchronously beating tissue that started contracting at day 4 of culture. **B)** Top perspective of the same working setup, where is also visible due to the transparency of the glass, the heterogenous-shaped tissue formed in the bottom sheet of the device. The scale bars were set using the Fiji Software.

After the several optimization steps performed regarding the assembly of the triple-layered stacks, as well as those concerning the generation and casting of the fibrin-based cardiac tissues in the stacks, encouraging results were obtained that highly contributed for the validation of the proof of concept of using this new approach. After accomplishing the successful culture of fibrin-based cardiac tissues inside of triple-layered stacks, the bonding of the channel layer to the working device was set as the next goal.

2.4.5. Channel Layer Design: Configuration projected for Plastic Stacks

The configuration envisioned for the channels intended to be bonded to the plastic stack, as well other dimensions relevant for its fabrication are depicted in Figure 34.

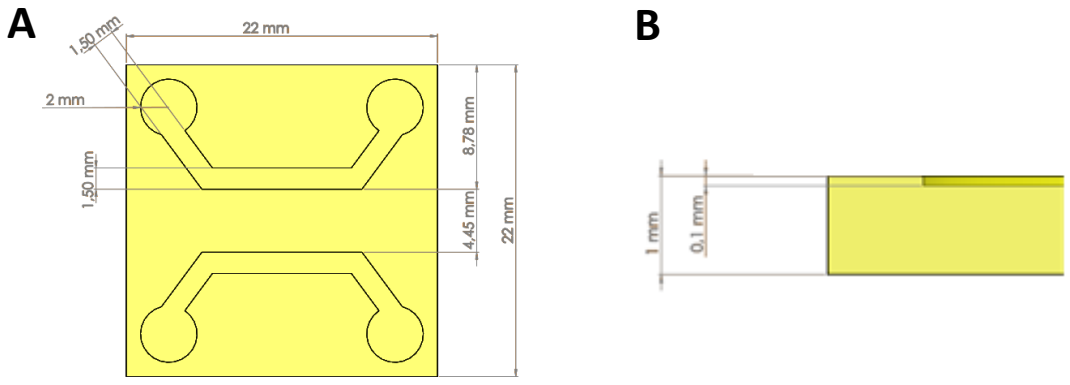

Figure 34: A) Top view of the channel layer envisioned to be assembled to a triple-layered plastic stack and some of its corresponding dimensions. B) Cross view of the concerned channel layer and associated thicknesses.

The yellow layer illustrates the channels layer whose relevant dimensions for its construction are properly discriminated in this Figure. All the views were obtained using SolidWorks® 2017 Software.

2.4.6. Attempting to Optimize the Bonding of PDMS to Plastic

A set of different approaches was tested to attempt the bonding of the channels to the plastic vinyl layer (bottom layer of the triple-layered plastic stack), namely plasma treatment (see Section “Channels Assembly to Triple-layered Glass Stacks), rolling a thin layer of PDMS and toluene (see Appendix “Rolling a Thin Layer of PDMS and Toluene”), or PDMS (see Appendix “Rolling a Layer of PDMS) or NOA81 (see Appendix “Rolling a Layer of NOA81) or by directly pipetting and curing NOA81 on top of the channel surface (see Appendix “Direct Pipetting of NOA81”).

Neither of these techniques have had successful results in providing the irreversible and non-leaking bonding of the PDMS to the vinyl surface. Since the exact chemical composition of the vinyl layer is unknown, it was not possible to make assumptions of the causes behind the failure of these techniques as well rethink new approaches to accomplish the desired bonding. For all these reasons, the use of triple-layered plastic stacks, although being more practical for drilling related motivations, was pushed aside, believing that the bonding of the PDMS to glass surfaces would be easily accomplished by plasma treatment, as reported by numerous authors, for instance by Katzenberg et al. (2005) [110]. Taken into consideration that the designed channel layer for triple-layered plastic stacks will not be used for further experiments, the presentation of the negative mold that enabled the obtention of the concerned layer was dismissed from the document.

2.4.7. Optimization of the Final Fluidic Device Design

Triple-Layered Glass Stack Design

Similar to the triple-layered plastic stacks but adapted to the higher dimensions of these new layers, a triple-layered glass stack was fabricated according to the projected design of Figure 35 and Figure 36 and taken into consideration the optimization performed before for the plastic stacks.

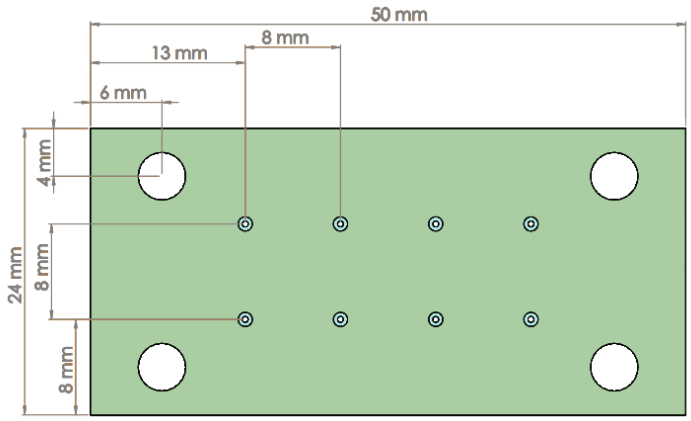

Figure 35: Top view of the current triple-layered glass stack and some of its corresponding dimensions. The green layer illustrates the first (glass slide) layer of the triple-layered glass stack, from a top to bottom perspective, whose some relevant dimensions for its construction are properly discriminated in this Figure. The concerned view was obtained using SolidWorks® 2017 Software.

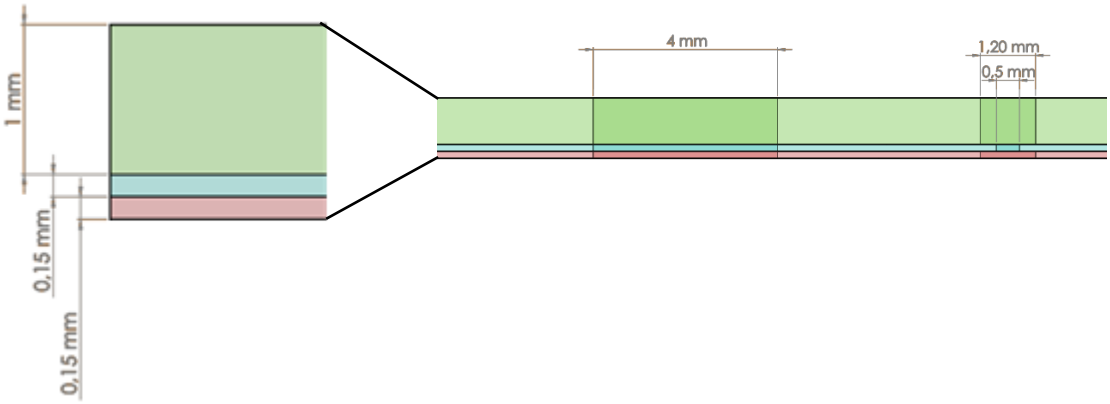

Figure 36: Cross view of the current triple-layered glass stack and associated thicknesses and diameter of holes.
The green, blue and pink layers illustrate the first (glass slide), second (glass coverslip) and third (glass coverslip) layers of the triple-layered glass stack, from a top to bottom perspective, whose some relevant dimensions for its construction are properly discriminated in this Figure. The concerned view was obtained using SolidWorks® 2017 Software.

The holes with 4 mm of diameter, drilled in each layer composing the stack and henceforth addressed as “inlets” and “outlets”, were drilled to allow the further communication to the channels, since both modules present the same external dimensions.

Channel Design

The height and width of each channel were carefully established and optimized so its hydraulic resistance (measurement of the resistance of the channel to the passage of a certain fluid flow) could be inferior to the hydraulic resistance of each row of holes. Otherwise, after applying the fluid into the channel, it would been diffused through the holes (since the fluid follows the way that offers a lower resistance) instead of being diffused through the channels.

The hydraulic resistance of each channel ($R_H\ (channel)$) was calculated by Equation 1 [111], by approximating the designed channels to rectangular-shaped and considering an aspect ratio that satisfies the condition $\frac{h}{w} \ll 1$.

$$R_H\ (channel) = \frac{12 \cdot \mu \cdot L}{w \cdot h^3} \qquad (1)$$

Wherein μ is the viscosity of the fluid $(Pa \cdot s)$, L is the channel length (m), w is the channel width (m) and h is channel height or in other words, its depth (m).

Specifically, Equation (1) was used to test different values of widths and heights that could ensure a hydraulic resistance in each channel ($R_H\ (channel)$) inferior to the hydraulic resistance offered by the set of working setups that each channel crosses. For a more detailed explanation, regarding the origin of this equation as well as the implementation of the equations that allow the calculation of the hydraulic resistance offered by the working setups, consult Appendix “Calculation of Hydraulic Resistances”.

The temporary hydrophily of the PDMS material after performing the surface functionalization step (see Section “Silane and Glutaraldehyde Functionalization”), was also taken into consideration in the selection of the final dimensions attributed to the channel, since it helps to reduce the resistance that the fluid is being subjected.

After performing all the calculations, the rectangular-shaped channels were projected to have 5 mm of width and 0,5 mm of height, as represented in Figure 37. Besides these dimensions, other relevant dimensions for their fabrication are also shown in Figure 37.

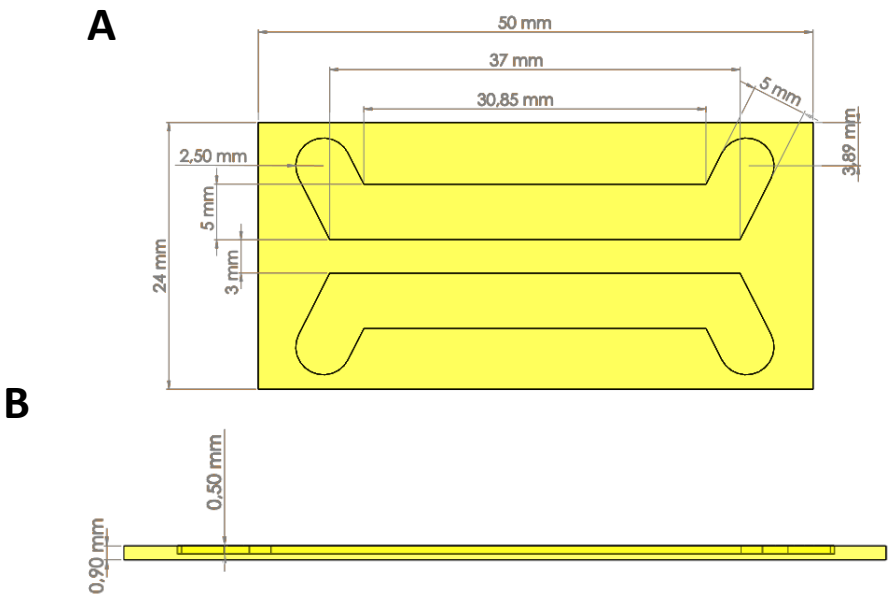

Figure 37: A) Top view of the current channel layer intended to be assembled to the triple-layered glass stack and some of its corresponding dimensions. B) Cross view of the current channel layer and associated thicknesses.
The yellow layer illustrates the channel layer whose relevant dimensions for its construction are properly discriminated in this Figure. All the views were obtained using SolidWorks® 2017 Software.

Design of the Negative Mold of the Channels

The negative mold of the channels was designed in order to present 5 mm of width and 0,5 mm of height above the surface of the PMMA material, in order to allow the impression of the original model of the channels (Figure 37) after the injection-molding process.

The frame created around the negative mold has a cavity with 0,9 mm of height and 2 mm of width as visible in Figure 38. Since the original mold of the channels will be obtained by an injection molding system using the aforementioned negative mold, the frame was designed to ensure a proper final thickness of the channel layer, particularly small enough, to allow the use of confocal microscopy to image the bottom of the fluidic device.

Additionally, one side of the frame is also composed by multiple spacers with variable lengths, that intend to allow the leakage of possible air bubbles formed during the injection molding procedure. The

aforesaid dimensions, as well as some other relevant measurements for the fabrication of the negative mold are also depicted in Figure 38.

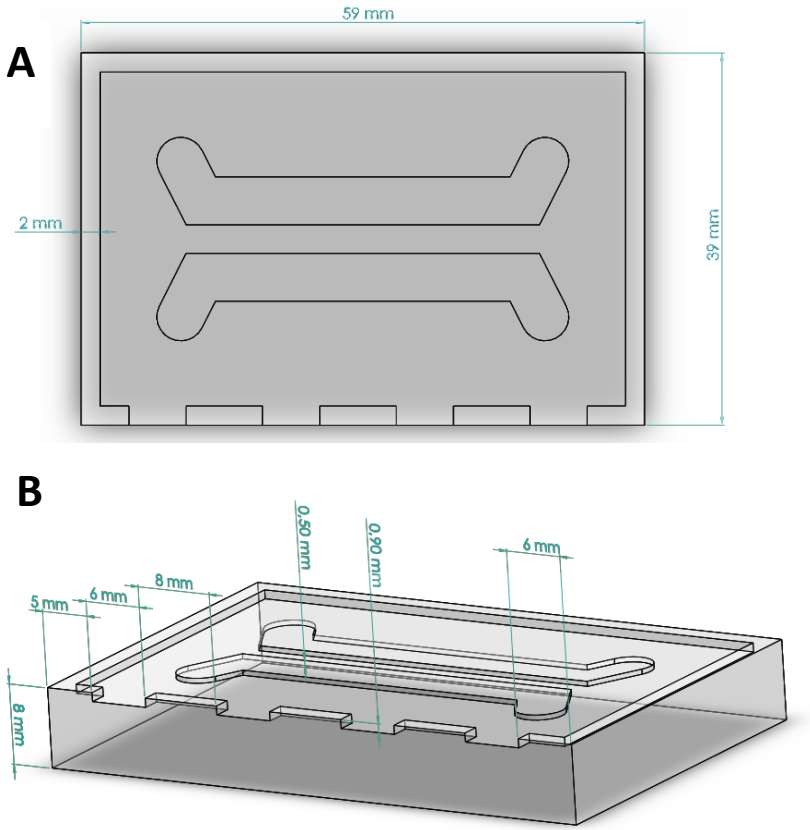

Figure 38: A) Top view of the negative mold of the channel layer impressed in a PMMA material and some of its respective dimensions. B) Cross view of the setup with additional dimensions.
Dimensions relevant to the design of the negative mold of the channel layer are properly discriminated in this Figure. All the views were obtained using SolidWorks® 2017 Software.

Optimizing Culturing Conditions in the Fluidic Device

Besides the fabrication of a shortened-volume petri dish to reduce the amount of medium needed to cover the entire chip (see Section “Practical Considerations”), four stoppers able to fit in the spaces of the inlets and outlets of the glass stack were fabricated by cutting small pieces of Pasteur pipettes tips with a height of 5 mm (approximately) and a suitable width (around 4 mm) to fit in the aforesaid spaces. Two of the stoppers were closed by filling their interior with PDMS that was subsequently cured; while the other two stoppers were left open. If both stoppers were closed, the liquid inside the channels would expand and fill the remaining spaces, which could lead to the displacement of the cardiac tissues, leading to their immediate disruption. The stoppers were projected to isolate and restrain the movement of medium in the channels. A schematic illustration of the aforementioned experimental setup is presented in Figure 39.

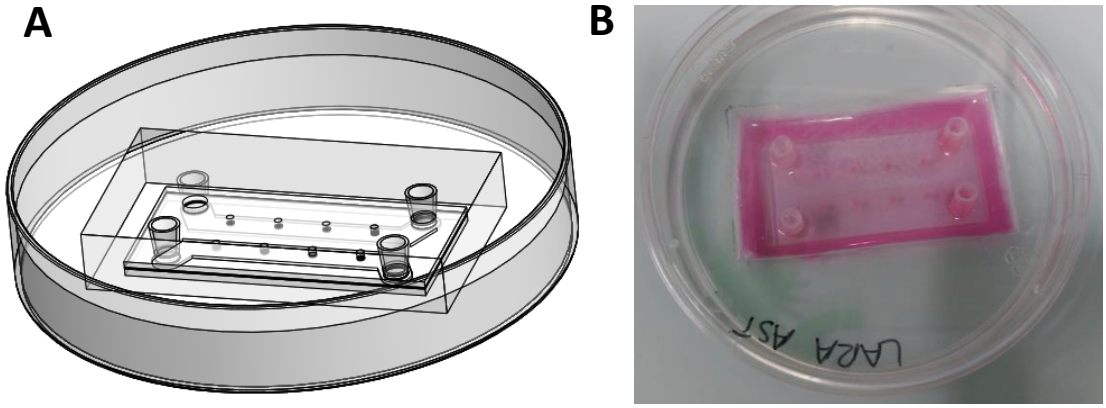

Figure 39: A) Schematic illustration of a cross view of the envisioned shortened-volume petri dish containing the assembled fluidic device with the stoppers placed in the inlets and outlets spacings. B) Photograph concerning the same subjects as illustration A.
The schematic cross view was obtained using SolidWorks® 2017 Software.

2.4.8. Bonding between PDMS and Glass

In fact, the bonding between the glass surface to the PDMS channels was easily accomplished, following the plasma treatment procedure (see Section “Channels Assembly to Triple-layered Glass Stacks”), leading to the effective replacement of the triple-layered plastic stacks for glass stacks in order to be possible to proceed with further experiments.

2.4.9. Optimization of the Material of the Triple-layered Stacks

Similar to the study for the plastic stacks, the triple-layered glass stacks assembled with NOA81 and previously bonded to the channel layer were also assessed in order to validate their usage. Some of the representative results are represented in Figure 40.

After all the troubleshooting and subsequent optimization, it was finally possible to obtain reproducible results in all the working setups, as attested by Figure 40, comprising extremely compacted and even denser tissues than the ones obtained with the previous experiments (either using triple-layered plastic stacks assembled with gelatin or NOA81).

As visible in Figure 40, in the triple-layered glass stacks, the cells were able to perform an extensive and complete remodeling around the middle hole that started right after the seeding and led to the formation of a spontaneously and synchronously contracting tissue-construct 4 days post-seeding. The engineered fibrin tissues were able to acquire a stable circular shape, not seen until this stage, as the cardiomyocytes were getting align along the multiple radial force lines created by the mechanical load to which they were being subjected due to their anchorage.

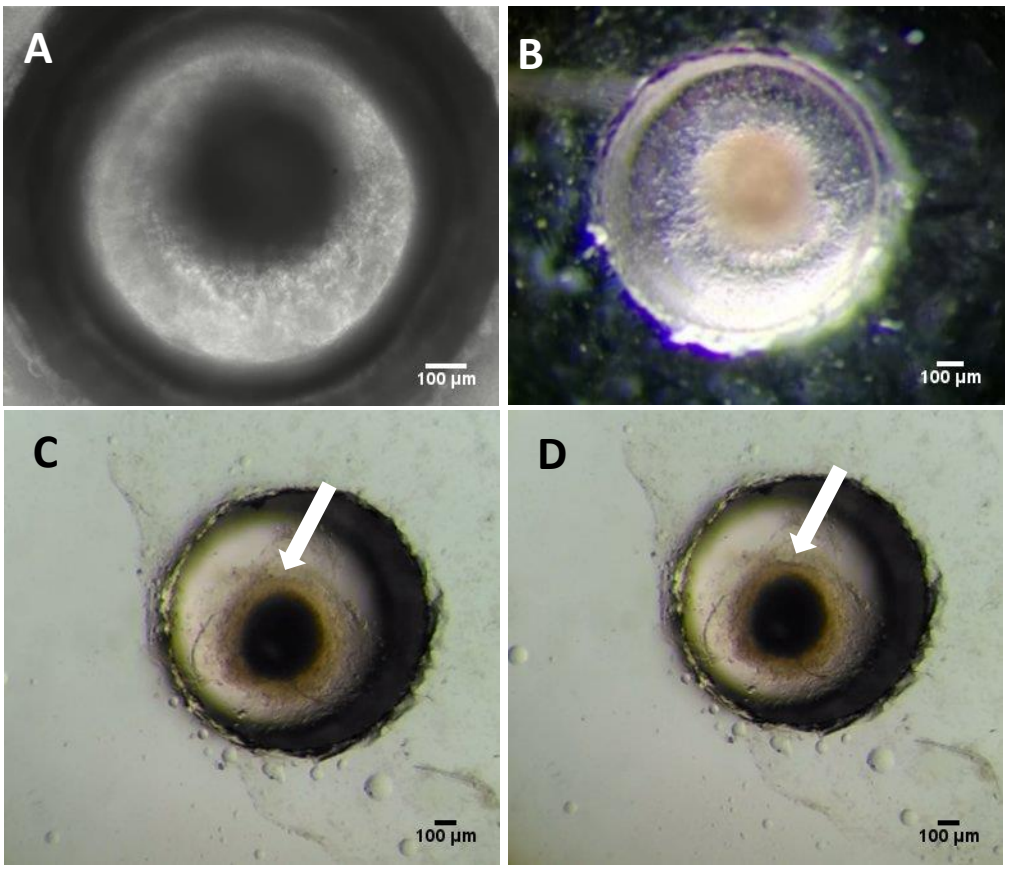

Figure 40: Micrographs taken to different working setups that composed a triple-layered glass stack, assembled with NOA81, at day 4 (micrographs A and B) and day 12 (micrographs C and D) of culture after optimization.
Micrographs C and D report to the same working setup at different stages of the contraction process (white arrows). **A)** Bottom perspective of a fibrin-based cardiac tissue at day 4 of culture. The remodeling of the tissue started immediately after the seeding with the appearance of a whole synchronously beating construct 4 days post-seeding. **B)** Top perspective of a fibrin-based cardiac tissue at day 4 of culture, where can be drawn the same conclusions taken from micrograph A. **C)** Top perspective of a fibrin-based cardiac tissue 12 days post-seeding taken during the relaxation of the cardiomyocytes. **D)** Top perspective of a fibrin-based cardiac tissue 12 days post-seeding taken during the contraction of the cardiomyocytes. Matrix compaction stabilized around day 12 post-seeding. All the scale bars were set using the Fiji Software.

The enormous stability of these fibrin-based cardiac tissues can be associated to the bonding of the channel layer that set the tissues under a lower hydraulic shear stress, caused by the constriction of the liquid movement that flows under them. It is important to notice that the thickness that goes from the bottom until the middle layer (where the tissue is anchored) is only of 150 µm, meaning that the bottom-located tissue is really thin being highly prone for rupturing under high stresses, contrary to the top-located tissue that is much thicker and consequently, much resistant; thereby the restriction of the medium in the bottom part of the fluidic device highly contributed for the protection of the more sensitive areas of the engineered tissue-construct, allowing its better development when in culture.

2.4.10. Final Considerations regarding the Final Design of the Fluidic Device

For the current project, it was chosen to use a static mechanical loading device since it is easier to implement and to control over large periods of time without theoretically incurring in the risk of tissue disruption comparing with cyclic stretching devices [112]. Nevertheless, engineering methods that can

promote auxotonic instead of isometric contractions on engineered heart tissues have been reported to improve not only the cardiac tissue structure but also its contractile performance [38], since they mimic the *in vitro* conditions of the heart beating against the hydrostatic pressure of the circulatory system. Hence, the employment of dynamic mechanical loads should be a high focus to be explored in advanced phases of the project in order to attempt to improve the maturation of the developing tissues.

Additionally to that, and besides glass being a really well-suitable material for the triple-layered stack as concluded before, its replacement by other synthetic or natural polymers easily prone to be sectioned should be brought to scope in order to allow future histological assays of the cardiac tissues.

3. Culturing hiPSC-derived Cardiac Endothelial Cells in the Fluidic Device

3.1. Analysis of the Experimental Data Before Optimization

After having optimized the procedure for culturing fibrin-based cardiac tissues inside the fluidic device, the next stage of the project was focused on the co-culture with hiPSC-derived cardiac endothelial cells, to further attempt to promote the vascularization inside these engineered-constructs. Having that in mind, the first set of experiments concerning this matter, were performed by seeding endothelial cells inside the channels using for that purpose a seeding density of 1×10^5 cells/mL in BPEL+VEGF+SB medium, being this based on the density used for monolayer culture in 6-well plates.

The conditions for seeding the fibrin-based cardiac tissues in the working setups that compose the triple-layered glass stack were kept the same as before, using CM+Gal+LowIns+T3+IGF+Glu+HS medium to fill in the volume of the petri dish, afterwards. Some of the representative results obtained for this set of experiments are presented in Figure 41.

Taken the results depicted in Figure 41 into consideration, it was clear that the seeding density needed to increase to enable the formation of a monolayer of hiPSC-derived cardiac endothelial cells, since the seeded number was not sufficient to allow the cells to self-organized in a packed layer. Besides that, it was impossible to distinguish the presence of endothelial cells on top of the tissues, despite being clear their presence on the same plane as the bottom-located tissues after the reinversion of the chip; therefore it was decided to perform the next set of experiments with fluorescently-labeled endothelial cells.

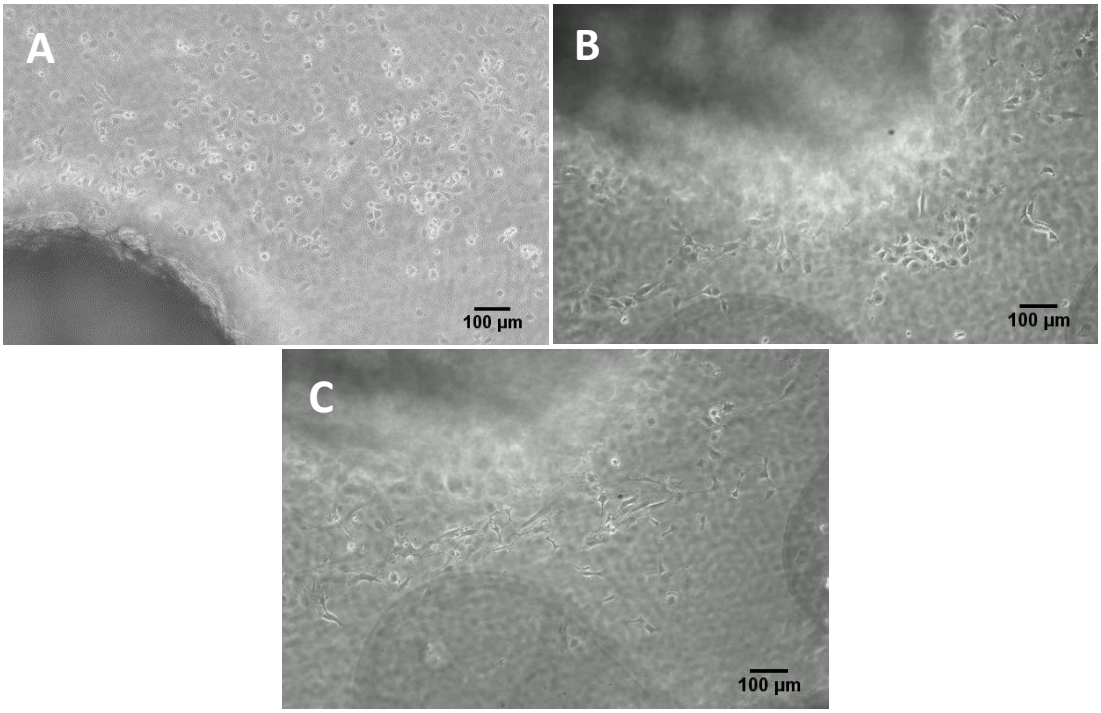

Figure 41: Micrographs taken on different channels seeded with hiPSC-derived cardiac endothelial cells at day 0 (micrograph A), day 1 (micrograph B) and day 5 (micrograph C) post-seeding.
Micrographs B and C were taken on the same position of a channel to enable the comparison of the morphological evolution of the endothelial cells. **A)** Endothelial cells 2 hours-post seeding, after the reinversion of the chip. As visible, the endothelial cells were able to attach to the top surface of the channels but it was impossible to distinguish their presence or absence on top of the tissues. **B)** Endothelial cells started to lose their round-shaped morphology at day 1 of culture, showing some signals of induced stress. **C)** After 5 days in culture, the endothelial cells were highly stressed with a major cell death associated. All the micrographs correspond to bottom views of the working device and the scale bars were set using the Fiji Software.

Along the days in culture, it was also visible that the endothelial cells started dying, whereas the alive ones where exhibiting morphological signs of induced stress, identified by the loss of their round-shaped morphology to a more elongated one; and it was also noticed an increase in the EC-EC communications, probably because they were trying to adapt their collective architecture to minimize the sensed stress [113]. This stress was possibly brought by the contact of the endothelial cells with the CM+Gal+LowIns+T3+IGF+Glu+HS medium (present in the petri dish) due to lack of proper sealing of the inlets and outlets. Parallel to that, the bottom-placed tissues that are directly exposed to the BPEL medium also started being negatively affected after a couple of days post-seeding of the endothelial cells, by starting to exhibit lower beating frequencies. All these findings clearly revealed the extreme importance of finding a matching medium suitable for co-culturing cardiomyocytes and endothelial cells in this fluidic device.

3.2. Matching Medium Formulation

In order to attempt to develop a matching medium adequate to the co-culture system, a combination of a CM-derived medium with a BPEL-derived medium was formulated and whose preparation is fully detailed in Appendix “Preparation of the BPEL+CM+VEGF+SB+IGF+HS Medium”.

This matching medium formulated had some prior known restrictions factors, namely the desired maintenance of the glucose levels to physiological-relevant values (around 5 mM) which led to the removal of the IMDM and Ham's F12 Nutrient Mix components from the BPEL-derived medium since they confer high levels of glucose to the medium, in fact, levels around 15 mM; and highly important for the co-culture of the engineered cardiac tissues, the removal of the ITS-X (100X) component from the BPEL-derived medium since it confers high-levels of insulin to the medium that is a known cardiac contractility inhibitor [114]. On the other hand, given that most of the others components that comprise the original BPEL medium were common to the CM medium, they were kept in the formulation of the BPEL-derived medium in their regular concentrations. Additional to these components, the supplementation of the BPEL-derived medium with VEGF and SB was known to be crucial from the beginning for enabling a viable co-culture including endothelial cells.

Concerning the CM-derived medium, some of their components were known to be essential for the cardiomyocytes, hence they were extended to the formulation of the CM-derived medium, namely: galactose; glucose; ITS-X component, since in the CM medium it is added in a low concentration, it might help to promote the switch from the glycolysis to the oxidative phosphorylation pathway since high-levels of insulin regulate the glycolysis mechanism [115]; DMEM component since it is a source of vitamins, amino acids, salts and others, clearly important to be added since the principal sources of these components in the BPEL-derived medium were withdrawn (IMDM and Ham's F12 components) and sodium carbonate since it helps to maintain the pH of the medium to physiological levels.

All the other components that comprise the regular CM+Gal+LowIns+T3+IGF+Glu+HS medium were individually tested since their presence for the cardiomyocytes was important but not mandatory, while their influence in the endothelial cells was completely unknown. Thus, all the components listed in Table 2 from Appendix "Preparation of the CM+Gal+LowIns Medium", plus the T3, IGF and HS components, were individually added to the formulated BPEL+CM medium supplemented with VEGF and SB, and tested in a culture of hiPSC-derived cardiac endothelial cells. The supplementation with IGF and HS was defined based on the next experiments.

3.3. Validation of the Matching Medium for Culturing Endothelial Cells

3.3.1. Morphological Analysis

For the aforementioned experiment, a culture of hiPSC-derived cardiac endothelial cells was seeded at a density of 1×10^4 cells/mL in BPEL+VEGF+SB medium in a 96-well format. On day 1 after the seeding, the medium from the wells was switched to the several testing combinations (BPEL+CM+VEGF+SB plus the testing component) in order to assess the behavior of the endothelial cells to each component belonging to the CM medium. The endothelial cells were also tested in BPEL+CM+VEGF+SB medium without any other supplementation and in the CM+Gal+LowIns+T3+IGF+Glu+HS medium. Each combination was tested in 2 wells in order to have replicates that could provide meaningful results. Micrographs were taken 4, 5 and 6 days-post seeding and compared against the micrographs concerning the control wells (in BPEL+VEGF+SB medium)

through three different criteria, each one visually evaluated in a scale from 1 (minimum) to 5 (maximum); in where the assignment of 5 meant that the testing well greatly resemble the control one in that criteria. Specifically, the three criteria evaluated were the proneness of the medium to enable the formation of a monolayer of hiPSC-derived endothelial cells and the grouping of the cells in a cobblestone-like structure and finally, the morphology of the cells that should ideally look flat and round-shaped. The final evaluation of each testing medium resulted from the sum of the score of the three criteria and can be found summarized in Figure 42.

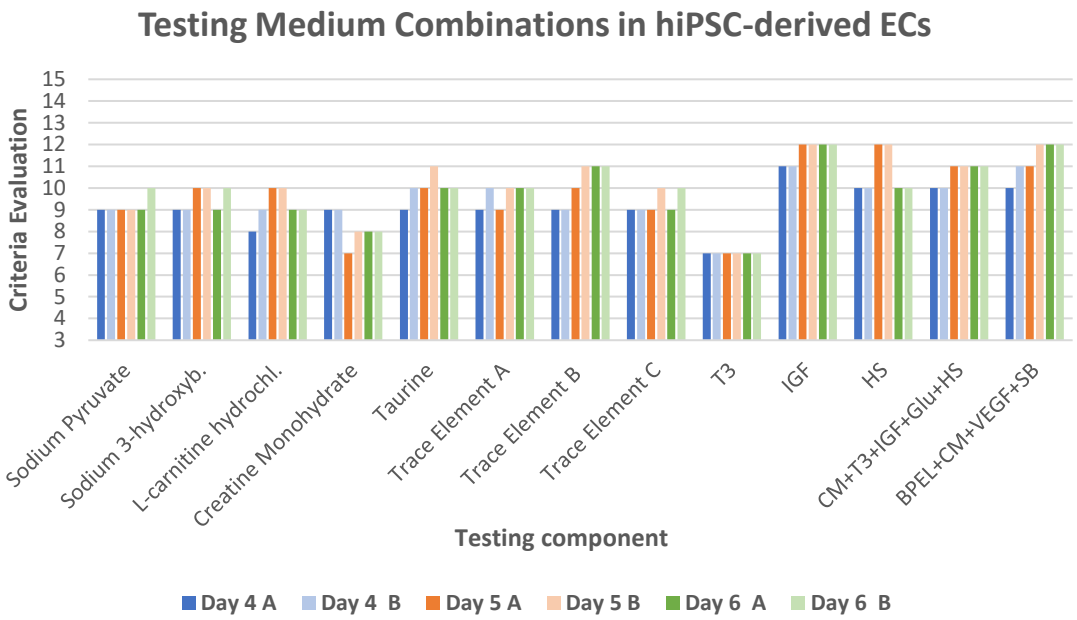

Figure 42: Representative illustration of the results obtained for each testing component added to the matching medium in study (BPEL+CM+VEGF+SB) and for the CM+T3+IGF+Glu+HS and BPEL+CM+VEGF+SB media 4 days post-seeding, 5 days post-seeding and 6 days post-seeding.

The presented results are discriminated for both replicates (A and B) for each condition in test and for each day. As visible by the bars, the medium in study (BPEL+CM+VEGF+SB) and the testing components IGF and HS were the components that provided the most positive effect in the cells in culture.

As seen in Figure 42, the IGF (insulin-like growth factor) and the HS (horse serum) were the components added to the matching medium in study (BPEL+CM+VEGF+SB) that had the most positive effect in the cells in culture, by more closely resembling the ones being cultured in the control medium (BPEL+VEGF+SB), as visible by the representative micrographs presented in Figure 43. In its turn, the matching medium in study, without any other supplementation, also led to some optimistic outcomes regarding the viability of using this medium to culture endothelial cells. On the other hand, the T3 hormone was the component that played the most negative effect in the cells in question, in fact as expected, since thyroid hormones are well-known activators of the transcriptional activity of recognized vasoconstrictors [116].

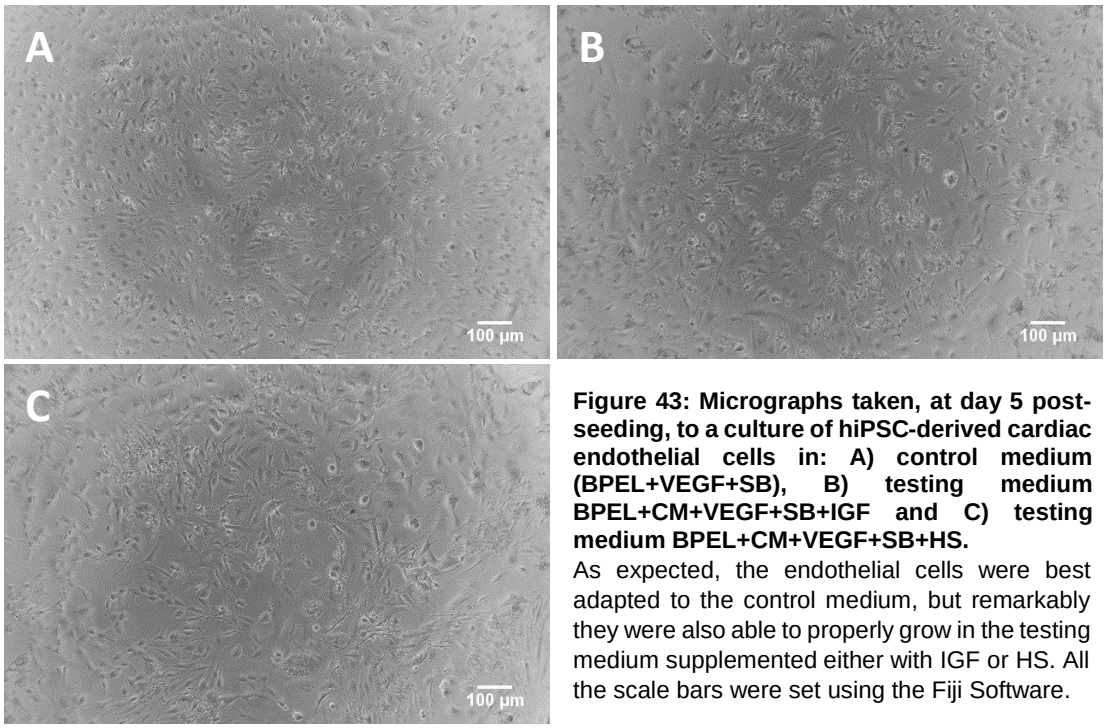

Figure 43: Micrographs taken, at day 5 post-seeding, to a culture of hiPSC-derived cardiac endothelial cells in: A) control medium (BPEL+VEGF+SB), B) testing medium BPEL+CM+VEGF+SB+IGF and C) testing medium BPEL+CM+VEGF+SB+HS.
As expected, the endothelial cells were best adapted to the control medium, but remarkably they were also able to properly grow in the testing medium supplemented either with IGF or HS. All the scale bars were set using the Fiji Software.

As visible by the micrographs of Figure 43, the endothelial cells cultured in the testing mediums supplemented with IGF and HS were able to positively adapt themselves to these mediums, showing only some residual signs of induced stress. Nevertheless, the monolayer formation and the grouping of the cells in a cobblestone-like structure was visibly close to the one exhibited by the control cells. Thus, from this point forward, the project was focused in the attempt of validating the BPEL+CM+VEGF+SB+IGF+HS medium as matching medium for co-culturing endothelial cells and cardiomyocytes.

The first step given in that direction was accomplished after culturing the endothelial cells in this final formulated medium (BPEL+CM+VEGF+SB+IGF+HS) and obtaining results as the ones presented in Figure 44.

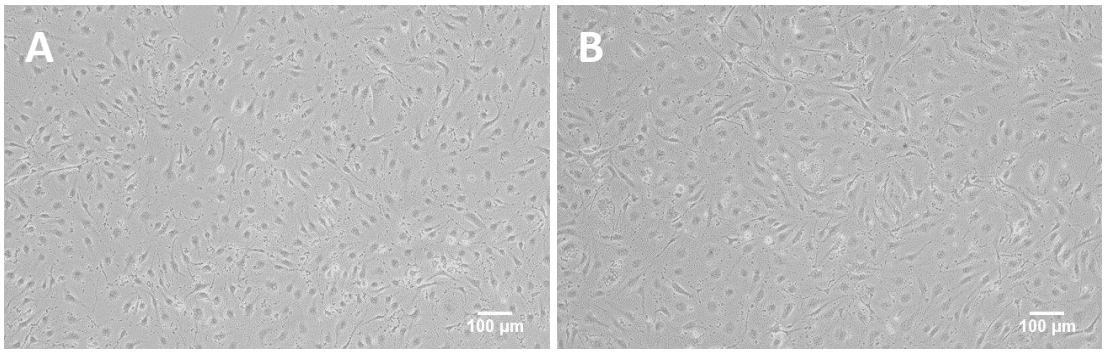

Figure 44: Micrographs taken at day 7 post-seeding of a culture of hiPSC-derived cardiac endothelial cells in: A) BPEL+VEGF+SB (control medium) and B) BPEL+CM+VEGF+SB+IGF+HS (matching medium).
Surprisingly, after the simultaneous addition of IGF and HS to the matching medium in study, it was visible that the cultured endothelial cells greatly resemble the ones in the control medium in every criteria possible to be visibly analyzed. All the scale bars were set using the Fiji Software.

After the simultaneous supplementation with IGF and HS to the matching medium in study (BPEL+CM+VEGF+SB), the obtained results were quite positive, revealing a perfect monolayer of endothelial cells in a visible cobblestone-like structure and in their majority round-shaped; giving in this way the first morphological evidences of the viability of using this new formulated medium to culture, at least, endothelial cells. As visible by Figure 44, the endothelial cells cultured in the matching medium were almost completely identical, morphologically speaking, to the ones in the control medium.

3.3.2. Flow Cytometry Analysis

In addition to the morphological analysis, the efficacy of using this matching medium (BPEL+CM+VEGF+SB+IGF+HS) for culturing endothelial cells was also evaluated and quantified though fluorescence analysis, of endothelial cells previously stained with the anti-human-CD31-APC conjugated antibody, by flow cytometry (Figure 45).

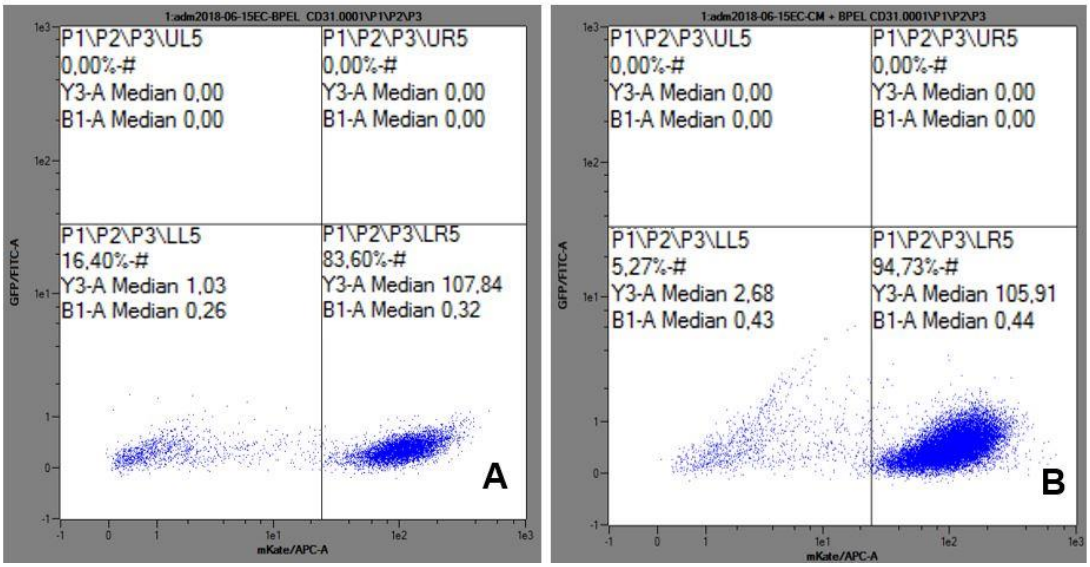

Figure 45: Flow cytometry analysis of endothelial cells stained with the anti-human-CD31-APC conjugated antibody and cultured using different media: A) BPEL+VEGF+SB and B) BPEL+CM+VEGF+SB+IGF+HS. Gating for Allophycocyanin (APC-A) (x axis) that is a fluorescent molecule that is chemically-crosslinked to the antibody to enable the identification of the CD31 positive cells ($CD31^+$) in each sample by fluorescence-based detection. As visible by the data plots, remarkably, a higher percentage of CD31 positive cells was obtained in the experimental medium (BPEL+CM+VEGF+SB+IGF+HS) than in the control medium (BPEL+VEGF+SB).

CD31, also known as platelet endothelial cell adhesion molecule-1 (PECAM-1), is a cell adhesion molecule and signaling receptor [117], expressed at high levels on early and mature endothelial cells and reported to be involved in cell migration and angiogenesis processes [118], being believed to be one of the main specific markers for endothelial cells.

As visible by Figure 45, around 84% of the cells in the control medium (BPEL+VEGF+SB) were positive for the CD31 cell surface marker, while around 95% were positive for this marker in the experimental medium in study (BPEL+CM+VEGF+SB+IGF+HS). This result showed that even a higher percentage of cells were positive for the CD31 marker in the matching medium, admittedly presenting an endothelial identity, giving the second validation proof of the viability of using this medium to culture endothelial cells. The higher percentage of positive endothelial cells in the matching medium can be justified by the

fact of this medium being composed by a serum component that is a well-known spreading factor in endothelial cells cultures [119]. Moreover, the validation of the model provided by the flow cytometer can be found in Appendix “Validation of the Flow Cytometry Model”.

3.4. Validation of the Matching Medium for Culturing Cardiomyocytes

After having enough evidences of the applicability of this medium to culture endothelial cells, the matching medium in study (BPEL+CM+VEGF+SB+IGF+HS) was used as the only culture medium in the fluidic device (including in the channels) from the moment post-seeding in order to assess the behavior of the fibrin-based cardiac tissues upon the exposure to this medium. In this set of experiments, the endothelial cells were labeled with a DiD®-labelling solution, to enable their distinction under the microscope by fluorescence imaging, and seeded in a reservoir setup, designed to be bonded to the top of the glass stack, instead in the channels, to allow the later imaging using confocal microscopy. The molded channels were designed to have a low thickness (0,9 mm) (see Section “Design of the Negative Mold of the Channels”), but deviations associated to the milling machine used, led to a final height of the frame of 1,2 mm, limiting their imaging using the confocal microscope.

3.4.1. Reservoir Design

The reservoir layer is composed by two rows of 4 holes with 5 mm of diameter each and whose center points perfectly align with the center points of the holes of the triple-layered glass stack. The external dimensions of the reservoir, the spatial distribution of the holes, as well as the distance of crucial points to its edge are properly reported in Figure 46. The reservoir was projected to confine the area of seeding of the endothelial cells, in order to assure that on top of every tissue endothelial cells could be present.

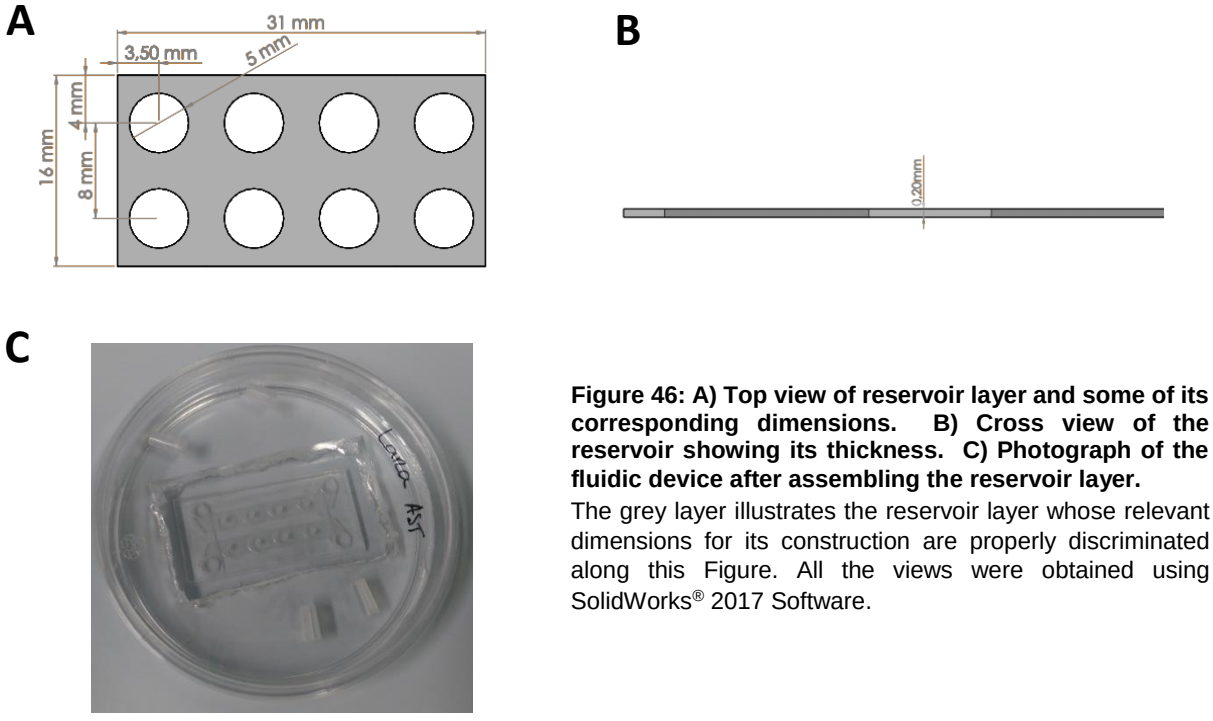

Figure 46: A) Top view of reservoir layer and some of its corresponding dimensions. B) Cross view of the reservoir showing its thickness. C) Photograph of the fluidic device after assembling the reservoir layer.
The grey layer illustrates the reservoir layer whose relevant dimensions for its construction are properly discriminated along this Figure. All the views were obtained using SolidWorks® 2017 Software.

3.4.2. Morphological Analysis

For the aforementioned experiment, involving the culture of both cardiac tissues and endothelial cells using the formulated matching medium, it was used an endothelial cell density of 5×10^5 cells/mL since after several attempts of optimization, this was the cell density that enabled the formation of a viable monolayer of endothelial cells in the coated surface. Some of the results obtained for this experiment are shown in Figure 47.

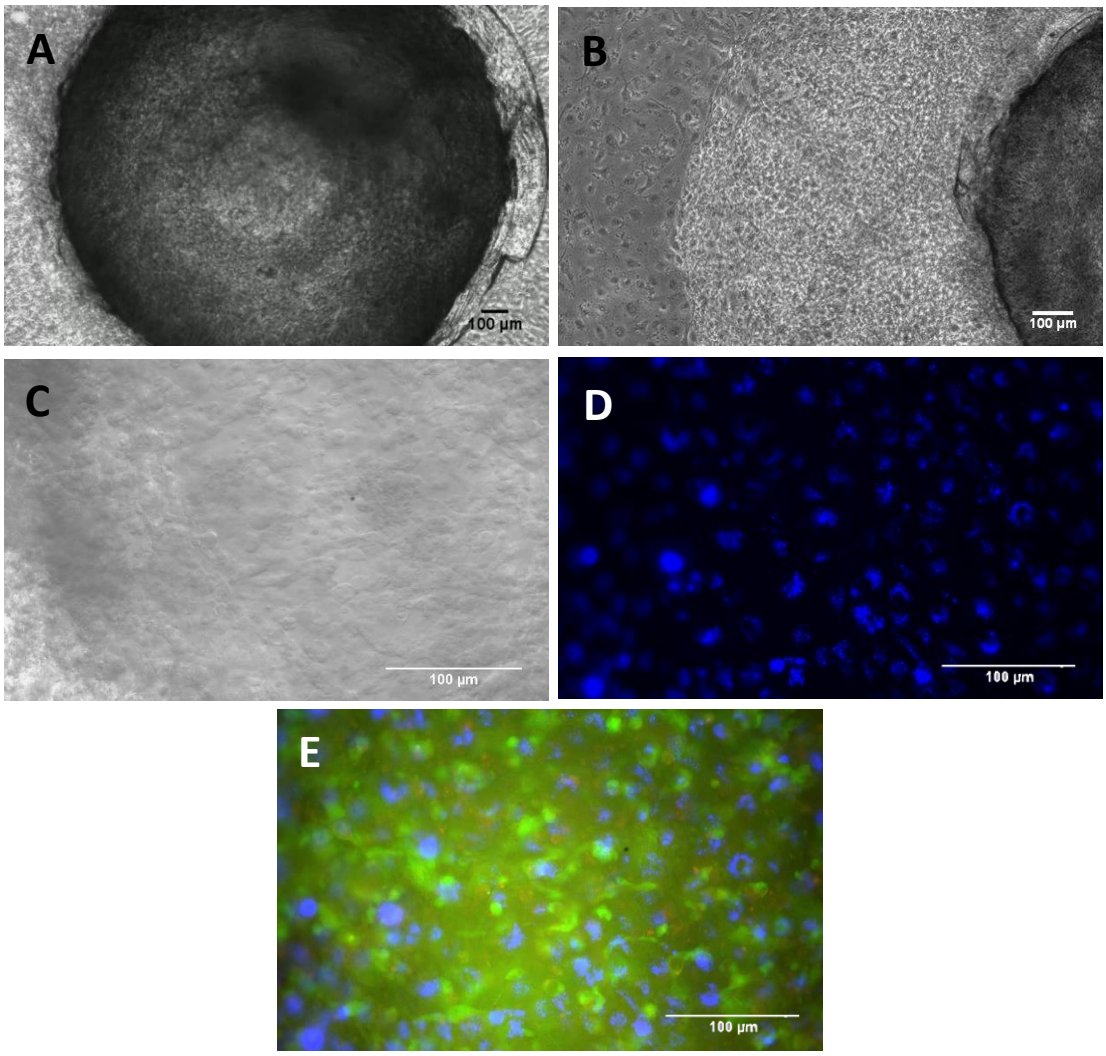

Figure 47: Brightfield and fluorescence micrographs taken at day 4 post-seeding to the co-culture system englobing cardiomyocytes and endothelial cells, both being cultured in the fluidic device using BPEL+CM+VEGF+SB+IGF+HS medium.
A) Brightfield micrograph concerning a top view of a fibrin-based cardiac tissue that was seeded on top with endothelial cells. The fibrin-based cardiac tissue started beating as a synchronous contracting tissue at day 4 post-seeding, showing the positive effect of the formulated matching medium for culturing cardiomyocytes, as well. **B)** Brightfield micrograph concerning a top view of the extremity of a fibrin-based cardiac tissue, where it is visible the monolayer of endothelial cells formed, at least, around the tissue. Pictures C, D and E concern micrographs taken from a fixed position in the center of the tissue. **C)** Brightfield micrograph. **D)** Fluorescence micrograph taken to the monolayer of endothelial cells stained with a DiD®-labelling solution, to which was applied a blue color filter resorting to Fiji Software. **E)** Overlapping of several fluorescence micrographs taken to the endothelial cells, cardiomyocytes and sarcomeres planes to which were applied a blue, green and red color filter, respectively, using the Fiji Software. All the micrographs were taken using the Nikon Eclipse Ts2 microscope and the scale bars were set using the Fiji Software.

In the experiment shown in Figure 47, both cardiomyocytes and endothelial cells were seeded at the same day in the fluidic device using BPEL+CM+VEGF+SB+IGF+HS medium. Remarkably, the formed fibrin-based cardiac tissues started beating as a whole at day 4 post-seeding in this new formulated medium, at a synchronous pace, showing the positive effect of this medium over the cardiomyocytes; therefore, giving the final validation proof of the viability of using this medium not only to culture endothelial cells, but cardiomyocytes as well. Moreover, the tissue engineered-cardiac constructs were kept under culture for longer than one month, without exhibiting any signs of induced stress or morphological instability, possible due to the cardiomyocyte-endothelial paracrine signaling established in this culturing system that may greatly contribute to enhance the tissue survival *in vitro* [120].

It is also visible from micrograph 47B that the endothelial cells density used, enabled the formation of a monolayer of these cells visible around the tissues under brightfield illumination and extended until the limits of the reservoir; although not being possible to distinguish the presence or absence of endothelial cells over the tissues from this micrograph. On the other hand, under fluorescence illumination, it was clear that the endothelial cells were able to aggregate themselves into an intact monolayer on top of the seeded tissues as well, as visible by micrographs 47D and 47E. The efficiency of the staining procedure of the endothelial cells was found to be very high, easily allowing the clear distinction of these cells from the remaining cardiac tissue.

3.5. Migration of the Endothelial Cells

Two days after the previous results, it was no longer possible to observe the same amount of stained endothelial cells on top of the tissues, as noticeable by micrographs 48B and 49B. This drastic decrease in the population of stained endothelial cells, in a timeframe of only 2 days of culture, could be due to multiple reasons, among them the possible reduced lifetime of the fluorescent dye, simple cell death or the expectedly migration of the endothelial cells into the tissue.

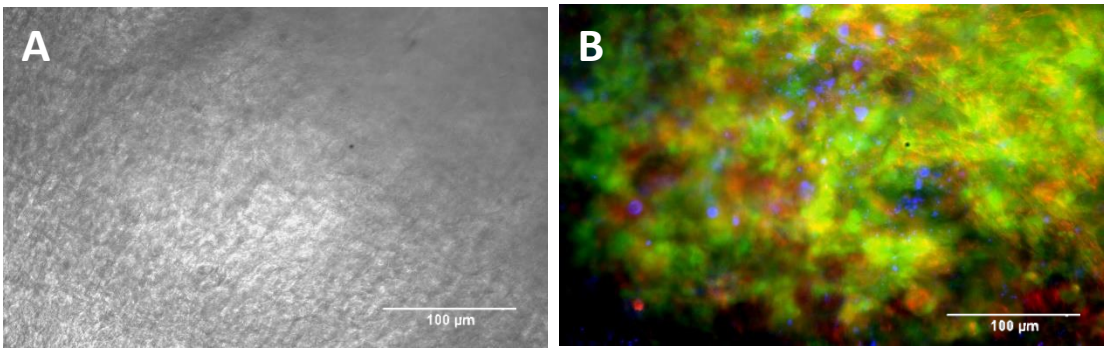

Figure 48: Brightfield and fluorescence micrographs taken at day 6 post-seeding of the co-culture system englobing cardiomyocytes and endothelial cells, both being cultured in the fluidic device using BPEL+CM+VEGF+SB+IGF+HS medium.
A) Brightfield micrograph taken to a position in the center of a tissue. **B)** Fluorescence micrograph, taken in the same position as the micrograph A, showing a much lower density of endothelial cells on top of the cardiac tissue, comparing to the micrographs taken at day 4 post-seeding. The color filters applied concern the same subjects as in Figure 47. All the micrographs were taken using the Nikon Eclipse Ts2 microscope and the scale bars were set using the Fiji Software.

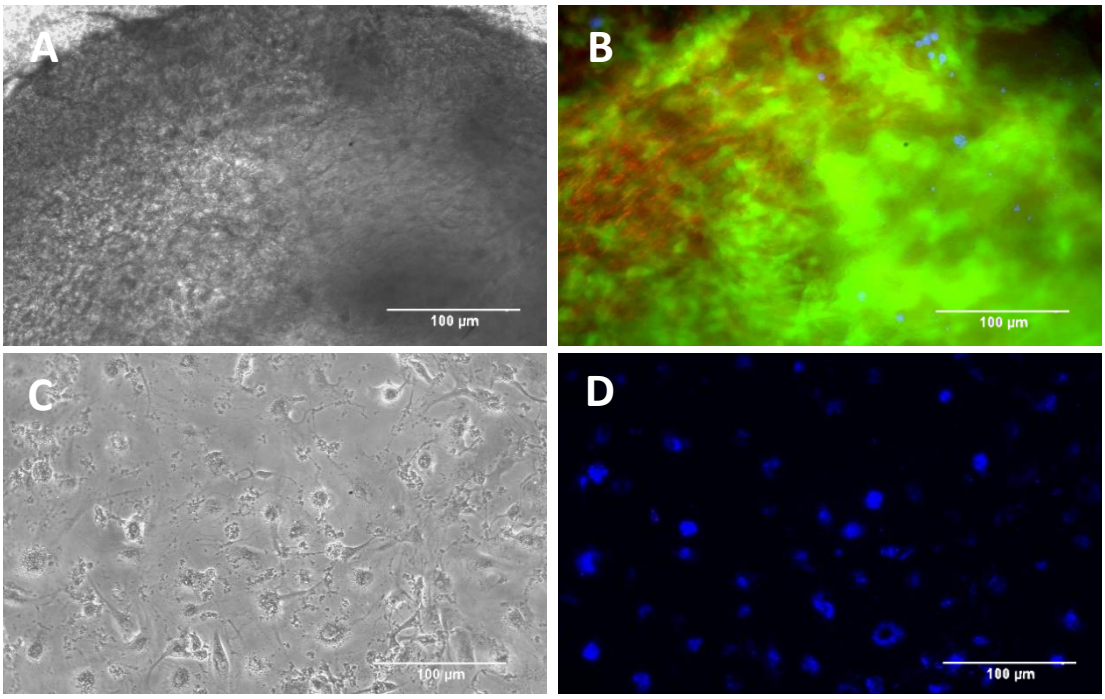

Figure 49: Brightfield and fluorescence micrographs taken at day 6 post-seeding of the co-culture system englobing cardiomyocytes and endothelial cells, both being cultured in the fluidic device using BPEL+CM+VEGF+SB+IGF+HS medium.

A) Brightfield micrograph taken to an extremity of a tissue. **B)** Fluorescence micrograph, taken in the same position as the micrograph A, showing just a few endothelial cells, no longer being possible to observe a monolayer. **C)** Brightfield micrograph taken to the extremity of the reservoir. **D)** Fluorescence micrograph, taken in the same position as the micrograph C, showing still the presence of a monolayer of endothelial cells. The color filters applied concern the same subjects as in Figure 47. All the micrographs were taken using the Nikon Eclipse Ts2 microscope and the scale bars were set using the Fiji Software.

The remote hypothesis of the lifetime of the fluorescent dye being decreasing rapidly was immediately withdrawal from the range of possibilities after imaging the extremity of the reservoir, since it was still possible to observe nicely stained endothelial cells in this region, as visible by micrograph 49D. To analyze the hypothesis of the recruitment of the endothelial cells into the tissue, a confocal microscopic analysis was performed, given that confocal microscopy allows the capturing of multiple 2D images at different depths of the tissue, enabling the subsequent reconstruction of its 3D-structure.

3.5.1. Confocal Analysis

The confocal microscope was used to image the center of several tissues and the reconstruction of their 3D-structure was accomplished through the overlap, according to the z-axis, of all the stacks taken with the system, resulting in a Z-stack projection, resorting to ImageJ Software.

In Figure 50A and 50B, the maximum intensity projection of the Z-stacks created from a 20x magnification and from a 60x magnification are, respectively, depicted. The maximum intensity projection concerns the creation of an output image whose pixels represent the maximum value over all the images that compose the stack, in that particular location of the pixel.

From the analysis of the Z-stack obtained for each magnification, it was possible to start by observing a monolayer of endothelial cells on top of the tissue, as expected, and then, planes that include cardiomyocytes (and endothelial cells), followed by planes that continue to comprise endothelial cells. Overall, this is an indication of endothelial cell migration within the cardiac tissue.

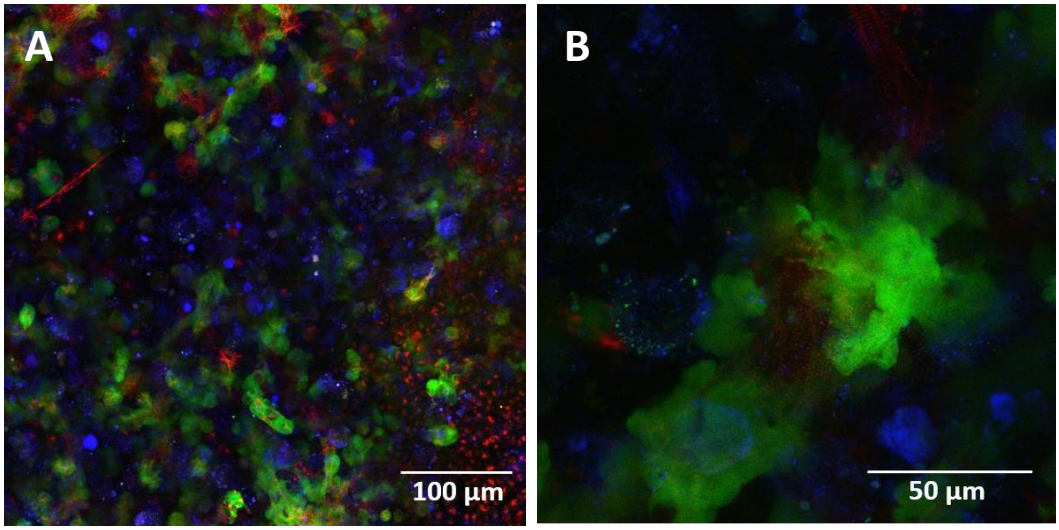

Figure 50: Maximum intensity projection obtained for the Z-stacks projected for a center of a fibrin-based cardiac tissue seeded with endothelial cells on its top.
Picture A concerns a 20x magnification and picture B concerns a 60x magnification. The projection of the Z-stack and the maximum intensity projection output were achieved using Fiji Software.

The migration of the endothelial cells can be explained by the supplementation to the medium with the vascular endothelial growth factor (VEGF) that is a critical inducer of the endothelial cell migration, mainly through the activation of the phosphatidylinositol 3-kinase (PI3K) and the GTPase Rac-1 pathways [121]. When the VEGF is diffusibly distributed, due to its widespread in the culture medium, endothelial cells can sense it and start slowly to migrate in random directions [122].

Unfortunately, due to time restraints, this was the last possible result. Nevertheless, after observing the initial recruitment of the endothelial cells into the tissue, it was clear that the present strategy is a promising methodology and futher insights on the utility of such engineered-constructs will be given in the next Chapter “Conclusions & Future Perspectives”.

V. Conclusions and Future Perspectives

In the project under study, the optimization of a fluidic device that allows the culture of hESC-derived fibrin cardiac tissues, providing the right cues for its development in a spontaneously and synchronously contracting construct, was successfully accomplished. The optimal seeding and culturing conditions to enable the complete remodel of these cellular structures was also achieved. Thanks to the troubleshooting, insight could be gained concerning the different parameters that influence the successful casting and formation of the tissues inside the fluidic device.

Moreover, the established fluidic device easily can support the scaling up of the engineered construct through several practical ways, conferring a distinct advantage over other fluidic devices. Nevertheless, the current dimensions of the engineered cardiac tissue are already up to the common dimensions of other similar approaches, being set in the millimeter-range. Additionally, the established platform allows the generation of multiple tissue-engineered cardiac constructs per device, also presenting an advantage over other established devices.

However, adjustments should be performed to the culture conditions, specifically regarding the use of serum-free media, since serum components lead to poor reproducibility between each experiment due to the serum dependent composition on the status of the donor animal [123]. Furthermore, the presence of unknown animal-derived factors limits the potential use of the cardiac model for therapeutic applications [123].

To attempt to promote the long-term survival of these structures, a co-culture approach including hiPSC-derived cardiac endothelial cells was brought to the fluidic device, aiming to promote the formation of vascular system in the engineered constructs. Factors such as the incompatibility of media, that interfered in the successful co-culture of both cells, were also identified and optimized allowing the subsequent formation of a visible monolayer of endothelial cells on top of the engineered constructs. The visualization of the monolayer was accomplished after applying a cell fluorescent stain to the endothelial cells. Nevertheless, an optimization to this strategy should be performed by using specific endothelial markers.

The migration of the endothelial cells into the tissue, possibly due to the supplementation of the medium with a pro-angiogenic factor, namely the vascular endothelial growth factor (VEGF), provided ground work to further develop the sprouting and formation of vascular network-like structures that could lately be perfused with culture medium, allowing the survival of increasingly thicker constructs. For that, several approaches can be followed, where can be highlighted the co-culture with fibroblasts, pro-angiogenic factors gradients and/or flow and pressure gradients.

The sprouting process is initiated when the endothelial cells start receiving pro-angiogenic signals, through paracrine signaling, that are released in their environment due to an increase demand within the tissue construct for oxygen and nutrients [124]. Some of the potential initiators of this sprouting process are the VEGF, fibroblast growth factor (FGF), angiopoietins and hypoxia inducible factors, for instance [124]. Hence, the angiogenic response of the endothelial cells can be manipulated through

extracellular gradients created using these pro-angiogenic factors, that will act as chemoattractant, inducing the cells to degrade their ECM, detach and sprout towards the gradient, directing the capillary growth [125]. For instance, Shin et al. (2011) had reported the collective sprouting angiogenesis process of endothelial cells under angiopoietin-1 (ANG-1) and VEGF gradients [105].

Also, apart from being involved in the migration and sprouting of endothelial cells [63], fibroblasts can also induce the tube formation in the sprouting process by the release of tubulogenesis-stimulating molecules, indispensable for lumen formation [124]. For instance, Newman et al. (2011) reported that in the absence of these fibroblast matrix-derived proteins, the endothelial cell sprouting could still occur but the formation of tubular-like structures failed to happen [126], revealing the importance of using co-culture systems including fibroblasts.

Moreover, endothelial cells are consistently subjected *in vivo* to fluidic shear stress resulting from the blood flow that circulates in each vessel; therefore the test of different flow conditions should also be taken into account when implementing vascularization strategies *in vitro* [127]. For instance, Hsu et al. (2001) reported that laminar and disturbed flows highly enhanced the endothelial cell migration *in vitro* [128]. Additionally, endothelial cells are also continuously exposed to high blood pressure *in vivo*, hence the application of pressure gradients should also be a concern, since they can induce morphological and mechanical responses in endothelial cells, as guiding the sprout elongation process, as reported by Ghaffari et al. (2015), for instance [129].

Despite not making part of the scope of the project, the development of appropriate cues to further promote the *in vitro* maturation of the cardiac engineered constructs could also be brought to analysis. For instance, mechanical stimulation either in the form of pulsatile flow or through cyclic stretch mechanisms and/or electrical stimulation with modulation of the frequency, pulse duration and other parameters have been reported to highly improve the maturation of engineered heart tissues *in vitro* [11]. In order to support these types of stimulation, some designing alterations may have to be performed to the fluidic device, but they would be highly beneficial for the underlying project.

To summarize, a novel fluidic device has been optimized to enable efficient co-culture between cardiomyocytes trapped in a fibrin matrix and endothelial cell monolayers. Here, promising results have been collected towards the prospect of formation of a primary network through the cardiac construct. Hence, the technology presented has an undoubtable value for advancing applications, especially in the field of vascularization for tissue engineering and regenerative medicine purposes.

VI. Appendixes

Appendix 1: Coating with Vitronectin

The vitronectin stock should be kept on ice during the entire procedure to avoid gelatinization. To coat a 6-well plate, the vitronectin stock was diluted to a concentration of 5 µg/mL in DPBS from where was taken 1 mL to add to each well. The 6-well plate was then incubated for 60 minutes at room temperature. After the incubation period, the plate was ready to be used; otherwise was stored at 4°C.

Appendix 2: Coating with Matrigel

Similar to the vitronectin, the Matrigel stock should be kept on ice during the entire procedure to prevent gelatinization. Firstly, the Matrigel stock was diluted to a concentration of 83 µg/mL, considering the coating of 6-well plates, using serum-free medium (DMEM-F12) (Gibco®, Life Technologies) and ice-cold pipette tips. Then, 1 mL of the prepared dilution was added to each well followed by the incubation of the plate for 60 minutes at room temperature. Afterwards, the plate could be used or stored for future experiments at 4°C.

Appendix 3: Coating with Fibronectin

To coat a 6-well plate, the fibronectin stock was diluted to a concentration of 50 µg/mL in DPBS; the stock should be kept on ice during the entire procedure. Then, 2 mL of the prepared dilution was added to each well that was thereafter incubated for 2 hours at 37°C. After the incubation period, the plate was ready to be used; otherwise was stored at 4°C.

Appendix 4: Preparation of the Fibrinogen Stock

The stock solution of fibrinogen was prepared at a concentration of 5 mg/mL (from a stock of 20 mg/mL in a 0,9% warm saline solution at 37°C), followed by the filtration of the solution using a sterile syringe (BD plastipak) and a sterile filter (Minisart®) with 0,2 µm of pore size. The filtered solution was aliquoted in plastic tubes and stored at 4°C for short-term periods or at -20°C for long-term periods.

Appendix 5: Preparation of the Aprotinin Stock

The stock solution of aprotinin was prepared at a concentration of 250 µg/mL in water followed by its filtration using a sterile syringe and a 0,2 µm filter. The solution was aliquoted in plastic tubes and store at 4°C for short-term storage or at -20°C for long-term storage.

Appendix 6: Preparation of the Thrombin Stock

The stock solution of thrombin was prepared at a concentration of 100 NIH units/mL (1 NIH unit = 0.324 ± 0.073 µg) in a 0,1% (w/v) BSA (Bovostar) solution in DPBS, following the manufacturer's instruction. Similar to the fibrinogen and the aprotinin, the stock solution was aliquoted in plastic tubes and kept at 4°C for short-term usages or stored at -20°C for long-term storage.

Appendix 7: Preparation of the BPEL Medium

Batches of 1L (1000 mL) of BPEL medium were prepared at a time. The BPEL medium is comprised by the components mentioned in Table 1, added without any specific order, but taken into account the following working solutions: BSA 10x (in IMDM), PVA 5% (w/v) (in cell culture grade water), αMTG (13 µL/mL in IMDM) and AA2P (5 mg/mL in water).

After adding all the components together, a sterile filtration was performed using a Stericup-GV sterile vacuum filtering system (Merck Millipore) with a pore size of 0,22 µm. The medium was then aliquoted and kept at 4°C for short-term storage or at -20°C for long-term storage.

Table 1: Formulation of the serum-free BPEL medium. All the listed components were added taking into consideration the preparation of a final medium volume of 1000 mL. The suppliers used for ordering each component are also discriminated in this listing.

Component	Supplier	For 1 L (1000 mL)
Iscove's Modified Dulbecco's Medium (IMDM), no phenol red	Gibco®	430
Ham's F12 Nutrient Mix, GlutaMAX™ Supplement	Gibco®	430
PFHM-II (Protein Free Hybridoma Medium-II)	Gibco®	50
Chemically Defined Lipid Concentrate	Gibco®	10
Insulin-Transferrin-Selenium-Ethanolamine (ITS-X) (100X)	Gibco®	5
GlutaMAX™ Supplement	Gibco®	10
Penicilin-Streptomycin (5000 U/mL)	Gibco®	1
Poly(vinyl alcohol) (PVA)	Sigma-Aldrich®	25
1-Thioglycerol (αMTG)	Sigma-Aldrich®	3
L-Ascorbic acid 2-phosphate sesquimagnesium salt hydrate (AA2P)	Sigma-Aldrich®	10
Bovine Serum Albumin (BSA)	Bovostar	25

Appendix 8: Preparation of the CM+Gal+LowIns Medium

Batches of 1L (1000 mL) of CM+Gal+LowIns medium were prepared at a time. The CM+Gal+LowIns medium is comprised by the components mentioned in Table 2 that were added without any specific order, expecting the sodium hydrogen carbonate ($NaHCO_3$) that should be the last to be added, to bring the final medium concentration of sodium to the pretended value (148 mM). Similar to the BPEL medium, the working solution of the AA2P compound is 5 mg/mL in water.

Table 2: Formulation of the CM+Gal+LowIns medium. All the listed components were added taking into consideration the preparation of a final medium volume of 1000 mL. The suppliers used for ordering each component are also discriminated in this listing.

Component	Supplier	For 1 L (1000 mL)
Dulbecco's Modified Eagle Medium (DMEM)	Gibco®	8,3 g
Galactose	Sigma-Aldrich®	1,8 g
Sodium Pyruvate	Sigma-Aldrich®	5 mL
Sodium 3-hydroxybutyrate	Sigma-Aldrich®	0,024 g
L-carnitine monohydrate	Sigma-Aldrich®	0,1 g
Creatine monohydrate	Sigma-Aldrich®	0,15 g
Taurine	Sigma-Aldrich®	0,626 g
Phenol Red	Sigma-Aldrich®	0,011 g
Distilled Water	Gibco®	957 mL
Trace elements A	Corning	1 mL
Trace elements B	Corning	1 mL
Trace elements C	Corning	1 mL
Chemically defined lipid concentrate	Gibco®	10 mL
GlutaMAX Supplement™	Gibco®	10 mL
1-Thioglycerol (α-MTG)	Sigma-Aldrich®	0,39 µL
Insulin-Transferrin-Selenium Ethanolamine (ITS-X)	Gibco®	100 µL
L-Ascorbic acid 2-phosphate sesquimagnesium salt hydrate (AA2P)	Sigma-Aldrich®	10 mL
Penicillin-Streptomycin (P/S)	Gibco®	5 mL
Sodium hydrogen carbonate ($NaHCO_3$)	Sigma-Aldrich®	3,7 g

After adding all the components to the medium solution, $NaOH$ should be added to bring the final pH to physiological relevant values (7,3-7,4). Finally, a sterile filtration was carried out using a Stericup-GV sterile vacuum filtering system with a pore size of 0,22 µm. Afterwards, the medium was aliquoted and kept at 4°C for short-term usage or at -20°C for long-term usage.

Appendix 9: Preparation of the BPEL+CM+VEGF+SB+IGF+HS Medium

The BPEL+CM+VEGF+SB+IGF+HS is composed of a BPEL-derived medium and a CM-derived medium that are mixtured in a ratio 1:1 (v/v) and posteriorly supplemented with 50 ng/mL of VEGF, 5 μM of SB431542, 100 ng/mL of IGF-1 and 10 nM of T3 hormone.

The composition of the BPEL-derived medium and the CM-derived medium are fully discriminated in Table 3 and 4, respectively. The BPEL-derived medium was prepared without any specific order, contrary to the CM-derived medium that has the particularity that the sodium hydrogen carbonate should be the last component to be added for the aforementioned reasons presented in Appendix "Preparation of the CM+Gal+LowIns Medium". The working solutions for the BSA, PVA, αMTG and AA2P components are the same listed in the Appendix "Preparation of the BPEL Medium". The only not mentioned working solution is the glucose concentration that englobes the CM-derived medium that should be of 4,5 mM.

An important detail, is that both mediums should be prepared two times concentrated, in order that after mixing the two mediums together in a ratio 1:1 (v/v), which will dilute two times both mediums, they can exhibit the pretended concentrations.

Table 3: Formulation of the BPEL-derived medium. All the listed components were added taking into consideration the preparation of a final medium volume of 1000 mL. The suppliers used for ordering each component are also discriminated in this listing.

Component	Supplier	For 1 L (1000 mL)
PFHM-II (Protein Free Hybridoma Medium-II)	Gibco®	50
Chemically Defined Lipid Concentrate	Gibco®	10
GlutaMAX™ Supplement	Gibco®	10
Poly(vinyl alcohol)	Sigma-Aldrich®	25
1-Thioglycerol (αMTG)	Sigma-Aldrich®	3
L-Ascorbic acid 2-phosphate sesquimagnesium salt hydrate (AA2P)	Sigma-Aldrich®	10
Bovine Serum Albumin (BSA)	Bovostar	25
Penicillin-Streptomycin	Gibco®	5
Distilled Water	Gibco®	862

Table 4: Formulation of the CM-derived medium. All the listed components were added taking into consideration the preparation of a final medium volume of 1000 mL. The suppliers used for ordering each component are also discriminated in this listing.

Component	Supplier	For 1 L (1000 mL)
Dulbecco's Modified Eagle Medium (DMEM)	Gibco®	8,3 g
Galactose	Sigma-Aldrich®	1,8 g
Distilled Water	Gibco®	1000 mL
Glucose	Sigma-Aldrich®	0,811 g
Insulin-Transferrin-Selenium Ethanolamine (ITS-X)	Gibco®	100 µL
Sodium hydrogen carbonate $(NaHCO_3)$	Sigma-Aldrich®	3,7 g

After the preparation of both mediums, they were filtered together in a Stericup-GV sterile vacuum filtering system (Merck Millipore) with a pore size of 0,22 µm. The final medium was aliquoted and store in the fridge at 4°C for short-term periods or in the freezer at -20°C for long-term periods. Before being applied to the culture system, it was supplemented with the VEGF, SB, IGF and HS components in the aforementioned concentrations.

Appendix 10: Rolling a Thin Layer of PDMS and Toluene

The rolling of a thin layer of PDMS and toluene on top of the channel surface consisted in the preparation of a solution of PDMS and toluene in a proportion of 5:3 (w/w), respectively, followed by the spin-coating of 200 µL of the prepared solution at 100 rpm for 2 minutes on a glass coverslip using a spin coater (Spin 150, Polos). The dilution with toluene intends to reduce the viscosity of the PDMS, allowing the obtention of thinner layers after the spin-coating [130]. Afterwards, an ink roller was used to remove the thin layer from the glass coverslip and to apply it in the PDMS surface that was then aligned and bonded to the vinyl layer by applying a subtle pressure between the layers. The samples were then placed in the oven at 67°C for at least 3 hours to allow the evaporation of the toluene in order to achieve a complete cross-linking between both layers.

Appendix 11: Rolling a Layer of PDMS

The rolling of a layer of PDMS on top of the channel surface was performed according to Appendix “Rolling a Thin Layer of PDMS and Toluene”, with the exception of the dilution step with toluene, in order to allow the testing of thicker layers (only composed of PDMS).

Appendix 12: Rolling a Layer of NOA81

The rolling of a layer of NOA81 on top of the channel surface was also performed according to Appendix “Rolling a Layer of PDMS”, with the exception of using NOA81 instead of PDMS.

Appendix 13: Direct Pipetting of NOA81

The direct pipetting of around 100 µL of NOA81 on the surface of the PDMS channels is self-explanatory. Afterwards, the PDMS layer was aligned and brought together with the vinyl layer, followed by the curing of the NOA81 to allow the posterior formation of an irreversible hard polymer between the layers.

Appendix 14: Calculation of Hydraulic Resistances

The calculation of the hydraulic resistance of a given microfluidic path can be based on the analogous comparison of hydraulic and electrical circuits, establishing correlations of pressure drop to voltage drop, volumetric flow rate to current and hydraulic resistance to electrical resistance, like described by Kwang et al. [111]. Following this analogy, Hagen-Poiseuille's law corresponds analogously to the Ohm's law and can be expressed by the following equation (Equation (i)) [111]:

$$Q = \frac{\Delta P}{R_H} \leftrightarrow \Delta P = Q \cdot R_H \qquad (i)$$

Wherein Q is the total volumetric flow rate $(m^3 \cdot s^{-1})$, ΔP is the pressure drop (Pa) and R_H is the hydraulic resistance $(Pa \cdot m^3 \cdot s^{-1})$.

In its turn, the hydraulic resistance can be defined by the following equation (Equation (ii)) [111]:

$$R_H = \frac{8 \cdot \mu \cdot L}{\pi \cdot {r_H}^4} \qquad (ii)$$

Wherein μ is the viscosity of the fluid $(Pa \cdot s)$, L is the channel length (m) and r_H is the hydraulic radius (m).

The hydraulic radius is a geometric constant that can be expressed as described in Equation (iii) [111]:

$$r_H = \frac{2A}{P} \qquad (iii)$$

Wherein A is the cross-sectional area of the channel (m^2) and P is the wetted perimeter (m). For circular channels, the hydraulic radius is equal to the channel radius (R) , meaning that: $r_H = R$.

For calculating the hydraulic resistance (R_H $(hole)$) offered by each drilled hole (approximate to a circular channel), composing a working setup, Equation (ii) was applied. In where, the channel length corresponds to the thickness of the layer drilled and the channel radius corresponds to the radius of the drilled hole.

After calculating the hydraulic resistance for each individual hole, the hydraulic resistance of a single working setup ($R_H\ (set)$), composed by three holes, was obtained by calculating the resistance in a series circuit, that can be expressed as elucidated in Equation (iv) [111]:

$$R_H\ (set) = R_H\ (hole\ 1) + R_H\ (hole\ 2) + R_H\ (hole\ 3) \qquad (iv)$$

After having the hydraulic resistance of a single working setup and taking into account that the fluid in each channel crosses 4 sets of these, the hydraulic resistance offered by the set of working setups ($R_H\ (total\ set)$) to the passage of fluid, was determined by calculating the resistance in a parallel circuit described by Equation (v) [111]:

$$\frac{1}{R_H\ (total\ set)} = \frac{1}{R_H\ (set\ 1)} + \frac{1}{R_H\ (set\ 2)} + \frac{1}{R_H\ (set\ 3)} + \frac{1}{R_H\ (set\ 4)} \qquad (v)$$

On the other hand, the hydraulic resistance for rectangular microchannels is calculated as the summation of a Fourier series like expressed in Equation (vi) [111]:

$$R_H = \frac{12 \cdot \mu \cdot L}{w \cdot h^3 \cdot \left(1 - \frac{h}{w} \cdot \left(\frac{192}{\pi^5} \cdot \sum_{n-1,3,5}^{\infty} \frac{1}{n^5} \cdot \tan h\left(\frac{n \cdot \pi \cdot w}{2h}\right)\right)\right)} \qquad (vi)$$

Wherein w is the width of the channel (m) and h is the height of the channel (m).

In cases when the aspect ratio is high $(e.g. \frac{h}{w} \ll 1)$, the hydraulic resistance of the rectangular channel can be assumed as stated in Equation (1) [111]:

$$R_H = \frac{12 \cdot \mu \cdot L}{w \cdot h^3} \qquad (1)$$

By approximating the geometry of the designed channels to rectangular-shaped and using an aspect ratio that satisfies the aforementioned condition, Equation (1) was used to test different pairs of values of widths and heights that could ensure a hydraulic resistance in the channels inferior to the hydraulic resistance in the holes above it.

Appendix 15: Validation of the Flow Cytometry Model

To validate the flow cytometry model, negative samples, not stained with the anti-human-CD31-APC conjugated antibody, were also subjected to a flow cytometric analysis (Figure 51).

As expected, negligible percentages of CD31 positive cells were found in the negative samples, specifically 0,07% for the BPEL+VEGF+SB medium and 0,17% for the BPEL+CM+VEGF+SB+IGF+HS medium, validating in this way the flow cytometry model that provided the final validation proof of the viability of the matching medium in course.

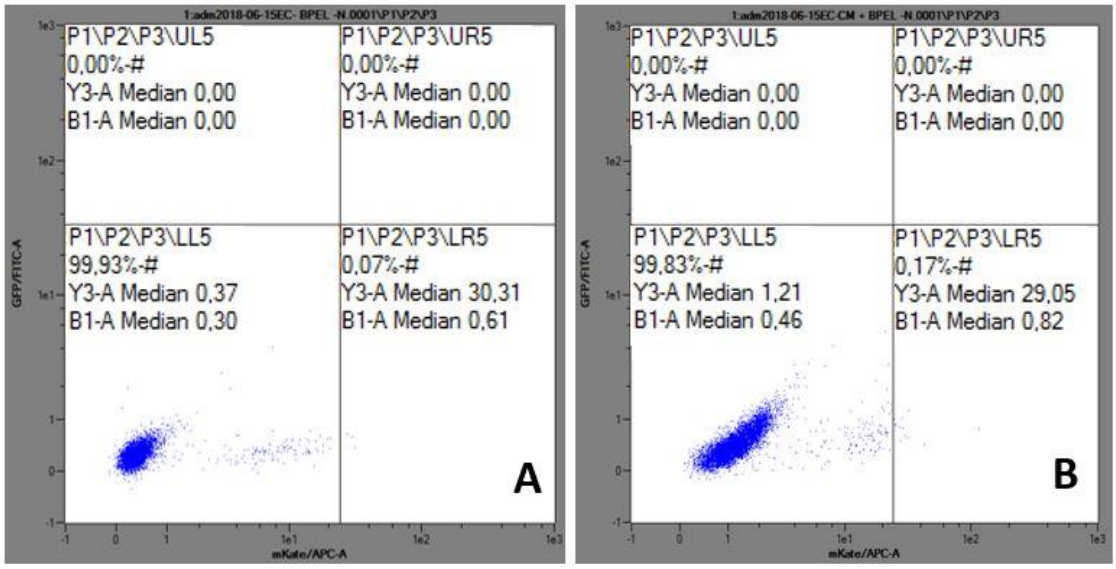

Figure 51: Flow cytometry analysis of populations of endothelial cells unstained with the anti-human-CD31-APC conjugated antibody, acting as a negative control, and cultured under different medium conditions: A) BPEL+VEGF+SB medium and B) BPEL+CM+VEGF+SB+IGF+HS medium.

Gating for Allophycocyanin (APC-A) (x axis). As visible by the data plots, negligible percentages of positive CD31 cells were obtained for the negative samples of both mediums.

VII. References

[1] "Cardiovascular diseases (CVDs)." [Online]. Available: http://www.who.int/news-room/fact-sheets/detail/cardiovascular-diseases-(cvds). [Accessed: 25-Jul-2018].

[2] M. Domenech, L. Polo-Corrales, J. E. Ramirez-Vick, and D. O. Freytes, "Tissue Engineering Strategies for Myocardial Regeneration: Acellular Versus Cellular Scaffolds?," Tissue Eng. Part B Rev., vol. 22, no. 6, pp. 438–458, 2016.

[3] V. Talman and H. Ruskoaho, "Cardiac fibrosis in myocardial infarction-from repair and remodeling to regeneration," Cell and Tissue Research, 2016.

[4] H. F. Lu et al., "Engineering a functional three-dimensional human cardiac tissue model for drug toxicity screening," Biofabrication, vol. 9, no. 2, May 2017.

[5] E. A. Woodcock and S. J. Matkovich, "Cardiomyocytes structure, function and associated pathologies," Int. J. Biochem. Cell Biol., vol. 37, no. 9, pp. 1746–1751, Sep. 2005.

[6] F. Weinberger, I. Mannhardt, and T. Eschenhagen, "Engineering Cardiac Muscle Tissue: A Maturating Field of Research.," Circ. Res., vol. 120, no. 9, pp. 1487–1500, Apr. 2017.

[7] A. H. Kashou and H. E. Kashou, Physiology, Sinoatrial Node (SA Node). StatPearls Publishing, 2018.

[8] "Cardiac Muscle and Electrical Activity | Anatomy and Physiology II." [Online]. Available: https://courses.lumenlearning.com/suny-ap2/chapter/cardiac-muscle-and-electrical-activity/. [Accessed: 13-Aug-2018].

[9] S. Nakano, T. Muramatsu, S. Nishimura, and T. Senbonmatsu, "Cardiomyocyte and Heart Failure," InTech, 2012.

[10] L. C. U. Junqueira, A. L. Mescher, and L. C. U. Junqueira, Junqueira's basic histology : text and atlas. McGraw-Hill Medical, 2010.

[11] G. J. Scuderi and J. Butcher, "Naturally Engineered Maturation of Cardiomyocytes," Front. Cell Dev. Biol., vol. 5, p. 50, May 2017.

[12] J. Li et al., "Impact of vitronectin concentration and surface properties on the stable propagation of human embryonic stem cells," Biointerphases, vol. 5, no. 3, pp. 132–142, Sep. 2010.

[13] T. Vazin and W. J. Freed, "Human embryonic stem cells: derivation, culture, and differentiation: a review.," Restor. Neurol. Neurosci., vol. 28, no. 4, pp. 589–603, 2010.

[14] H. Baharvand et al., "Generation of new human embryonic stem cell lines with diploid and triploid karyotypes," Dev. Growth Differ., vol. 48, no. 2, pp. 117–128, 2006.

[15] J. Nichols et al., "Formation of Pluripotent Stem Cells in the Mammalian Embryo Depends on the POU Transcription Factor Oct4," Cell, vol. 95, no. 3, pp. 379–391, Oct. 1998.

[16] I. Chambers et al., “Functional Expression Cloning of Nanog, a Pluripotency Sustaining Factor in Embryonic Stem Cells,” Cell, vol. 113, no. 5, pp. 643–655, May 2003.

[17] H. Fong, K. A. Hohenstein, and P. J. Donovan, “Regulation of Self-Renewal and Pluripotency by Sox2 in Human Embryonic Stem Cells,” Stem Cells, vol. 26, no. 8, pp. 1931–1938, Aug. 2008.

[18] K. Takahashi and S. Yamanaka, “Induction of pluripotent stem cells from mouse embryonic and adult fibroblast cultures by defined factors.,” Cell, vol. 126, no. 4, pp. 663–76, Aug. 2006.

[19] K. Takahashi et al., “Induction of Pluripotent Stem Cells from Adult Human Fibroblasts by Defined Factors,” Cell, vol. 131, no. 5, pp. 861–872, Nov. 2007.

[20] J. Yu et al., “Induced Pluripotent Stem Cell Lines Derived from Human Somatic Cells,” Science (80-.)., vol. 318, no. 5858, pp. 1917–1920, Dec. 2007.

[21] S. Diecke, S. M. Jung, J. Lee, and J. H. Ju, “Recent technological updates and clinical applications of induced pluripotent stem cells.,” Korean J. Intern. Med., vol. 29, no. 5, pp. 547–57, Sep. 2014.

[22] X. Q. Xu and W. Sun, “Perspective from the heart: The potential of human pluripotent stem cell-derived cardiomyocytes,” J. Cell. Biochem., vol. 114, no. 1, pp. 39–46, Jan. 2013.

[23] I. Kehat et al., “Human embryonic stem cells can differentiate into myocytes with structural and functional properties of cardiomyocytes.,” J. Clin. Invest., vol. 108, no. 3, pp. 407–14, Aug. 2001.

[24] C. Mummery, “Differentiation of Human Embryonic Stem Cells to Cardiomyocytes: Role of Coculture With Visceral Endoderm-Like Cells,” Circulation, vol. 107, no. >21, pp. 2733–2740, Jun. 2003.

[25] C. L. Mummery, J. Zhang, E. S. Ng, D. A. Elliott, A. G. Elefanty, and T. J. Kamp, “Differentiation of human embryonic stem cells and induced pluripotent stem cells to cardiomyocytes: a methods overview.,” Circ. Res., vol. 111, no. 3, pp. 344–58, Jul. 2012.

[26] S. A. Langhans, “Three-Dimensional in Vitro Cell Culture Models in Drug Discovery and Drug Repositioning,” Front. Pharmacol., vol. 9, Jan. 2018.

[27] J. Zhang et al., “Extracellular matrix promotes highly efficient cardiac differentiation of human pluripotent stem cells: the matrix sandwich method.,” Circ. Res., vol. 111, no. 9, pp. 1125–36, Oct. 2012.

[28] M. A. Laflamme et al., “Cardiomyocytes derived from human embryonic stem cells in pro-survival factors enhance function of infarcted rat hearts,” Nat. Biotechnol., vol. 25, no. 9, pp. 1015–1024, Sep. 2007.

[29] C. Zuppinger, “3D culture for cardiac cells,” Biochim. Biophys. Acta - Mol. Cell Res., pp. 1873–1881, 2016.

[30] R. R. Besser, M. Ishahak, V. Mayo, D. Carbonero, I. Claure, and A. Agarwal, “Engineered Microenvironments for Maturation of Stem Cell Derived Cardiac Myocytes,” Theranostics, vol. 8, no. 1, pp. 124–140, 2018.

[31] J. Li et al., “Human Pluripotent Stem Cell-Derived Cardiac Tissue-like Constructs for Repairing the Infarcted Myocardium,” Stem Cell Reports, vol. 9, no. 5, pp. 1546–1559, Nov. 2017.

[32] I. Klein and S. Danzi, “Thyroid Disease and the Heart,” Circulation, vol. 116, no. 15, pp. 1725–1735, Oct. 2007.

[33] Y.-K. Lee et al., “Triiodothyronine Promotes Cardiac Differentiation and Maturation of Embryonic Stem Cells via the Classical Genomic Pathway,” Mol. Endocrinol., vol. 24, no. 9, pp. 1728–1736, Sep. 2010.

[34] Y.-H. Song, M. Godard, Y. Li, S. R. Richmond, N. Rosenthal, and P. Delafontaine, “Insulin-Like Growth Factor I-Mediated Skeletal Muscle Hypertrophy Is Characterized by Increased mTOR-p70S6K Signaling without Increased Akt Phosphorylation,” J. Investig. Med., vol. 53, no. 3, pp. 135–142, Apr. 2005.

[35] C. Freund et al., “Insulin Redirects Differentiation from Cardiogenic Mesoderm and Endoderm to Neuroectoderm in Differentiating Human Embryonic Stem Cells,” Stem Cells, vol. 26, no. 3, pp. 724–733, Mar. 2008.

[36] C. Correia et al., “Distinct carbon sources affect structural and functional maturation of cardiomyocytes derived from human pluripotent stem cells,” Sci. Rep., vol. 7, no. 1, 2017.

[37] E. T. Kase et al., “Remodeling of oxidative energy metabolism by galactose improves glucose handling and metabolic switching in human skeletal muscle cells.,” PLoS One, vol. 8, no. 4, p. e59972, 2013.

[38] M. N. Hirt, A. Hansen, and T. Eschenhagen, “Cardiac Tissue Engineering: State of the Art,” Circ. Res., vol. 114, no. 2, pp. 354–367, Jan. 2014.

[39] T. Eschenhagen, M. Didié, F. Munzel, P. Schubert, K. Schneiderbanger, and W.-H. Zimmermann, “3D engineered heart tissue for replacement therapy,” Basic Res. Cardiol., vol. 97, no. 7, pp. 1–1, May 2002.

[40] I. M. El-Sherbiny and M. H. Yacoub, “Hydrogel scaffolds for tissue engineering: Progress and challenges.,” Glob. Cardiol. Sci. Pract., vol. 2013, no. 3, pp. 316–42, 2013.

[41] Z. Li and J. Guan, “Hydrogels for Cardiac Tissue Engineering,” Polymers (Basel)., vol. 3, no. 2, pp. 740–761, Apr. 2011.

[42] A. Hansen et al., “Development of a Drug Screening Platform Based on Engineered Heart Tissue,” Circ. Res., vol. 107, no. 1, pp. 35–44, Jul. 2010.

[43] E. Cholewinski, M. Dietrich, T. C. Flanagan, T. Schmitz-Rode, and S. Jockenhoevel, “Tranexamic Acid—An Alternative to Aprotinin in Fibrin-Based Cardiovascular Tissue Engineering,” Tissue Eng. Part A, vol. 15, no. 11, pp. 3645–3653, Nov. 2009.

[44] K. Yuan Ye, K. E. Sullivan, and L. D. Black, “Encapsulation of Cardiomyocytes in a Fibrin Hydrogel for Cardiac Tissue Engineering,” J. Vis. Exp., no. 55, Sep. 2011.

[45] A. S. Wolberg, “Thrombin generation and fibrin clot structure,” Blood Rev., vol. 21, no. 3, pp. 131–142, May 2007.

[46] T. Eschenhagen et al., “Three-dimensional reconstitution of embryonic cardiomyocytes in a collagen matrix: a new heart muscle model system.,” FASEB J., vol. 11, no. 8, pp. 683–94, Jul. 1997.

[47] W.-H. Zimmermann et al., “Tissue engineering of a differentiated cardiac muscle construct.,” Circ. Res., vol. 90, no. 2, pp. 223–30, Feb. 2002.

[48] S. S. Nunes et al., “Biowire: a new platform for maturation of human pluripotent stem cell derived cardiomyocytes,” Nat Methods, vol. 10, no. 8, pp. 781–787, 2013.

[49] S. R. Caliari and J. A. Burdick, “A practical guide to hydrogels for cell culture.,” Nat. Methods, vol. 13, no. 5, pp. 405–14, 2016.

[50] R. K. Li, Z. Q. Jia, R. D. Weisel, D. A. Mickle, A. Choi, and T. M. Yau, “Survival and function of bioengineered cardiac grafts.,” Circulation, vol. 100, no. 19 Suppl, pp. II63-9, Nov. 1999.

[51] R. L. Carrier et al., “Cardiac tissue engineering: cell seeding, cultivation parameters, and tissue construct characterization.,” Biotechnol. Bioeng., vol. 64, no. 5, pp. 580–9, Sep. 1999.

[52] J. Leor et al., “Bioengineered cardiac grafts: A new approach to repair the infarcted myocardium?,” Circulation, vol. 102, no. 19 Suppl 3, pp. III56-61, Nov. 2000.

[53] M. Radisic et al., “Functional assembly of engineered myocardium by electrical stimulation of cardiac myocytes cultured on scaffolds,” Proc. Natl. Acad. Sci., vol. 101, no. 52, pp. 18129–18134, Dec. 2004.

[54] K. Y. Ye, L. D. Black, and III, “Strategies for tissue engineering cardiac constructs to affect functional repair following myocardial infarction.,” J. Cardiovasc. Transl. Res., vol. 4, no. 5, pp. 575–91, Oct. 2011.

[55] N. Nakamura, T. Kimura, and A. Kishida, “Overview of the Development, Applications, and Future Perspectives of Decellularized Tissues and Organs,” ACS Biomater. Sci. Eng., 2016.

[56] J. P. Guyette et al., “Bioengineering Human Myocardium on Native Extracellular MatrixNovelty and Significance,” Circ. Res., vol. 118, no. 1, pp. 56–72, Jan. 2016.

[57] T. Shimizu, “Fabrication of Pulsatile Cardiac Tissue Grafts Using a Novel 3-Dimensional Cell Sheet Manipulation Technique and Temperature-Responsive Cell Culture Surfaces,” Circ. Res., vol. 90, no. 3, p. 40e–48, Feb. 2002.

[58] E. C. Novosel, C. Kleinhans, and P. J. Kluger, “Vascularization is the key challenge in tissue engineering,” Adv. Drug Deliv. Rev., vol. 63, no. 4–5, pp. 300–311, Apr. 2011.

[59] P. C. H. Hsieh, M. E. Davis, L. K. Lisowski, and R. T. Lee, “Endothelial-cardiomyocyte interactions in cardiac development and repair.,” Annu. Rev. Physiol., vol. 68, pp. 51–66, 2006.

[60] D. L. Brutsaert, “Cardiac Endothelial-Myocardial Signaling: Its Role in Cardiac Growth, Contractile Performance, and Rhythmicity,” Physiol. Rev., vol. 83, no. 1, pp. 59–115, 2003.

[61] “Blue Histology - more about Endothelial Cells.” [Online]. Available: http://www.lab.anhb.uwa.edu.au/mb140/moreabout/endothel.htm. [Accessed: 05-Mar-2018].

[62] C. W. Peak, L. Cross, A. Singh, and A. K. Gaharwar, “Microscale Technologies for Engineering Complex Tissue Structures,” in Microscale Technologies for Cell Engineering, Cham: Springer International Publishing, 2016, pp. 3–25.

[63] K. Haase and R. D. Kamm, “Advances in on-chip vascularization,” Regen. Med., vol. 12, no. 3, pp. 285–302, 2017.

[64] J. B. Hoying, Genetics of angiogenesis. Bios Scientific, 2003.

[65] S. Hauser, F. Jung, and J. Pietzsch, “Human Endothelial Cell Models in Biomaterial Research,” Trends Biotechnol., vol. 35, no. 3, pp. 265–277, Mar. 2017.

[66] T. Vag, T. Schramm, W. A. Kaiser, and I. Hilger, “Proliferating and quiescent human umbilical vein endothelial cells (HUVECs): a potential in vitro model to evaluate contrast agents for molecular imaging of angiogenesis,” Contrast Media Mol. Imaging, vol. 4, no. 4, pp. 192–198, Jul. 2009.

[67] D. J. Nolan et al., “Bone marrow-derived endothelial progenitor cells are a major determinant of nascent tumor neovascularization,” Genes Dev., vol. 21, no. 12, pp. 1546–1558, 2007.

[68] L. Li et al., “VEGF promotes endothelial progenitor cell differentiation and vascular repair through connexin 43.,” Stem Cell Res. Ther., vol. 8, no. 1, p. 237, Oct. 2017.

[69] B. Lin et al., “High-purity enrichment of functional cardiovascular cells from human iPS cells,” Cardiovasc. Res., vol. 95, no. 3, pp. 327–335, Aug. 2012.

[70] D. Taura et al., “Induction and Isolation of Vascular Cells From Human Induced Pluripotent Stem Cells--Brief Report,” Arterioscler. Thromb. Vasc. Biol., vol. 29, no. 7, pp. 1100–1103, Jul. 2009.

[71] S. Sagnella, E. Anderson, N. Sanabria, R. E. Marchant, and K. Kottke-Marchant, “Human endothelial cell interaction with biomimetic surfactant polymers containing Peptide ligands from the heparin binding domain of fibronectin.,” Tissue Eng., vol. 11, no. 1–2, pp. 226–36, 2005.

[72] T. Watabe, J. K. Yamashita, K. Mishima, and K. Miyazono, “TGF-β Signaling in Embryonic Stem Cell-Derived Endothelial Cells,” in Embryonic Stem Cell Protocols, New Jersey: Humana Press, pp. 341–352.

[73] D. I. R. Holmes and I. Zachary, “The vascular endothelial growth factor (VEGF) family: angiogenic factors in health and disease.,” Genome Biol., vol. 6, no. 2, p. 209, 2005.

[74] M. Lovett, K. Lee, A. Edwards, and D. L. Kaplan, “Vascularization Strategies for Tissue Engineering,” Tissue Eng. Part B Rev., vol. 3, pp. 353–370.

[75] M. Montgomery, B. Zhang, and M. Radisic, “Cardiac Tissue Vascularization,” J. Cardiovasc. Pharmacol. Ther., vol. 19, no. 4, pp. 382–393, Jul. 2014.

[76] R. Soares, “The Relevance of Vascularisation in Tissue Engineering,” Eur. Cells Mater., vol. 28, pp. 51–67, 2014.

[77] D. A. Narmoneva, “Endothelial Cells Promote Cardiac Myocyte Survival and Spatial Reorganization: Implications for Cardiac Regeneration,” Circulation, vol. 110, no. 8, pp. 962–968, Aug. 2004.

[78] H. D. Devalla and R. Passier, “Cardiac differentiation of pluripotent stem cells and implications for modeling the heart in health and disease,” Sci. Transl. Med., vol. 10, no. 435, Apr. 2018.

[79] H. Sekine et al., “In vitro fabrication of functional three-dimensional tissues with perfusable blood vessels,” Nat. Commun., vol. 4, pp. 1310–1399, 2013.

[80] T. Dvir, B. P. Timko, D. S. Kohane, and R. Langer, “Nanotechnological strategies for engineering complex tissues,” Nat. Nanotechnol., vol. 6, no. 1, pp. 13–22, Jan. 2011.

[81] X. HAO et al., “Angiogenic effects of sequential release of VEGF-A165 and PDGF-BB with alginate hydrogels after myocardial infarction,” Cardiovasc. Res., vol. 75, no. 1, pp. 178–185, Jul. 2007.

[82] B. M. Leung and M. V Sefton, “A Modular Approach to Cardiac Tissue Engineering,” Tissue Eng. Part A, vol. 16, no. 10, pp. 3207–3218, 2010.

[83] A. D. van der Meer and A. van den Berg, “Organs-on-chips: breaking the in vitro impasse,” Integr. Biol., vol. 4, no. 5, p. 461, 2012.

[84] J. T. Borenstein, H. Terai, K. R. King, E. J. Weinberg, M. R. Kaazempur-Mofrad, and J. P. Vacanti, “Microfabrication Technology for Vascularized Tissue Engineering,” Biomed. Microdevices, vol. 4, no. 3, pp. 167–175, 2002.

[85] J. N. Lee, C. Park, and G. M. Whitesides, “Solvent Compatibility of Poly(dimethylsiloxane)-Based Microfluidic Devices,” Anal. Chem., vol. 75, no. 23, pp. 6544–6554, Dec. 2003.

[86] T. Gervais, J. El-Ali, A. Günther, and K. F. Jensen, “Flow-induced deformation of shallow microfluidic channels,” Lab Chip, vol. 6, no. 4, p. 500, 2006.

[87] S. Kuddannaya, Y. J. Chuah, M. H. A. Lee, N. V. Menon, Y. Kang, and Y. Zhang, “Surface Chemical Modification of Poly(dimethylsiloxane) for the Enhanced Adhesion and Proliferation of Mesenchymal Stem Cells,” ACS Appl. Mater. Interfaces, vol. 5, no. 19, pp. 9777–9784, Oct. 2013.

[88] B. J. van Meer et al., “Small molecule absorption by PDMS in the context of drug response bioassays,” Biochem. Biophys. Res. Commun., vol. 482, no. 2, pp. 323–328, Jan. 2017.

[89] C.-W. Chi, A. R. Ahmed, Z. Dereli-Korkut, and S. Wang, “Microfluidic cell chips for high-throughput drug screening,” Bioanalysis, vol. 8, no. 9, pp. 921–937, May 2016.

[90] A. S. Curtis, “The Mechanism of Adhesion of Cells to Glass. A stufy by interference reflection microscopy.,” J. Cell Biol., vol. 20, no. 2, pp. 199–215, Feb. 1964.

[91] A. P. Golden and J. Tien, “Fabrication of microfluidic hydrogels using molded gelatin as a sacrificial element,” Lab Chip, vol. 7, no. 6, p. 720, 2007.

[92] D. A. Elliott et al., “NKX2-5 eGFP/w hESCs for isolation of human cardiac progenitors and cardiomyocytes,” Nat. Methods, vol. 8, no. 12, pp. 1037–1040, Dec. 2011.

[93] E. S. Ng, R. Davis, E. G. Stanley, and A. G. Elefanty, “A protocol describing the use of a recombinant protein-based, animal product-free medium (APEL) for human embryonic stem cell differentiation as spin embryoid bodies,” Nat. Protoc., vol. 3, no. 5, pp. 768–776, May 2008.

[94] F. L. Crespo, V. R. Sobrado, L. Gomez, A. M. Cervera, and K. J. McCreath, “Mitochondrial Reactive Oxygen Species Mediate Cardiomyocyte Formation from Embryonic Stem Cells in High Glucose,” Stem Cells, p. N/A-N/A, May 2010.

[95] E. Moonen, R. Luttge, and J.-P. Frimat, “Single cell trapping by capillary pumping using NOA81 replica moulded stencils,” Microelectron. Eng., vol. 197, pp. 1–7, Oct. 2018.

[96] “Norland Products.” [Online]. Available: https://www.norlandprod.com/lightsourc.html#led200. [Accessed: 03-Jun-2018].

[97] A. Note, “Plasma Treated PDMS for improved bonding performance of microfluidic devices,” Henniker Plasma.

[98] J. Kim, M. K. Chaudhury, and M. J. Owen, “Hydrophobic Recovery of Polydimethylsiloxane Elastomer Exposed to Partial Electrical Discharge,” J. Colloid Interface Sci., vol. 226, pp. 231–236, 2000.

[99] “Fluorescence SpectraViewer - NL.”

[100] S. Kredel et al., “mRuby, a Bright Monomeric Red Fluorescent Protein for Labeling of Subcellular Structures,” PLoS One, vol. 4, no. 2, Feb. 2009.

[101] S. Pecha, T. Eschenhagen, and H. Reichenspurner, “Myocardial tissue engineering for cardiac repair,” J. Hear. Lung Transplant., 2016.

[102] T. Eschenhagen, C. Mummery, and B. C. Knollmann, “Modelling sarcomeric cardiomyopathies in the dish: from human heart samples to iPSC cardiomyocytes,” Cardiovasc. Res., vol. 105, no. 4, pp. 424–438, Apr. 2015.

[103] A. Gishto, “Scaffold Composition and Architecture Critically Regulate Extracellular Matrix Synthesis by Cardiomyocytes,” ETD Arch., 2013.

[104] Y.-S. Zhao et al., “Construction of a Unidirectionally Beating 3-Dimensional Cardiac Muscle Construct,” J. Hear., vol. 24, no. 8, pp. 1091–1097, 2005.

[105] Y. Shin et al., “In vitro 3D collective sprouting angiogenesis under orchestrated ANG-1 and VEGF gradients,” Lab Chip, vol. 11, no. 13, p. 2175, 2011.

[106] S. A. Sell, P. S. Wolfe, K. Garg, J. M. McCool, I. A. Rodriguez, and G. L. Bowlin, “The Use of Natural Polymers in Tissue Engineering: A Focus on Electrospun Extracellular Matrix Analogues,” Polymers (Basel)., vol. 2, no. 4, pp. 522–553, Nov. 2010.

[107] C. J. Connon and I. W. Hamley, “Hydrogels in Cell-based Therapies,” RSC Publ., 2014.

[108] “Microfluidic device for chemical and mechanical manipulation of suspended cells,” J. Phys. D Appl. Phys, vol. 51.

[109] Y. Li, H. Meng, Y. Liu, and B. P. Lee, “Fibrin gel as an injectable biodegradable scaffold and cell carrier for tissue engineering.,” ScientificWorldJournal., 2015.

[110] F. Katzenberg, “Plasma-bonding of poly(dimethylsiloxane) to glass,” E-Polymers, no. 060, 2005.

[111] K. W. Oh, K. Lee, B. Ahn, and E. P. Furlani, “Design of pressure-driven microfluidic networks using electric circuit analogy,” Lab Chip, vol. 12, no. 3, pp. 515–545, 2012.

[112] W.-H. Zimmermann, “Biomechanical regulation of in vitro cardiogenesis for tissue-engineered heart repair,” Stem Cell Res. Ther., vol. 4, no. 6, p. 137, 2013.

[113] S. Ohta, S. Inasawa, and Y. Yamaguchi, “Alignment of vascular endothelial cells as a collective response to shear flow,” J. Phys. D. Appl. Phys., vol. 48, no. 24, Jun. 2015.

[114] Q. Fu et al., “Insulin Inhibits Cardiac Contractility by Inducing a Gi-Biased 2-Adrenergic Signaling in Hearts,” Diabetes, vol. 63, no. 8, pp. 2676–2689, Aug. 2014.

[115] L. B. Bockus et al., “Cardiac Insulin Signaling Regulates Glycolysis Through Phosphofructokinase 2 Content and Activity,” J. Am. Heart Assoc., vol. 6, no. 12, Dec. 2017.

[116] E. Guzmán-Gutiérrez, C. Veas, A. Leiva, C. Escudero, and L. Sobrevia, “Is a low level of free thyroxine in the maternal circulation associated with altered endothelial function in gestational diabetes?,” Front. Pharmacol., vol. 5, p. 136, 2014.

[117] J. R. Privratsky and P. J. Newman, “PECAM-1: regulator of endothelial junctional integrity.,” Cell Tissue Res., vol. 355, no. 3, pp. 607–19, Mar. 2014.

[118] P. Lertkiatmongkol, D. Liao, H. Mei, Y. Hu, and P. J. Newman, “Endothelial functions of platelet/endothelial cell adhesion molecule-1 (CD31),” Curr. Opin. Hematol., vol. 23, no. 3, pp. 253–259, May 2016.

[119] B. Hennig, G. A. Boissonneault, and H. P. Glauert, “Effects of serum type on growth and permeability properties of cultured endothelial cells.,” Exp. Cell Res., vol. 181, no. 2, pp. 589–96, Apr. 1989.

[120] A. Lesman, L. Gepstein, and S. Levenberg, “Vascularization shaping the heart.,” Ann. N. Y. Acad. Sci., vol. 1188, pp. 46–51, Feb. 2010.

[121] Y. Wang et al., “Regulation of VEGF-induced endothelial cell migration by mitochondrial reactive oxygen species.,” Am. J. Physiol. Cell Physiol., vol. 301, no. 3, pp. C695-704, Sep. 2011.

[122] H. Gerhardt, “VEGF and endothelial guidance in angiogenic sprouting.,” Organogenesis, vol. 4, no. 4, pp. 241–6, Oct. 2008.

[123] B. Baron, “Biochemical Formulation of Chemically-Defined and Non-Xenogeneic Culture Media for Research and Clinical Applications of Human Stem Cells 2 Basic Biochemistry,” Austin Publ., 2016.

[124] M. W. Irvin, A. Zijlstra, J. P. Wikswo, and A. Pozzi, “Techniques and assays for the study of angiogenesisa,” Exp Biol Med, vol. 239, no. 11, pp. 1476–1488, 2014.

[125] F. Mac Gabhann, J. W. Ji, and A. S. Popel, “VEGF gradients, receptor activation, and sprout guidance in resting and exercising skeletal muscle,” J. Appl. Physiol., vol. 102, no. 2, pp. 722–734, Feb. 2007.

[126] A. C. Newman, M. N. Nakatsu, W. Chou, P. D. Gershon, and C. C. W. Hughes, “The requirement for fibroblasts in angiogenesis: fibroblast-derived matrix proteins are essential for endothelial cell lumen formation.,” Mol. Biol. Cell, vol. 22, no. 20, pp. 3791–800, Oct. 2011.

[127] C. Wang, B. M. Baker, C. S. Chen, and M. A. Schwartz, “Endothelial cell sensing of flow direction.,” Arterioscler. Thromb. Vasc. Biol., vol. 33, no. 9, pp. 2130–6, Sep. 2013.

[128] P.-P. Hsu et al., “Effects of Flow Patterns on Endothelial Cell Migration into a Zone of Mechanical Denudation,” Biochem. Biophys. Res. Commun., vol. 285, no. 3, pp. 751–759, Jul. 2001.

[129] S. Ghaffari, R. L. Leask, and E. A. V Jones, “Flow dynamics control the location of sprouting and direct elongation during developmental angiogenesis.,” Development, vol. 142, no. 23, pp. 4151–7, Dec. 2015.

[130] J. Park, H. S. Kim, and A. Han, “Micropatterning of poly(dimethylsiloxane) using a photoresist lift-off technique for selective electrical insulation of microelectrode arrays,” J. Micromech Microeng., 2009.